DEVELOPMENT AND VALIDATION OF AN ANALYTICAL MODEL FOR THE NOTCHED POCKET DAMPER SEAL

A Thesis

by

BHARATHWAJ KANNAN SRINIVAS

Submitted to the Office of Graduate Studies of
Texas A&M University
in partial fulfillment of the requirements for the degree of

MASTER OF SCIENCE

May 2003

Major Subject: Mechanical Engineering

DEVELOPMENT AND VALIDATION OF AN ANALYTICAL MODEL FOR THE NOTCHED POCKET DAMPER SEAL

A Thesis

by

BHARATHWAJ KANNAN SRINIVAS

Submitted to Texas A&M University
in partial fulfillment of the requirements
for the degree of

MASTER OF SCIENCE

Approved as to style and content by:

John M. Vance (Chair of Committee)	Dara W. Childs (Member)
Maurice Rahe (Member)	John Weese (Head of Department)

May 2003

Major Subject: Mechanical Engineering

ABSTRACT

Determination and Validation of an Analytical Model for
the Notched Pocket Damper Seal. (May 2003)
Bharathwaj Kannan Srinivas, B.E., University of Madras, India
Chair of Advisory Committee: Dr. John M. Vance

Experiments conducted at the Texas A&M Turbomachinery Laboratory and field applications have shown that pocket damper seals (PDS) can be used to suppress vibrations in compressors. A mathematical model is presented for the notched PDS. The notch is a prominent feature in all the PDS manufactured in recent times. The notch is provided at the exit blades of the PDS to act as a diverging clearance, which is one of the conditions for the damper seal to perform satisfactorily. The model to be presented has been adapted from a theory previously developed to predict the direct stiffness and damping coefficients. The flow equations are numerically solved and a computer program is developed correspondingly. The predictions from this notched model are compared with the existing model to highlight the effect of the notch in the analysis. These predictions correlate well with the experimental results from the notched PDS. Also experimental results from testing of a two bladed PDS are compared to the code predictions thus validating the notched model. The notched model performs satisfactorily to predict the direct damping coefficients.

Coastdown tests are conducted on a four bladed eight pocket PDS with a partial arc notch of large radius across the exit blades. The PDS offers positive direct damping which increases with an increase in seal inlet pressure. The low stiffness of the test rig combined with the negative stiffness of the seal made it impracticable to conduct testing above inlet pressures of 64.7 psia (4.461 bar). The existing theoretical models are compared with the experimental data collected up to 64.7 psia (4.461 bar).

DEDICATION

To my

Family

&

the *Turbo Lab*

If we knew what we were doing, it wouldn't be called research, would it?

- Albert Einstein

ACKNOWLEDGEMENTS

I would like to express my sincere gratitude to Dr. John M. Vance, my advisor, for giving me an opportunity to work with him and for guiding me throughout my research at the Turbomachinery Laboratory. He has been a great teacher sharing his invaluable ideas and wisdom. His broad and profound knowledge, his patience in making me understand concepts have been of enormous help to me. I greatly appreciate Dr. Dara W. Childs and Dr. Maurice Rahe for agreeing to be part of my thesis committee and I would like to thank them for all their interest and valuable suggestions in completing my thesis. I am also grateful to:

Dr. Luis San Andres for his help in the early stages of the development of the analytical model,

Mr. Eddie Denk and John Cox for their superb ideas in the machine shop, without which I would have spent a lot more time trying to do what I wanted,

Anand Srinivasan for his involvement in my work and numerous discussions from which I have immensely benefited,

Nirmal Ganatra and Avijit Bhattacharya for their support in programming,

Bugra Ertas and Ashish Sharma for their assistance and suggestions while working on the damper seal project, and

Ahmed Ghamal, my co-worker, for a number of not-so technical discussions which made working at the Turbomachinery lab a nice experience.

NOMENCLATURE

$\dot{m}_1$	-	Mass flow rate at the inlet blade [M/T]
$\dot{m}_2$	-	Mass flow rate at the exit [M/T]
$\dot{m}_3$	-	Mass flow rate through the notch [M/T]
$\dot{m}_4$	-	Mass flow rate through the exit clearance [M/T]
p_1	-	Seal inlet pressure [F/L^2]
p_2	-	Seal pocket pressure (Static) [F/L^2]
p_3	-	Seal exit pressure [F/L^2]
cr_inlet	-	Seal clearance at the inlet (radial) [L]
cr_exit	-	Seal clearance at the exit (radial) [L]
T	-	Temperature [T]
γ	-	Specific heat ratio for the gas [-]
R	-	Universal gas constant [FL/(MT)]
Fa_1	-	Flow area at the inlet clearance [L^2]
Fa_2	-	Flow area at the exit clearance [L^2]
Fa_3	-	Flow area of the notch [L^2]
r	-	Density of the gas [M/L^3]
f	-	Friction factor of the notch [-]
L	-	Length of the notch [L]
h	-	Hydraulic diameter of the notch [L]
m	-	Viscosity of the gas [MT/L^2]
Re	-	Reynolds number [-]
V_p	-	Volume of the one damper pocket [L^3]
ω	-	Angular whirling frequency of the rotor [T^{-1}]
X	-	Amplitude of vibration [L]
δ	-	Variation in seal clearance (radial) [L]

C_{xx}	-	Direct damping in the horizontal direction [FT/L]
K_{xx}	-	Direct stiffness in the horizontal direction [F/L]
A_e	-	Area on which the pocket pressure acts [L^2]
Cd_1	-	Coefficient of discharge at the inlet [-]
Cd_2	-	Coefficient of discharge at the exit [-]
Cd_3	-	Coefficient of discharge at the notch [-]

TABLE OF CONTENTS

Page

CHAPTER Page

CHAPTER Page

LIST OF FIGURES

Page

Page

Page

Page

Page

LIST OF TABLES

Page

Page

CHAPTER I

INTRODUCTION

BACKGROUND OF DAMPER SEALS

Modern turbomachines operate at speeds and bearing clearances that were thought improbable in the early 1960's. This has been made possible due to extensive research in the field of rotordynamics. The next generation of turbomachines will demand decreased vibration amplitudes for superior performance. These machines will be stretched to their limits but at the same time will be expected to give fewer or no rotordynamics problems. Annular gas seals are used in high-speed machines to minimize leakage due to pressure differentials. These seals have known to cause a variety of rotordynamics problems. Hence, a lot of understanding has been accomplished with regard to their effects on rotating machinery. A seal with a useful amount of damping characteristics is known as a damper seal.

Many rotating machines have fluid film bearings and labyrinth seals. Bearings cannot always be used to dampen vibrations because they may be placed near the nodes of the bending mode shape and therefore are at a place where vibration levels are already at a minimum level. The problem with the labyrinth seals is that they produce cross-coupled forces which sometimes tend to drive the system unstable. This is also true for some types of bearings which contribute destabilizing forces and excite subsynchronous vibrations. A damper seal with no or minimal cross-coupled force can be of significant advantage. A new pocket damper seal with the trade name TAMSEAL^{TM} was invented at the Turbomachinery Laboratory, Texas A&M University in 1991. Continuous testing since then has shown that PDS are very effective in suppressing vibration amplitudes.

This thesis follows the style and format of ASME Journal of Engineering for Gas Turbines and Power.

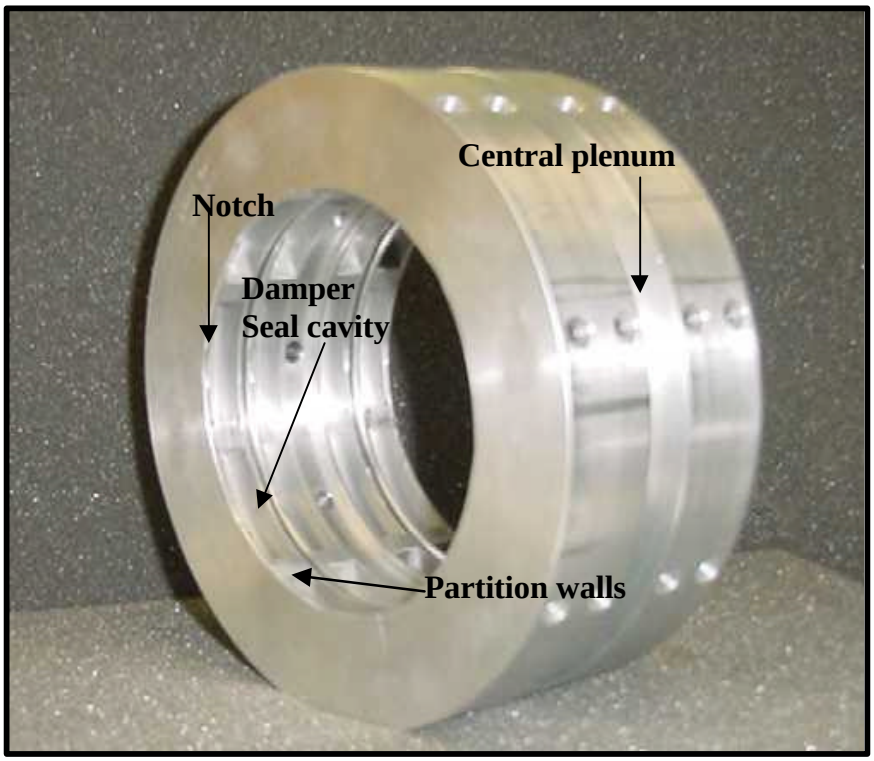

Fig. 1 Photograph of a typical pocket damper seal

Photograph of a typical PDS is shown in Figure 1. One major advantage of this PDS is that it can be placed at a strategic position along the length of the rotor to achieve effective vibration suppression. The two main features of the PDS responsible for providing the damping are:

(a) Diverging seal clearances. This causes the pressure in the cavities (pockets) to always oppose the rotor vibratory velocity. The latest design of PDS have notches cut across in their exit blades to substitute for the diverging clearances.

(b) The presence of separation walls minimizes the circumferential flow or the swirl which is known to cause cross-coupled stiffness. (Cross-coupled stiffness reduces the effective damping).

A major concern about the applicability of the PDS is their high leakage rates. Compared to conventional labyrinth seals of similar dimensions, a PDS has higher leakage rates. A number of experiments have been conducted at the Turbomachinery Laboratory with numerous PDS configurations to validate the relatively simple existing theoretical model. The damping capability of the PDS is well understood but more work has to be done to come up with a PDS design which has lesser leakage. More test data are required to thoroughly understand the static and dynamic performance and limitations of the PDS for current and proposed applications in high speed rotating machinery. In the best interest of the industry more PDS designs are needed which have low leakage (with swirl blockage) and just enough damping to suppress instability.

LITERATURE REVIEW

Alford [1] showed analytically that the dynamic pressure oscillations around the circumference of the seal due to rotor vibration would be stabilizing for diverging seal designs and destabilizing for converging seal designs. Although he predicted this considering labyrinth seals, there is no account of the circumferential swirl of the gas through the seal or propagation of the pressure around the circumferential grooves. Experiments [2] conducted to test Alford's analysis proved it to be incorrect. Vance reviewed Alford's work and proposed that to fully realize the pressure forces, partition walls must be installed to create pockets in the annular grooves.

Benckert and Wachter [3] conducted experiments with labyrinth seals and showed that circumferential flow produces a tangential force that drives the system unstable. They also recommended that the use of swirl brakes could have the effect of stabilizing the system by avoiding cross-coupled forces. Vance & Sundararajan [4] introduced a novel gas pocket bearing damper as a replacement for conventional squeeze film dampers. They developed an isentropic flow model without viscous effects to predict the dynamic force coefficients. This model was entirely based on orifice flow equations (St. Venant's equation). Based on the working principle of the gas pocket

bearing damper, Vance and Shultz [5] introduced a novel type of damper seal, the TAMSEAL^{TM} to be used in turbomachines to suppress vibrations. Non-rotating tests with two bladed PDS conducted by Shultz [6] showed that PDS have more damping than the analogous labyrinth seal. A computer code described in [7] showed good correlation with the experimental results.

Li and Vance [8,9] presented the first test results on two and three bladed notched TAMSEAL's using a rotating test rig. They studied experimentally the effect of clearance ratios and number of teeth to come up with an optimum design to maximize damping coefficients and at the same time decreasing leakage rates. Test results demonstrated that the notched configuration gives twice as much damping as the conventional design.

Li and San Andres [10] developed a code (in Fortran 90) for the rotating journal case. The code was based upon one-control volume bulk flow model. The equations of continuity, momentum in the circumferential direction and the equations for the flow along the partition walls were used to obtain dynamic pressure distribution and the velocity field along a grid prepared for the fluid inside the cavity. The use of a number of second-order parameters in this analysis made the code unpopular for predicting the seal coefficients.

Laos [11,12] conducted a series of tests on the six bladed labyrinth seal and four bladed notched (rectangular) PDS with both four and eight pockets. The notches at the exit blades were rectangular in shape. The tests showed that damping values for the two PDS configurations were much higher than the labyrinth seal. A mathematical model was developed to predict the rotordynamic coefficients for the offcentered PDS. Although this model considered the flow between pockets in the circumferential direction, it did not account for the effect of notches. The existing model highly overpredicted the direct stiffness and damping coefficients when compared with test results. After some scrutiny, this overprediction of the force coefficients was found to be because of incorrect pressure measurements. The section describing the comparison of

predictions and experimental results in [12] has been redone in this thesis which shows that the corrected damping coefficients are actually lesser than the measured values.

Testing of a two bladed eight pocket damper seal by Sharma [13] revealed that if the central supply plenum dimensions were insufficient to handle the volumetric flow through the seal, then the damping capability of the PDS would be severely affected. A comparison of predictions versus measurements made by Li [8] showed that the earlier model [4] overpredicts the seal damping coefficients. A more realistic flow model of multiple-tooth, notched PDS is needed to improve prediction of leakage and dynamic force coefficients.

JUSTIFICATION FOR THE CURRENT RESEARCH

- Continuous testing and research have resulted in modifications to the original damper seal design. One of them is the provision of notches in the exit blades to increase the flow area at the exit to twice the inlet clearance area. Initially inlet and exit blades were of altogether different clearances. However, in the latest PDS design, the notch is provided at the exit blade so as to double the effective clearance. In other words, the dimensions of the notch are such that when summed up the exit area is twice the inlet clearance area. Tests conducted at the Turbomachinery Laboratories revealed that the notched PDS gave better results. In the previously developed one control volume model, the notch is not considered. Even though the present seals come with the notched configuration, the design geometry is currently optimized using the original code. Thus it becomes necessary to have an analysis which includes the notch.
- The 4 bladed PDS to be tested has an active to inactive pitch ratio of 5.1:1. Most of the PDS tested previously have a ratio of 2:1. This means that more area is devoted to the active pockets and might possibly lead to more damping. Results from the experiments conducted would be useful to compare the effect of increasing the pitch ratio.

RESEARCH OBJECTIVES

The following are the objectives to be achieved as part of this research work:

a) Develop a mathematical model to include the flow through the notch in the PDS.
b) Implement the model as a computer code to be used to predict the rotordynamic coefficients and the pocket pressures.
c) Compare the theoretical predictions of the notched model with the predictions from the existing non-notched model to justify the inclusion of the notch in the analysis.
d) Compare the theoretical predictions from the code to the previous test results (Laos and Sharma) of experiments with damper seals.
e) Conduct coastdown tests on a new four bladed damper seal with a notch configuration different from the ones tested.
f) Compare experimental results with the predictions from the two available computer codes, one developed without the notch by Vance and that with the notch.

THESIS OVERVIEW

The background and the literature review are presented in Chapter I along with the research objectives and the justification for the current work. Chapter II is devoted to the presentation of the mathematical model. Predictions from the model are compared with the earlier model in Chapter III. Also theoretical predictions for the case of two bladed PDS are compared with the actual test results in Chapter III. The detailed specification of the test facility, test apparatus and the required instrumentation support is presented in Chapter IV. An overview of the rotordynamic model used in the extraction of rotordynamic coefficients from the experimental Bode plots is discussed in Chapter V. Experimental results for the four bladed PDS are presented in Chapter VI. Chapter VII details on the comparisons between the test results and the predictions from the existing computer codes for damper seals. Conclusions are described along with some discussion in Chapter VIII.

CHAPTER II

ANALYTICAL MODEL FOR THE NOTCHED POCKET DAMPER SEAL

This Chapter describes the analytical model for the PDS incorporating the effect of flow through the notch in the exit blades. The original model developed for the bearing damper [4] has been adapted here in this analysis. The flow equations are analyzed using basic laws of thermodynamics and modeled to calculate the damping and stiffness coefficients due to the dynamically oscillating pressure forces. The average pressures in each of the cavities are calculated based on the gross flow rates into and out of the cavities.

The control volume for this analysis is shown in Figure 2. The annulus of the damper seal is divided into cavities by the partition walls. A typical PDS can have any number of blade pairs but for the sake of simplicity, only two blades have been shown here. The seal has the same inner diameter on the inlet and the exit blades. The notches are cut across the exit blades in such a way as to provide a diverging clearance for the seal. The figure also shows a representation of the notch.

The direction of the fluid flow is from left to right. The vibratory amplitude of the rotor causes flow modulations at the exit and inlet clearances. A dynamically varying pressure force, always opposing the rotor velocity is developed due to the diverging clearance of the seal. The stiffness and the damping coefficients can be calculated from this pressure force.

GOVERNING FLOW EQUATIONS

The flow through the exit clearance is modeled in a manner similar to the analysis of the inlet clearance. However, the flow through the notch is considered as flow through a duct. The following are the assumptions in the analysis:

a) Perfect gas with constant specific heat capacity is considered.

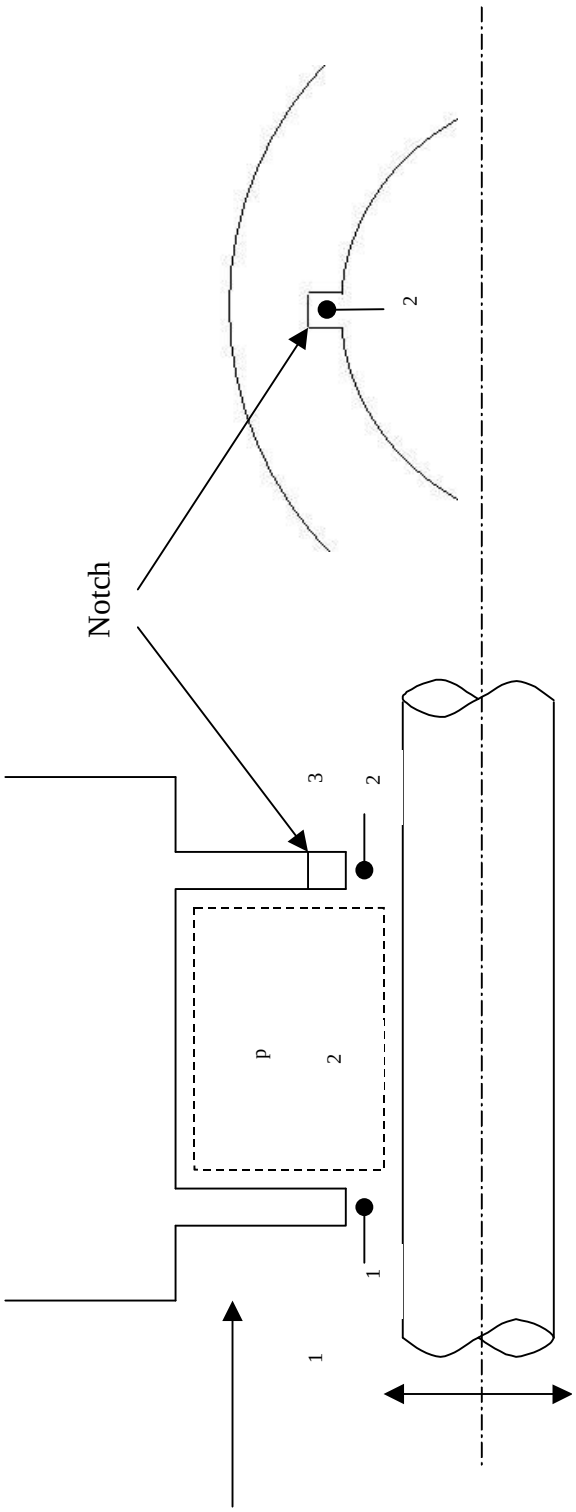

Fig. 2 One control volume for a two bladed PDS with notched exit blade

b) Temperature of the gas is assumed to be a constant. (Experiments at the Turbomachinery Laboratory have shown that temperature variation across the tested seals is less than 5% of the fluid inlet temperature).
c) Circumferential flow is assumed negligible.
d) Viscous effects of the working fluid are neglected.
e) Pressure variations within the pockets are negligible compared to the pressure difference across a seal blade.
f) Flow through the notch is modeled as isothermal flow with friction through a duct.

For no vibration of the journal, the flow through the seal is a constant. In steady state we have

$$\dot{m} = \dot{m}_1 = \dot{m}_2 \quad \text{.....(1)}$$

Considering flow through the seal clearance as isentropic, the mass flow rate through the seal is calculated from St. Venant's equation.

For the inlet blade, the equation for unchoked flow is given by

$$\dot{m}_1 = cd_1 \frac{p_1 Fa_1}{\sqrt{g\,RT}} \sqrt{\frac{2g^2}{g-1}\left[\left(\frac{p_2}{p_1}\right)^{\frac{2}{g}} - \left(\frac{p_2}{p_1}\right)^{\frac{(g+1)}{g}}\right]} \quad \text{.....(2)}$$

The flow at the exit consists of two parts: flow through the exit clearance and flow through the notch. The mass flow through the clearance at the exit is given by

$$\dot{m}_4 = cd_2 \frac{p_2 Fa_2}{\sqrt{g\,RT}} \sqrt{\frac{2g^2}{g-1}\left[\left(\frac{p_3}{p_2}\right)^{\frac{2}{g}} - \left(\frac{p_3}{p_2}\right)^{\frac{(g+1)}{g}}\right]} \quad \text{.....(3)}$$

The mass flow through the notch is obtained by considering isothermal flow through a constant area duct with friction [14].

$$\dot{m}_3 = cd_3 Fa_3 \sqrt{\frac{\left(p_2{}^2 - p_3{}^2\right)}{RT\left[\left(\frac{fL}{h}\right) + 2\ln\left(\frac{p_2}{p_3}\right)\right]}} \quad \text{.....(4)}$$

Hence the total mass flow through the exit is

$$\dot{m}_2 = \dot{m}_3 + \dot{m}_4 \quad \text{.....(5)}$$

The equations for steady state mass flow rates are used in an Excel spreadsheet to calculate the mass flow rate and the pocket pressure for different upstream pressures. But again the friction factor is an unknown parameter. The following iterative procedure is used to calculate the friction factor and hence the steady state mass flow rates.

ITERATIVE PROCEDURE FOR CALCULATING FRICTION FACTOR

1) An initial value for the friction factor 'f' is assumed.
2) $\dot{m}_1$ and $\dot{m}_2$ are calculated from the equations by assuming an initial pocket pressure $p_2 = \left(\frac{p_1 + p_3}{2}\right)$.
3) The pocket pressure is varied until equation (1) is satisfied.
4) After each of the iteration, pressure ratios are checked for choking. In choked conditions for air, the pressure ratio drops below the critical pressure ratio of 0.5283. For choked flow at either the upstream or downstream blade the mass flow rate equations for air are given by

$$\text{At the inlet, } \dot{m}_1 = \frac{0.532\, Cd_1\ p_1\ Fa_1}{T} \quad \text{.....(6)}$$

$$\text{At the exit, } \dot{m}_4 = \frac{0.532\, Cd_2\ p_2\ Fa_2}{T} \quad \text{.....(7)}$$

5) The outlet velocity of the gas is calculated from

$$v_2 = \frac{\dot{m}_3}{r\ Fa_3} \quad \text{.....(8)}$$

6) The Reynolds number at the notch outlet is calculated as

$$\mathrm{Re} = \frac{r\ h\ v_2}{m} \quad \text{.....(9)}$$

7) Considering turbulent flow in smooth pipes, the friction factor of the duct is given by the VonKarman Nikuradse formula [14].

$$\frac{1}{\sqrt{4f}} = -0.8 + 2\log_{10}\left(\frac{\mathrm{Re}}{\sqrt{4f}}\right) \quad \text{.....(10)}$$

The friction factor is calculated from the above equation by iteration because it appears on both the sides of the equation.

8) This value of ‘f’ is then compared with the assumed friction factor.
9) Steps 1 – 8 are repeated until the assumed friction factor value matches with the calculated one.

A schematic of the above iterative process is shown in Figure 3.

The mass flow rates and the pressure conditions are used as inputs for the dynamic pressure model to calculate the damping and stiffness provided by the seal. Now when the journal begins to move, the variations in the inlet and exit clearances will cause a variation in the pocket pressure.

For the control volume defined by a pocket shown we have

$$m_1(t) = m_2(t) + \frac{\partial\left(rV_p\right)}{\partial t} \quad \text{.....(11)}$$

For a perfect gas the relationship between pressure and density in an isentropic process

$$\frac{p}{r^{g}} = const \quad \text{……(12)}$$

$$p = rRT \quad \text{…….(13)}$$

$$\frac{\partial\left(rV_p\right)}{\partial t} = V_p \frac{\partial r}{\partial t} + r \frac{\partial V_p}{\partial t} \quad \text{…….(14)}$$

$$\Rightarrow m_1(t) = m_2(t) + V_p \frac{\partial r}{\partial t}\frac{\partial p}{\partial t} + r \frac{\partial V_p}{\partial t} \quad \text{……..(15)}$$

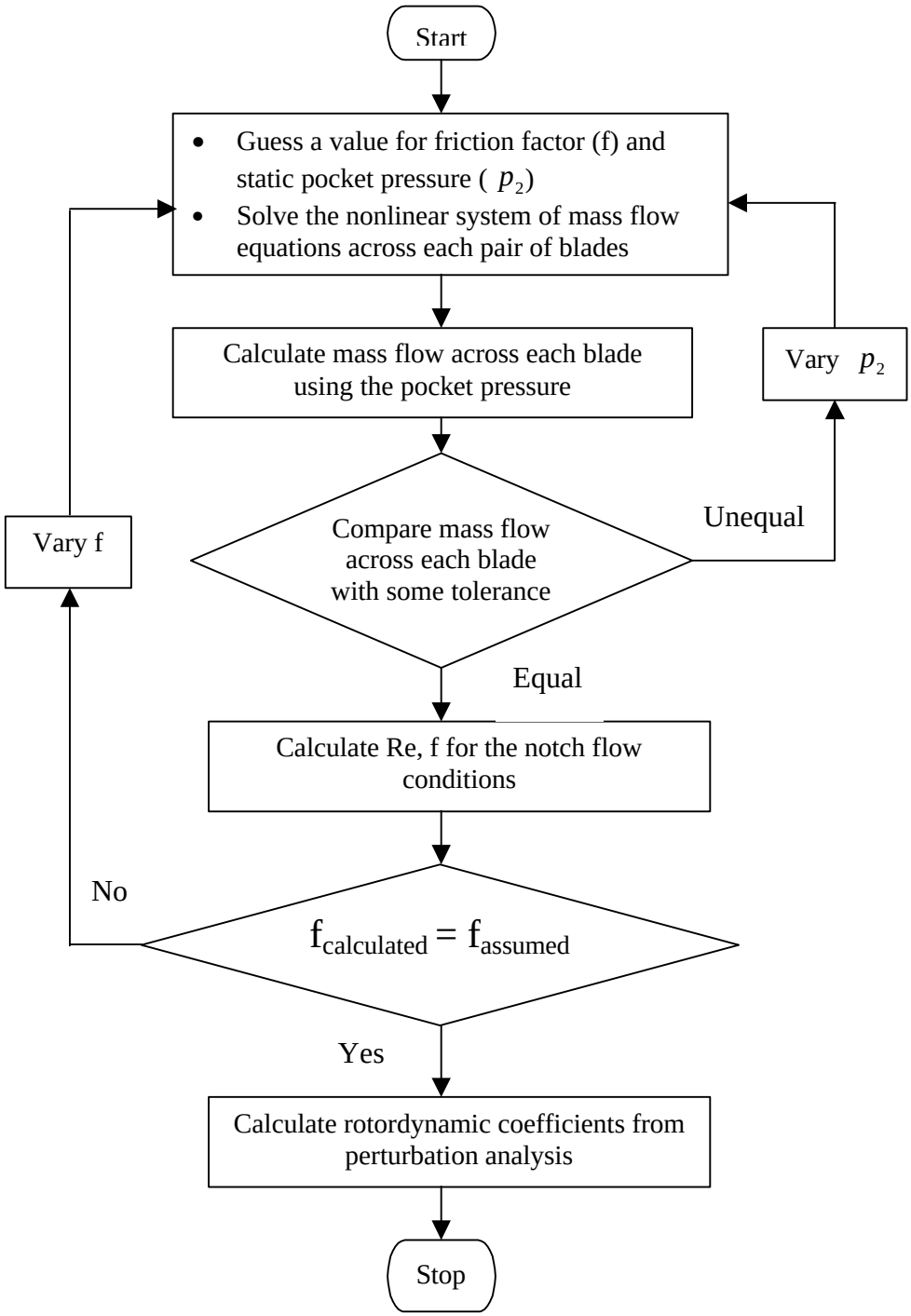

Fig. 3 Flow chart of the notched code

PERTURBATION ANALYSIS

All time varying quantities are assumed to be a sum of a steady state value plus a dynamic value. The mass flow rates vary with time. The mass flow rates vary as a function of p_2 and clearance δ, i.e, we have

$$m_1(t) = \dot{m}_1[p_2(t), d(t)] \quad \text{.....(16)}$$

$$m_2(t) = \dot{m}_2[p_2(t), d(t)] \quad \text{.....(17)}$$

The flow through the notch varies only because of the change in the pocket pressure. Change in the value of δ has no effect on the mass flow across it. In other terms, m_3 is a function of p_2 only, assuming p_3 is fixed.

$$m_2(t) = m_3(t) + m_4(t) \quad \text{.....(18)}$$

$$m_3(t) = \dot{m}_3[p_2(t)] \quad \text{.....(19)}$$

$$m_4(t) = \dot{m}_4[p_2(t), d(t)] \quad \text{.....(20)}$$

The expressions for $m_1(t)$ and $m_2(t)$ are written as sums of steady state and dynamic flow by considering Taylor series expansions and neglecting higher order terms

$$m_1(t) = \dot{m}_1 + \left(\frac{\partial \dot{m}_1}{\partial p_2}\right)_{p_2} p_2(t) + \frac{\partial \dot{m}_1}{\partial d} d(t) \quad \text{.....(21)}$$

$$m_2(t) = \dot{m}_2 + \left(\frac{\partial \dot{m}_2}{\partial p_2}\right)_{p_2} + \frac{\partial \dot{m}_2}{\partial d} d(t) \quad \text{.....(22)}$$

The journal displacement can be assumed to be of the form

$$d(t) = X \sin(w\, t) \quad \text{.....(23)}$$

$$\frac{\partial d}{\partial t} = w\ X\cos(w\ t) \ldots\ldots\ldots\ldots\ldots\ldots\ldots\ldots\ldots\ldots\ldots\ldots(24)$$

Since the journal displacement is assumed to be sinusoidal, the variation in the pocket pressure can also be assumed sinusoidal. The dynamic pressure in the pocket can be expressed as a sum of sine and cosine terms as shown below

$$p_2(t) = p_2 + \bar{p}_2(t) \ldots\ldots\ldots\ldots\ldots\ldots\ldots\ldots\ldots\ldots\ldots\ldots(25)$$

$$\bar{p}_2(t) = p_{2c}\cos(w\ t) + p_{2s}\sin(w\ t) \ldots\ldots\ldots\ldots\ldots\ldots\ldots\ldots\ldots\ldots\ldots(26)$$

$$\frac{\partial p_2(t)}{\partial t} = -w\ \bar{p}_{2c}\sin(w\ t) + w\ \bar{p}_{2s}\cos(w\ t) \ldots\ldots\ldots\ldots\ldots\ldots\ldots\ldots\ldots\ldots..(27)$$

Substituting equations 21, 22, 24, 26 and 27 in 15 we have an equation of the form below:

$$a\left(\frac{\partial d}{\partial t}\right) + b\left(\frac{\partial \bar{p}_2}{\partial t}\right) + c(p_2(t)) + d(d(t)) = 0\,, \ldots\ldots\ldots\ldots\ldots\ldots\ldots\ldots\ldots\ldots(28)$$

where the dummy variables are given by

$$a = \frac{p_2\ A_e}{R\ T} \ldots\ldots\ldots\ldots\ldots\ldots\ldots\ldots\ldots\ldots\ldots\ldots\ldots\ldots\ldots\ldots\ldots\ldots\ldots\ldots\ldots\ldots..(29)$$

$$b = \frac{V_p}{g\ R\ T} \ldots\ldots\ldots\ldots\ldots\ldots\ldots\ldots\ldots\ldots\ldots\ldots\ldots\ldots\ldots\ldots\ldots\ldots\ldots\ldots\ldots\ldots\ldots\ldots\ldots\ldots(30)$$

$$c = \left(\frac{\partial \dot{m}_1}{\partial p_2} - \frac{\partial \dot{m}_2}{\partial p_2}\right) \ldots\ldots\ldots\ldots\ldots\ldots\ldots\ldots\ldots\ldots\ldots\ldots\ldots\ldots\ldots\ldots\ldots\ldots\ldots\ldots\ldots\ldots\ldots\ldots\ldots\ldots\ldots\ldots...(31)$$

$$d = \left(\frac{\partial \dot{m}_1}{\partial d} - \frac{\partial \dot{m}_2}{\partial d}\right) \ldots\ldots\ldots\ldots\ldots\ldots\ldots\ldots\ldots\ldots\ldots\ldots\ldots\ldots\ldots\ldots\ldots\ldots\ldots\ldots\ldots\ldots\ldots\ldots\ldots\ldots\ldots\ldots..(32)$$

The mass flow derivatives due to pocket pressure variation are calculated using

$$\frac{\partial \dot{m}_1}{\partial p_2} = \frac{\dot{m}_1}{2\ p_1\ g} \frac{\left[2\left(\frac{p_2}{p_1}\right)^{\frac{(2-g)}{g}} - (g+1)\left(\frac{p_2}{p_1}\right)^{\frac{1}{g}} \right]}{\left[\left(\frac{p_2}{p_1}\right)^{\frac{2}{g}} - \left(\frac{p_2}{p_1}\right)^{\frac{(g+1)}{g}} \right]} \quad \text{.....(33)}$$

$$\frac{\partial \dot{m}_3}{\partial p_2} = \frac{\dot{m}_3}{p_2^2 - p_3^2} \frac{p_2 \left[\left(\frac{f\ L}{h}\right) + 2\ln\left(\frac{p_2}{p_3}\right) - \frac{p_2^2 - p_3^2}{p_2} \right]}{\left[\left(\frac{f\ L}{h}\right) + 2\ln\left(\frac{p_2}{p_3}\right) \right]} \quad \text{.....(34)}$$

$$\frac{\partial \dot{m}_4}{\partial p_2} = \frac{\dot{m}_4}{2\ p_3\ g} \frac{\left[2\,(g-1)\left(\frac{p_3}{p_2}\right)^{\frac{(2-g)}{g}} + (1-g)\left(\frac{p_3}{p_2}\right)^{\frac{1}{g}} \right]}{\left[\left(\frac{p_3}{p_2}\right)^{\frac{(2-2g)}{g}} - \left(\frac{p_3}{p_2}\right)^{\frac{(1-g)}{g}} \right]} \quad \text{.....(35)}$$

The mass flow derivatives due to change in flow areas are calculated using

$$\frac{\partial \dot{m}_1}{\partial d} = \frac{\dot{m}_1}{cr\_inlet} \quad \text{.....(36)}$$

$$\frac{\partial \dot{m}_2}{\partial d} = \frac{\dot{m}_4}{cr\_exit} \quad \text{.....(37)}$$

Equation 28 is solved for p_{2c} and p_{2s}. Cosine and sine coefficients are separated to form two equations with unknowns.

$$(a\,w\,x + b\,w\,p_{2s} + c\,p_{2c})\cos(w\,t) = 0 \quad \text{.....(38)}$$

$$(-b\,w\,p_{2c} + c\,p_{2s} + d\,x)\sin(w\,t) = 0 \quad \text{.....(39)}$$

SEAL ROTORDYNAMIC COEFFICIENTS

The seal force coefficients (direct stiffness and damping) are calculated by solving the above system of linear equations.

$$\begin{pmatrix} c & bw \\ -bw & c \end{pmatrix}\begin{pmatrix} p_{2c} \\ p_{2s} \end{pmatrix} = \begin{pmatrix} -awx \\ -dx \end{pmatrix} \quad \text{.....(40)}$$

Solving, using Cramer's rule,

$$p_{2c} = \frac{(b\,d - a\,c)w\,x}{(c^2 + b^2)w^2} \quad \text{.....(41)}$$

$$p_{2s} = \frac{(c\,d + a\,b\,w^2)\,X}{(c^2 + b^2w^2)} \quad \text{.....(42)}$$

The damping and stiffness values are calculated as given by

$$\text{Damping}\,C_{xx} = \frac{p_{2c}\,A_e}{w\,X} \quad \text{.....(43)}$$

$$\text{Stiffness}\,K_{xx} = \frac{p_{2s}\,A_e}{w} \quad \text{.....(44)}$$

CHAPTER III

THEORETICAL PREDICTIONS FROM THE NOTCHED MODEL

In this Chapter, predictions from the theoretical model explained earlier in Chapter II are presented. The predictions described are in essence an attempt to validate the inclusion of the effect of the notch in the model. First, predictions from the two existing damper seal models are compared and further to validate the notched model, experimental results from previous testing of a two bladed PDS are compared with the predictions.

It is worthwhile to compare contrast the approaches underlying the two existing computer codes before discussing their actual predictions. The earlier model by Vance will be referred to as Code 1 and the notched model will be denoted as Code 2 in the remaining of this thesis. Apart from including the effect of notch in Code 2 there are some other minor but notable differences in the structure of these two codes. The key points have been summarized below:

- The algorithm followed in the two codes for calculating the mass flow rates across each of the blades is different.
- As a consequence of the above, the predicted mass flow rates as well as the pocket pressures are different in the two codes, even when the effect of the notch is neglected in Code 2. Another important point to be noted is that both the codes verify the mass flows across each of the blades to make sure that they are equal. Interestingly in Code 1 the mass flows for each blade slightly differ from each other. However the mass flow rates from Code 2 predict the same value across all the blades.
- Code 1 uses the minimum of all the mass flows for its perturbation analysis whereas Code 2 uses a mass flow which is same for all the blades.
- During perturbation of the system in Code 2, only the inlet and exit clearance area is affected by the vibration and the notch area is assumed to be unmodulated.

- In codes 1 and 2, the coefficients of discharge for flow across the inlet and exit were assumed to be 0.95 and 1.1 respectively. A coefficient of discharge of 1.0 was assumed for the flow through the notch. However, the flow model for the notch includes a friction factor.

COMPARISON FROM THE TWO EXISTING PDS CODES

A specific set of PDS geometry and other parameters were chosen to be used as input for various simulations with the two existing theoretical models (Vance and the notched model). The input values chosen were of an existing two bladed PDS. The assumed simulation parameters such as seal inlet pressure, air temperature, etc., are values which typically occur in the testing of a PDS at the Turbomachinery Laboratory. Table 1 gives the input values for the various code runs.

Table 1 Input parameters used for the comparison of PDS codes

Seal parameter	Dimensions Inches (mm)
Diameter of the journal	4.0 (101.6)
Inlet seal clearance	0.004 (0.102)
Exit seal clearance	0.008 (0.204)
Seal length	1.056 (26.822)
Radial depth of pocket	0.4 (10.16)
Wall thickness	0.25 (6.35)
Blade thickness	0.075 (1.905)
Number of blades	2
Number of pockets	8

The inlet pressure was varied from 24.7 psia (1.703 bar) to 64.7 psia (4.462 bar). The temperature of the gas was assumed to be 80 °F (26.7 °C) and the properties of the fluid were taken to be that of air.

As mentioned earlier Code 2 deals with the flow at the exit in two parts. By modifying the code, it is possible to exclude the effect of notch. The predictions from such a modified Code when compared with predictions from Code 1 can justify including the flow through the notch in the analysis of the PDS.

Accordingly, Code 2 was modified not to include the effect of the notch. Now the two codes are based on the same analysis but differ in the methodology (algorithm). The codes were run to predict the direct damping and stiffness coefficients for different seal inlet pressures. Figure 4 shows a comparison of the predictions from the two codes after modifying Code 2. Also the mass flow rates are compared in Figure 5.

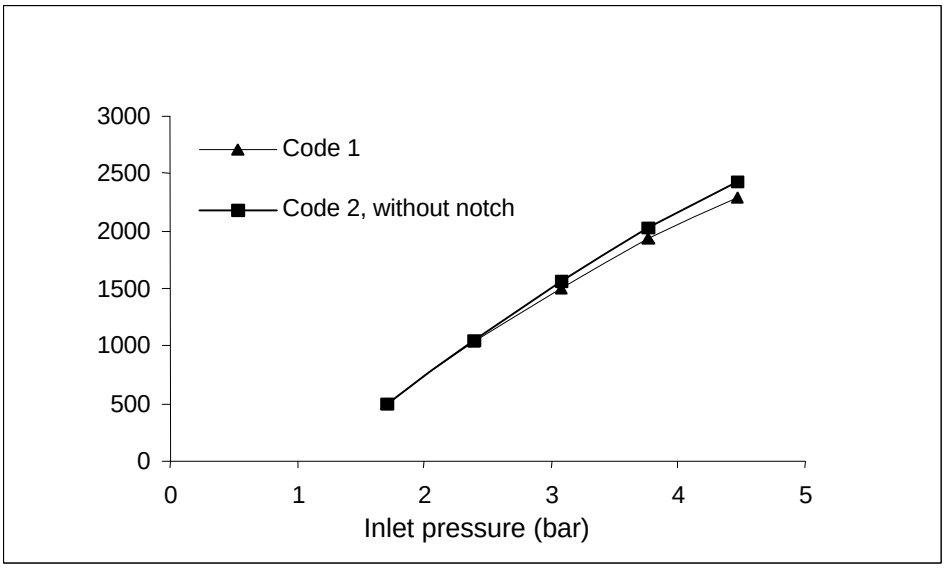

Fig. 4 Comparison of direct damping from Code 1 and Code 2 without notch

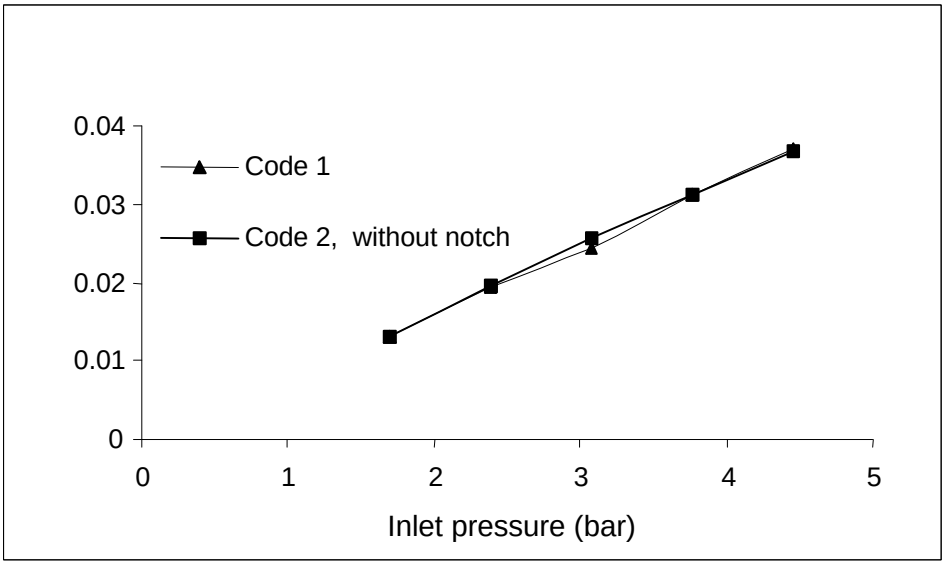

Fig. 5 Comparisons of mass flow from Code 1 and Code 2 without notch

Table 2 gives a better comparison of the damping and mass flow rates predictions along with the percentage deviation from Code 1.

Table 2 Comparison of direct damping with percentage deviation between the two codes no notch case

Inlet pressure psia (bar)	Direct damping coefficients				% difference from Code 1
	Code 1		Code 2, without notch		
	lbs/in	Ns/m	lbs/in	Ns/m	
24.7 (1.703)	2.826	494.714	2.857	500.111	1.090
34.7 (2.392)	5.930	1037.78	6.016	1052.86	1.453
44.7 (3.080)	8.558	1497.65	8.917	1560.61	4.203
54.7 (3.771)	11.055	1934.74	11.199	1959.86	1.297
64.7 (4.462)	13.076	2288.74	13.246	2318.15	1.298

Table 3 Comparison of mass flow with percentage deviation between the two codes- no notch case

Inlet pressure psia (bar)	Mass flow rate				% difference from Code 1
	Code 1		Code 2, without notch		
	lb/s	kg/s	lb/s	kg/s	
24.7 (1.703)	0.028	0.012	0.028	0.013	0.876
34.7 (2.392)	0.042	0.019	0.043	0.019	1.317
44.7 (3.080)	0.054	0.024	0.056	0.025	4.273
54.7 (3.771)	0.068	0.031	0.068	0.031	-0.104
64.7 (4.462)	0.081	0.036	0.080	0.036	-0.712

As seen from Figure 4 and Table 2 the direct damping from the two codes agree well with each other. The slight difference between the two predictions is because of the difference in the algorithm used. The percentage difference seems to be greater at higher pressures. The predicted mass flow rates from the two codes are shown in Table 3. A comparison of the mass flow rates emphasizes the fact that the two codes are based on the same equations for the flow. The maximum difference between the two mass flow predictions is 4.27 % at a seal inlet pressure of 44.7 psia (3.08 bar). For all other inlet pressure ranges the two values are very close to each other. These comparisons assure that there is a strong similarity between the two codes when the notch is not considered. At this point simulations with the Code 2 should give us a good idea of including the notch in the analysis.

Before proceeding with the simulations for the notched case, an interesting case with regard to the notched PDS is worth mentioning. Results from the testing of a two bladed PDS by Li [9] reveal that the damping coefficients are almost doubled for the notched configuration as compared with the non-notched PDS of similar geometry. To

give a better idea the following Figure 6 is reproduced which evidently shows the increased damping coefficients of the same PDS when notches are cut across the exit blades.

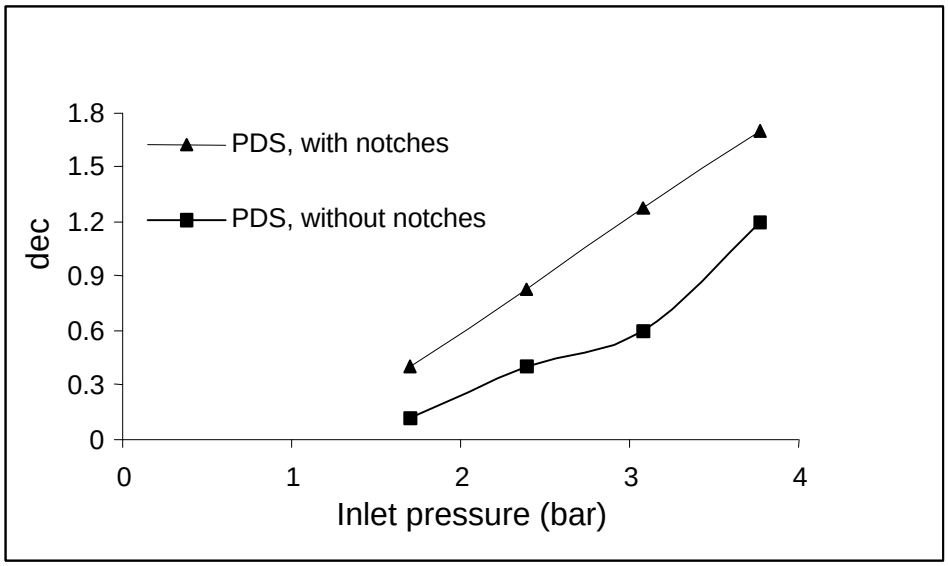

Fig. 6 Comparison of logarithmic decrements for the PDS with and without notch [9]

Code 2 was now used to simulate for each of the above cases with the notch for the same inlet pressure range and the direct damping and mass flow coefficients are tabulated below in Tables 4 and 5 respectively. Figures 7 and 8 depict the direct damping and mass flow coefficients for similar runs but with the notch included.

Table 4 Comparison of direct damping with percentage deviation between the two codes

Inlet pressure psia (bar)	Direct damping coefficients				% deviation from Code 1
	Code 1		Code 2, notched		
	lbs/in	Ns/m	lbs/in	Ns/m	
24.7 (1.703)	2.826	494.714	3.228	564.903	14.187
34.7 (2.392)	5.930	1037.78	8.155	1427.27	37.531
44.7 (3.080)	8.558	1497.65	10.042	1757.47	17.348
54.7 (3.771)	11.055	1934.74	12.398	2169.65	12.141
64.7 (4.462)	13.076	2288.44	13.650	2388.83	4.3867

Table 5 Comparison of mass flow with percentage deviation between the two codes

Inlet pressure psia (bar)	Mass flow rate				% deviation from Code 1
	Code 1		Code 2, notched		
	lb/s	kg/s	lb/s	kg/s	
24.7 (1.703)	0.0286	0.0129	0.0307	0.0139	7.309
34.7 (2.392)	0.0427	0.0193	0.0439	0.0198	2.819
44.7 (3.080)	0.0540	0.0244	0.0565	0.0256	4.727
54.7 (3.771)	0.0689	0.0312	0.0691	0.0311	0.381
64.7 (4.462)	0.0815	0.0369	0.0813	0.0368	-0.192

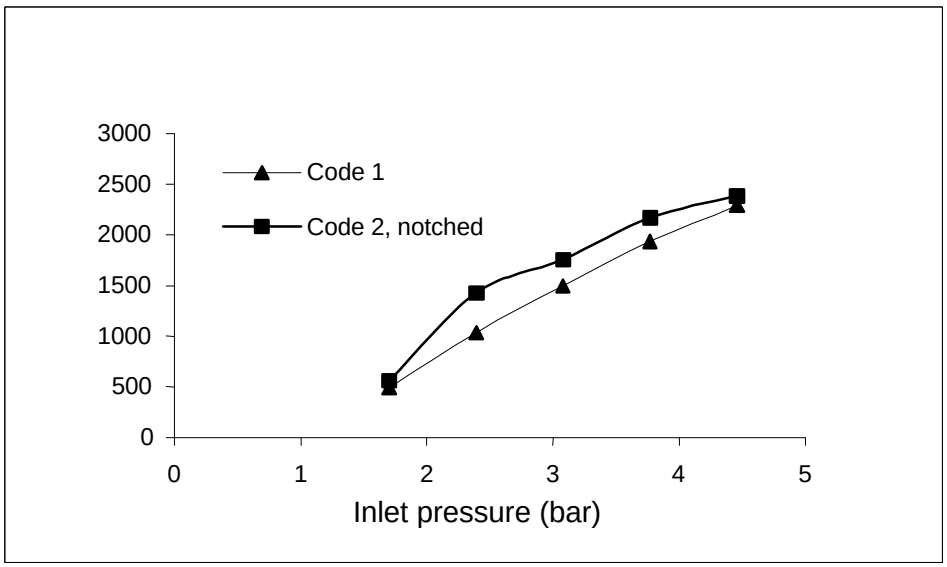

Fig. 7 Comparison of direct damping coefficients from code 1 and code 2, notched

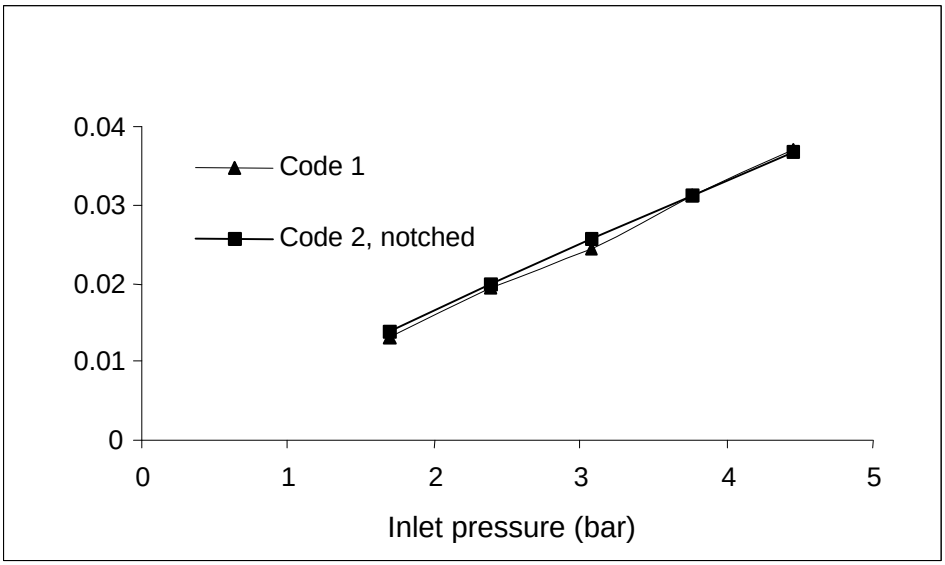

Fig. 8 Comparisons of mass flow from code 1 and code 2, notched

The direct damping obtained from Code 2 is higher than those obtained from Code 1. This clearly indicates that the inclusion of the notch in the analysis increases the predicted damping values. The direct damping values predicted by Code 2 are between 5

% and 35 % greater than those of Code 1 depending on the seal inlet pressure. The above comparison are in qualitative agreement with the various tests results conducted at the Turbomachinery Laboratory where the notched PDS have been shown to exhibit higher damping values than PDS without the notch.

A look at Figure 8 shows that the mass flow rate does not differ for a notched and non-notched PDS. However the damping values have been shown to be drastically different. This can be explained by going back to equations (28) and (41) in the perturbation analysis in Chapter II. The flow through the notch is assumed to be unmodulated. Hence the perturbation of the rotor does not affect the flow through the notch. This means that the term 'd' in equation (28) is increased. As a consequence of this, the calculated value of 'P_{2c}' is more when the notch is included in the analysis. The predicted direct damping is thus more for the notched case. The static pocket pressure values obtained for the above case is shown in Figure 9 and the deviation from Code 1 is shown in Table 6.

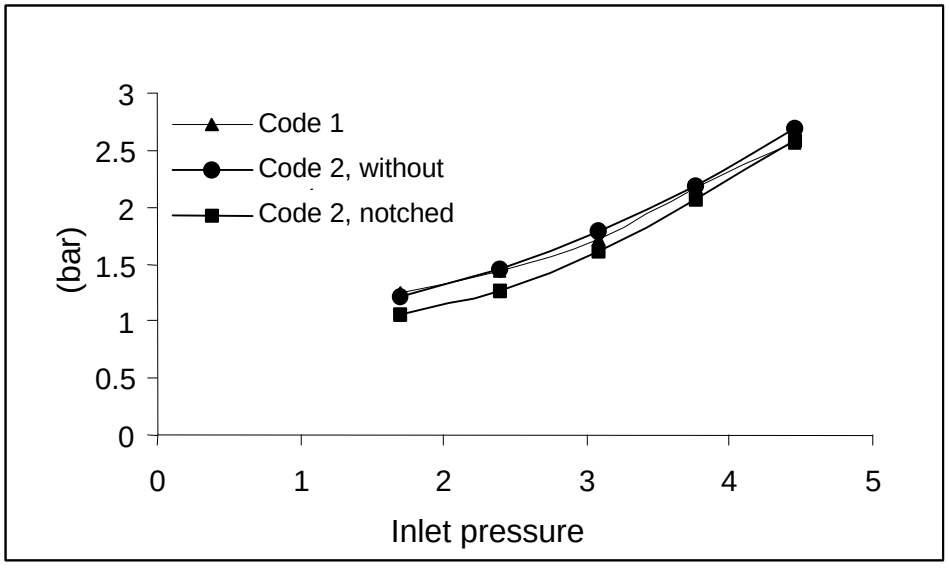

Fig. 9 Comparison of static pocket pressures between the codes

Table 6 Comparison of pocket pressure with percentage deviation between the two codes

Inlet pressure psia (bar)	Static pocket pressure psia (bar)		% deviation from Code 1
	Code 1	Code 2, notched	
24.7 (1.703)	17.474 (1.205)	15.418 (1.063)	-11.767
34.7 (2.392)	20.97 (1.446	18.457 (1.272)	-11.998
44.7 (3.080)	24.896 (1.716)	23.458 (1.617)	-5.774
54.7 (3.771)	31.519 (2.173)	29.952 (2.065)	-4.970
64.7 (4.462)	37.281 (2.57)	37.463 (2.583)	0.489

As seen above, there is a significant difference in the predicted static pocket pressures between the two codes. The percentage difference seems to be lesser for higher values of seal inlet pressures. Interestingly, the same trend is also observed in case of the direct damping coefficients.

Effect of friction factor

The friction factor is an important parameter in the iterative analysis of the notched code. It is seen that the mass flow rate decreases as the friction factor increases. Figure 10 shows the variation of the leakage rate predicted from Code 2 for different values of the friction factor. The variation is minimal for friction factor values in the range 0 to 0.1.

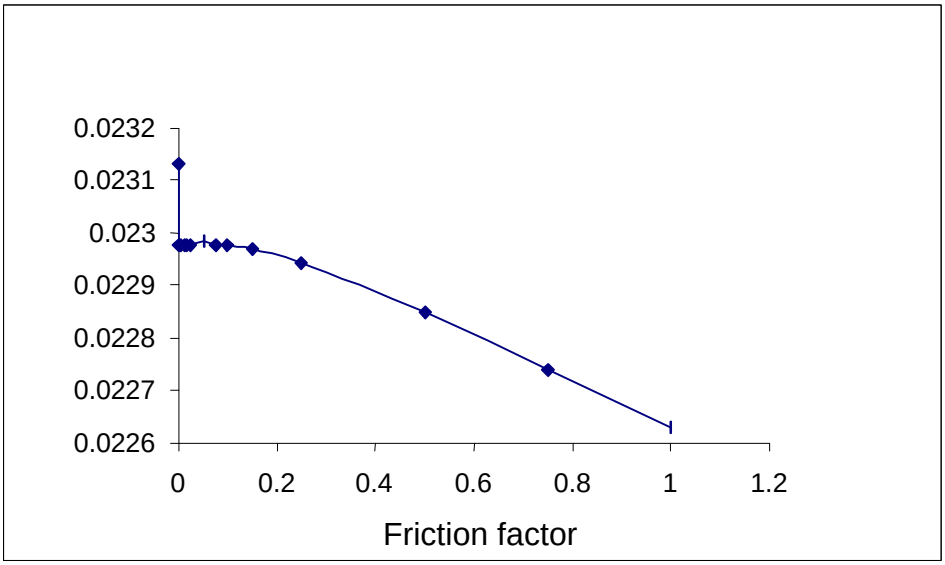

Fig. 10 Mass flow vs Friction factor

COMPARISON OF THEORETICAL PREDICTIONS WITH EXPERIMENTAL RESULTS

In this section predictions from the analytical model will be compared with experimental results from the testing of a two bladed PDS. A two bladed PDS was tested in May 2000 [13]. This PDS was designed by Lockheed Martin and had notches cut across the exit blades. The test results are compared with two theoretical models available at present. Code 1 is the original theoretical model developed by Vance and Sundarajan [4]. Code 2 refers to the new analytical model with the notch.

The seal used for the experiments is very similar to the one shown in Figure 1. The main geometrical parameters of the seal are detailed in Table 7**.** The exit pressure for all the cases was the atmospheric pressure - 14.7 psia (1.0135 bar). The inlet pressure was varied from 24.7 psia (1.703 bar) to 84.7 psia (5.898 bar). The discharge coefficients used for the inlet and exit blades were 1.1 and 0.95 respectively. All the values obtained from the codes were calculated at a whirl frequency of 12600 cpm. Code 2 deals with the flow at the exit separately; one part through the notch and the other one through the exit clearance between the rotor and the seal blade. Hence, while running the code, care is

taken to keep both the inlet and the outlet clearances the same and the notch part is included separately. The code even calculates the notch dimensions so as to make the flow areas equivalent to an exit to inlet clearance ratio of 2:1. This requires that the notch area be equal to the inlet clearance area.

Table 7 Parameters of the two bladed PDS tested

Seal parameter	Dimensions
	Inches (mm)
Diameter of the journal	7.75 (196.85)
Width of the seal pocket	0.6 (15.24)
Seal length (back to back)	2.00 (50.8)
Radial depth of the pocket	0.19 (4.826)
Blade thickness	0.125 (3.175)
Inlet clearance	0.009 (0.229)
Exit clearance	0.009 (0.229)
Number of blades	2
Number of pockets	8

The experimental results listed here are from non-rotating rap tests. The damping values were calculated from the logarithmic decrements of a pure single frequency decaying trace.

Comparison of the seal mass flow rates

Both tests and computed results [9] show that rotor speed has negligible influence on the seal mass flow rate (leakage). The flow rate vs inlet pressure is depicted in Figure 11. The comparison shows that the new model slightly overpredicts the leakage rate but it gives much better values for leakage as the inlet pressure goes up. But at lower pressures

the earlier model predicts the seal leakage better than the new model. As expected, the mass flow increases as the inlet pressure is increased.

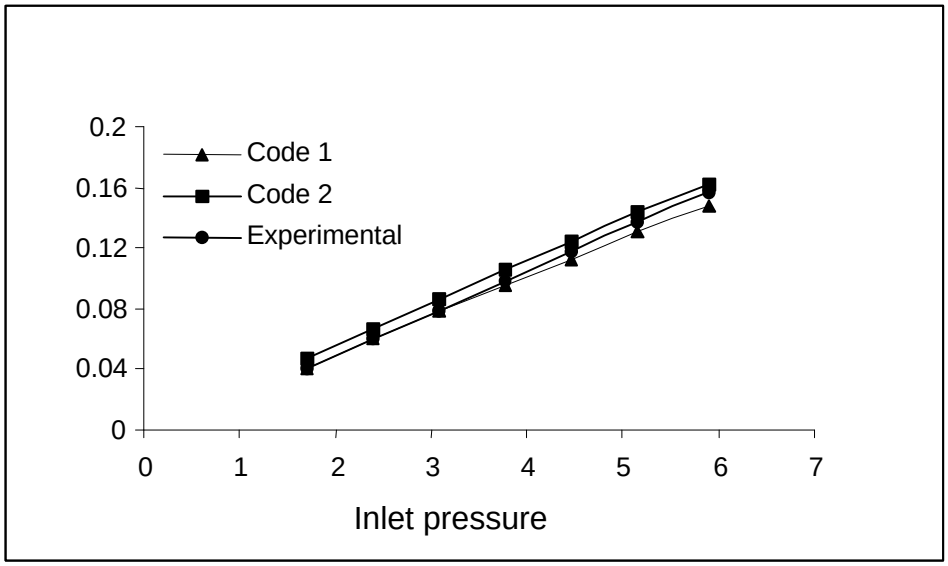

Fig. 11 Comparison of mass flow rates for a two bladed PDS

Comparisons of direct damping coefficients

Figure 12 illustrates the measured direct damping coefficients of the seal and the predictions from the two models. In all these measurements the whirl frequency of the rotor is 12600 rpm. In general, both the models do not give exact predictions for the seal damping coefficients. Again the margin of error with the new model decreases as the inlet pressure increases. The model correctly predicts the direct damping coefficients to be positive and to increase with increasing inlet pressure.

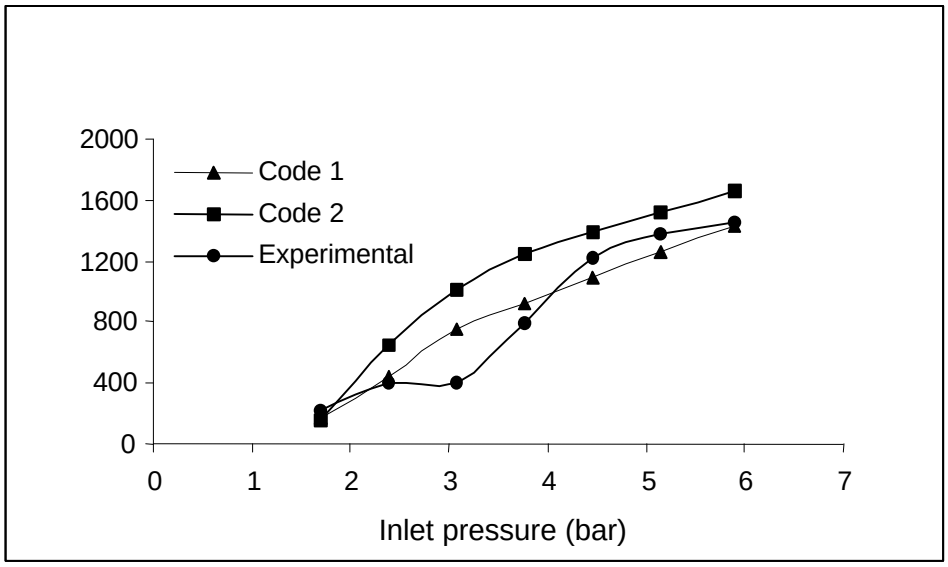

Fig. 12 Comparison of damping coefficients for a two bladed PDS

Comparison of direct stiffness coefficients

The predicted direct stiffness coefficients for the two models and the measured values are shown in Figure 13. Both codes always overpredict (in magnitude) the direct stiffness and the error involved with the previous model is lesser than the new model. The trend with both models is that the stiffness goes more negative as the inlet pressure increases.

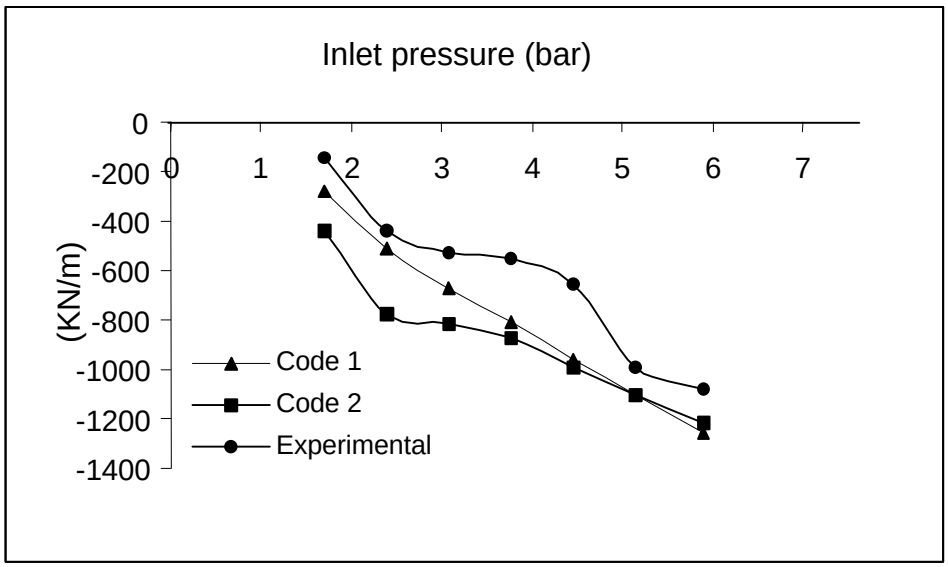

Fig. 13 Comparison of direct stiffness coefficients for the two bladed PDS

Comparison of pocket pressures between the two codes

Figure 14 shows the static pocket pressures as a function of the inlet pressure obtained from the two codes. There was no provision for measuring the pocket pressure during the testing, so only the theoretical predictions from the two codes are shown. The pocket pressures from the two codes slightly differ when the inlet pressure is low. As the inlet pressure goes up the two codes are in clear agreement. The difference in the pressure values can be attributed to the kind of iterative procedures for the flow used in the two codes. The predicted pressures are also tabulated below in Table 8.

Table 8 Comparison of pocket pressures between the two codes

Inlet pressure psia (bar)	Pocket pressure psia (bar)	Pocket pressure psia (bar)
	Code1	Code 2
84.7 (5.898)	48.805 (3.337)	49.357 (3.430)
74.7 (5.150)	43.043 (2.967)	42.662 (2.941)

64.7 (4.460)	37.281 (2.570)	35.980 (2.480)
54.7 (3.771)	31.519 (2.173)	29.304 (2.020)
44.7 (3.081)	24.896 (1.716)	23.610 (1.627)
34.7 (2.392)	20.974 (1.446)	18.452 (1.272)
24.7 (1.703)	17.474 (1.204)	15.198 (1.047)

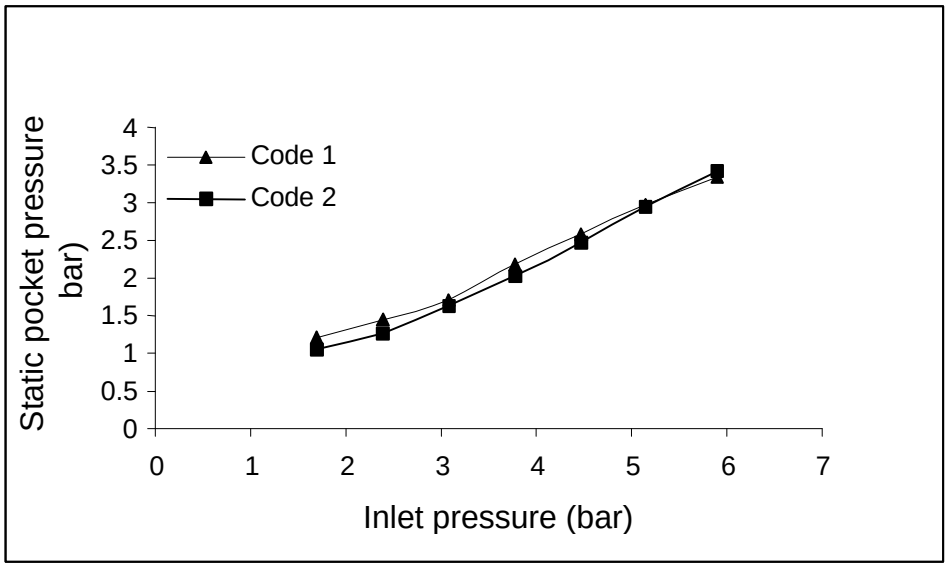

Fig. 14 Comparison of pocket pressure between the two codes for the two bladed PDS

CHAPTER IV

TEST HARDWARE, APPARATUS AND METHODOLOGY

DESCRIPTION OF THE PDS TESTED

A four bladed PDS was designed and used for the experiments conducted. Although this is a new seal, this design was adapted from an earlier PDS design template used by Laos [12]. The parameters for the new PDS were optimized using the TAMSEAL code. The pitch ratio (active/inactive) and the notch geometry were the major variations from the previous PDS. Figures 15 and 16 show detailed drawings of the modified PDS designed at the Turbomachinery Laboratory for the tests. The seal insert was designed using a back-to-back arrangement in order to minimize the axial loading (thrust) on the bearings. Hence, this insert actually has two pocket damper seals.

This PDS has eight pockets at equal angles separated by partition walls. The partition walls are provided only in the active pockets and thus the fluid can flow circumferentially in the inactive pockets. The inlet to the seal is through eight radial holes drilled in the central supply plenum of the PDS. The fluid enters the supply plenum and then separates to flow (axially) through the two PDS in opposite directions. The seal is made of 6061-T6 aluminum, which has good resistance to abrasion in case of rubbing with the journal. The overall length of a single seal is 1.056 inches (26.822 mm). The method of attachment of the partition walls is worth noting here. The walls are machined separately (component is referred as ‘key’) from the same material and are inserted in the PDS axially. Then the full key is secured to the seal with the help of machine screws [# 6-32 * 5/8 inches (15.875 mm)]. The ends of the seal are chamfered to allow easier assembly and prevent any damage to the seal in case of an accidental fall.

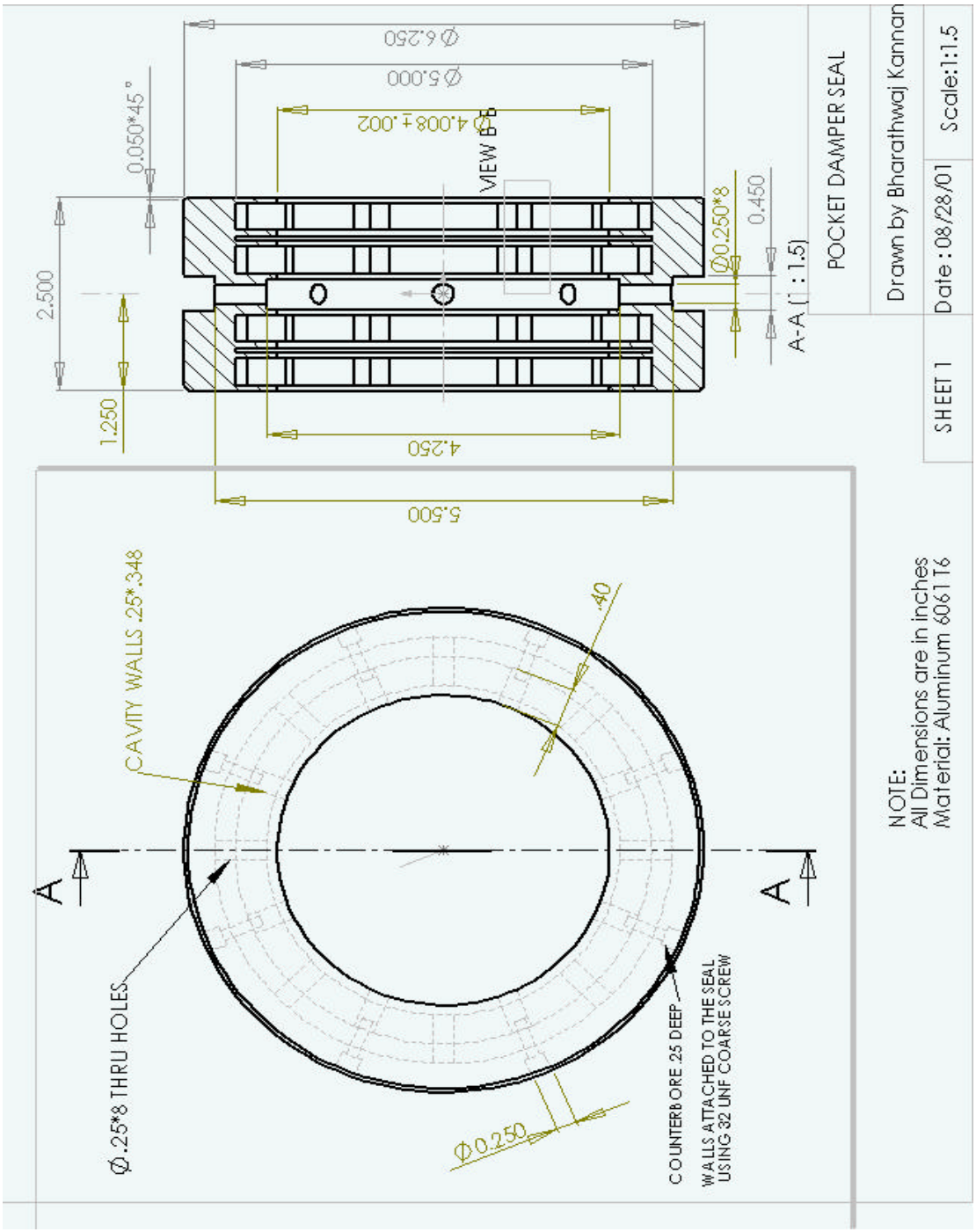

Fig. 15 Detailed drawing of the PDS used in the rotating tests (Sheet I)

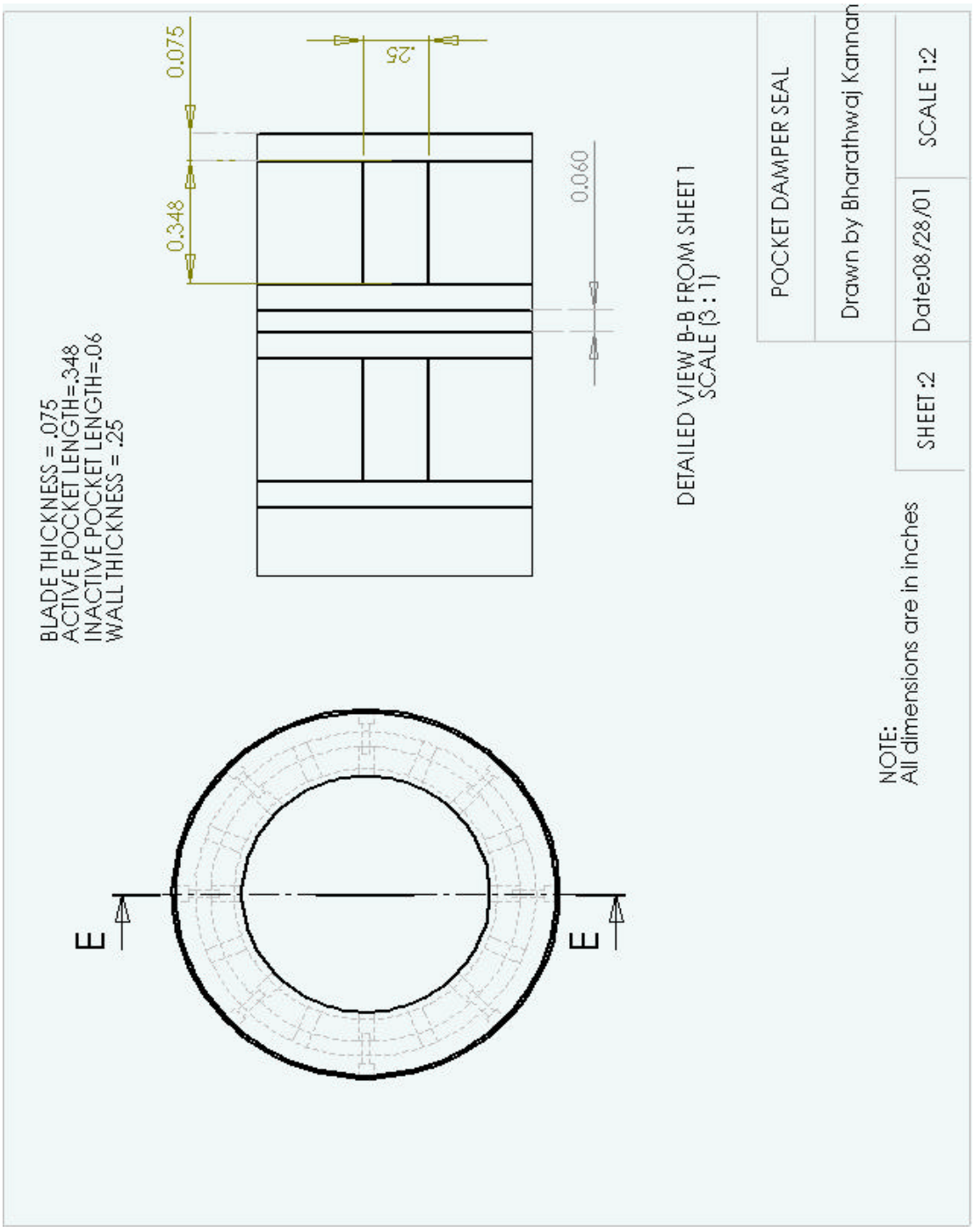

Fig. 16 Detailed drawing of the PDS used in the rotating tests (Sheet II)

The photograph of the seal is shown in Figure 1 and the dimensions are listed in Table 9. The effective clearance ratio between blades at the exit and the inlet ends is 2:1. This is incorporated by providing notches in the exit blades. A semi-circular notch was chosen in this design. This design was considered favorable considering the ease of manufacture and its relative lower cost. In comparison, the previous design had rectangular notches at the exit blades to double the clearance. This notch is manufactured using a three-axis milling machine to scrape off material to a calculated depth from the inner edge of the seal (usually with the help of CNC). A representation of this new feature is shown in Figure 17.

Table 9 Parameters of the four bladed PDS used in the experiments

Seal parameter	Dimensions Inches (mm)
Overall length (two seals)	2.5 (63.5)
Active pocket pitch	0.3040 (7.722)
Inactive pocket pitch	0.06 (1.524)
Blade width	0.075 (1.905)
Wall thickness	0.25 (6.35)
Pocket radial depth	0.4 (10.16)
Number of blades	4
Number of pockets	8
Inlet blade clearance (Radial)	0.004 (0.1016)
Exit blade clearance (Radial) (Notches cut in the exit blades to give exit flow area = 2* inlet flow area)	0.004(0.1016)

As shown in the Table, the pocket radial depth is 0.4 inches (10.16 mm) and the wall thickness is 0.25 inches (6.35 mm). The journal used in the testing has an outer diameter of 4.000 inches (101.6 mm). The seal housing has two hose fittings to allow pressurized air to enter the seal.

(a) Old notch design (b) New notch design

Fig. 17 Representation of the notch designs

During the initial stages of this research it was decided to test the PDS at pressures as high as 300 psi (20.684 bar). A 3D model of the PDS was developed using SOLIDWORKS™ software and a detailed stress analysis was performed to validate the design. COSMOS™ package was used in supplement to do the finite element analysis. The analysis was done for two different cases. Firstly without the partition walls to get a conservative estimate of the stresses and then again with the partition walls. The pressure forces were applied in the annulus with restraints imposed on the outer surface of the PDS. The mesh plot during one such analysis is shown in Appendix C.

TEST JOURNAL

A new test journal was manufactured to be used with the seal in the rotating tests. The journal has a diameter of 4.000 ± 0.002 inches (101.6 ± 0.0508 mm). This tight tolerance on the outer diameter is extremely important, as the proper functioning of the PDS is dependent on accurate clearances between the seal and the journal. The

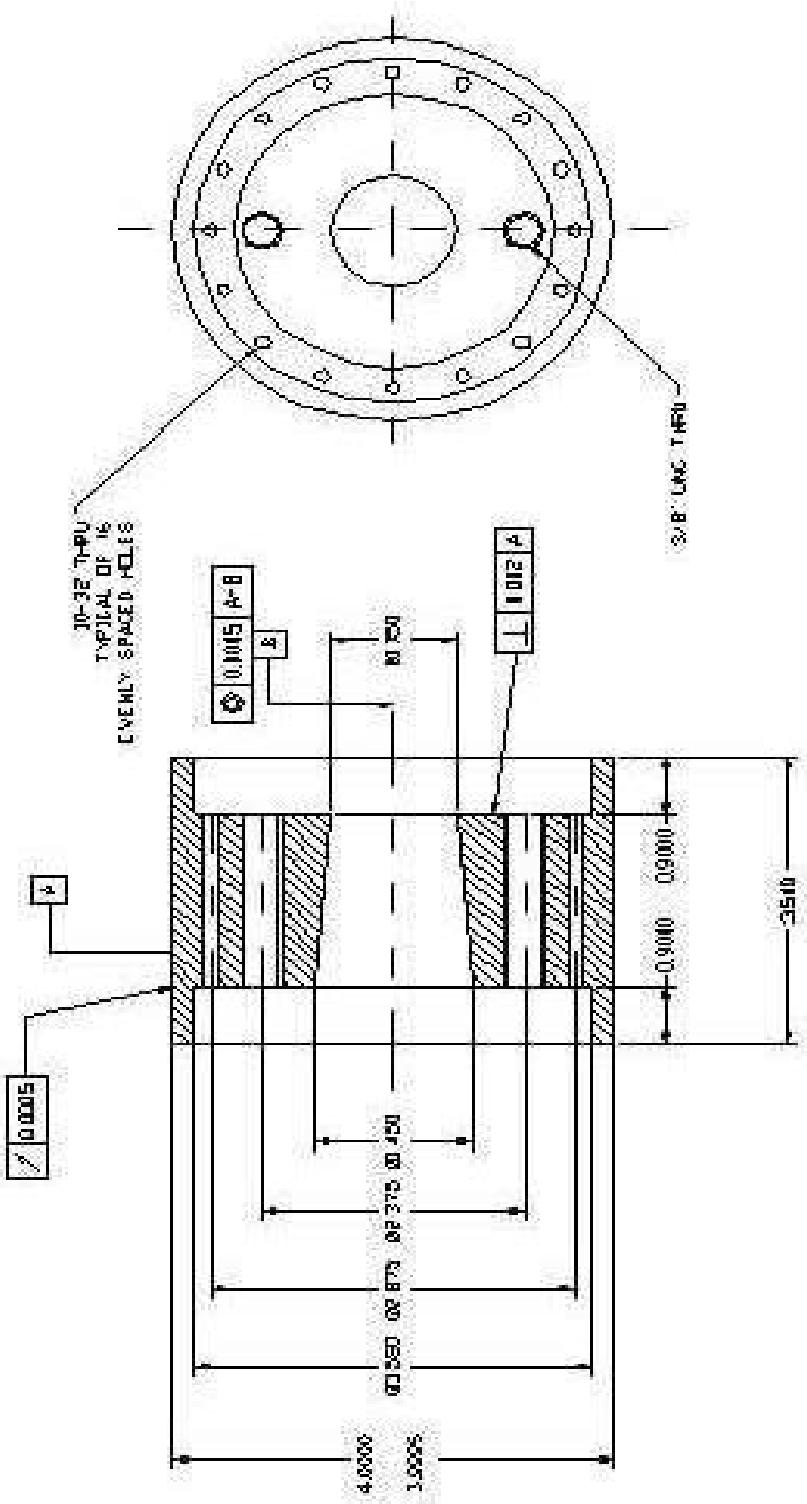

Fig. 18 Drawing of the rotor journal

preliminary machining was undertaken at the Turbomachinery Laboratory and was given to the TEES machine shop for the work on the inside taper. Figure 18 shows the dimensions of the journal.

DESCRIPTION OF THE TEST FACILITY

The air line system

The test rig had two independent air line systems

i. 125 psig (8.618 bar) line from three identical Ingersoll Rand compressors to drive the Pelton wheel type air turbine connected to the rotor.
ii. 300 psig (20.684 bar) line from Atlas Copco compressor for conducting pressurized tests on the PDS.

Both the air line systems were operated through two Masoneilan valves controlled by throttle switches located in the control room. The 300 psig air line was made available to the test rig only recently for this testing thus opening up the possibility of future experiments with damper seals on this rig at higher pressures than previously been possible. Air from this system was supplied to the housing with the help of two ¾ inch (19.05 mm) hoses. The housing has fixtures on its opposite sides to connect the air hoses. A turbine flowmeter (Omega FTB-938) along with a Bourdon type pressure gauge [0-350 psig (20.684 bar)] was connected to this line to monitor the flow parameters while testing. The other air line [125 psig (8.618 bar)], which was primarily used as a drive for the rotor, was directed at the Pelton wheel turbine through nozzles. The rotor was also connected to an electric motor capable of running at a maximum speed of 25,000 rpm through a one way clutch. But all of the testing in this research was carried out using the air line system and thus the services of the motor were not required

Description of the test rig

Figure 19 shows the end view of the test rig. The following gives a brief description of the different components of the test rig:

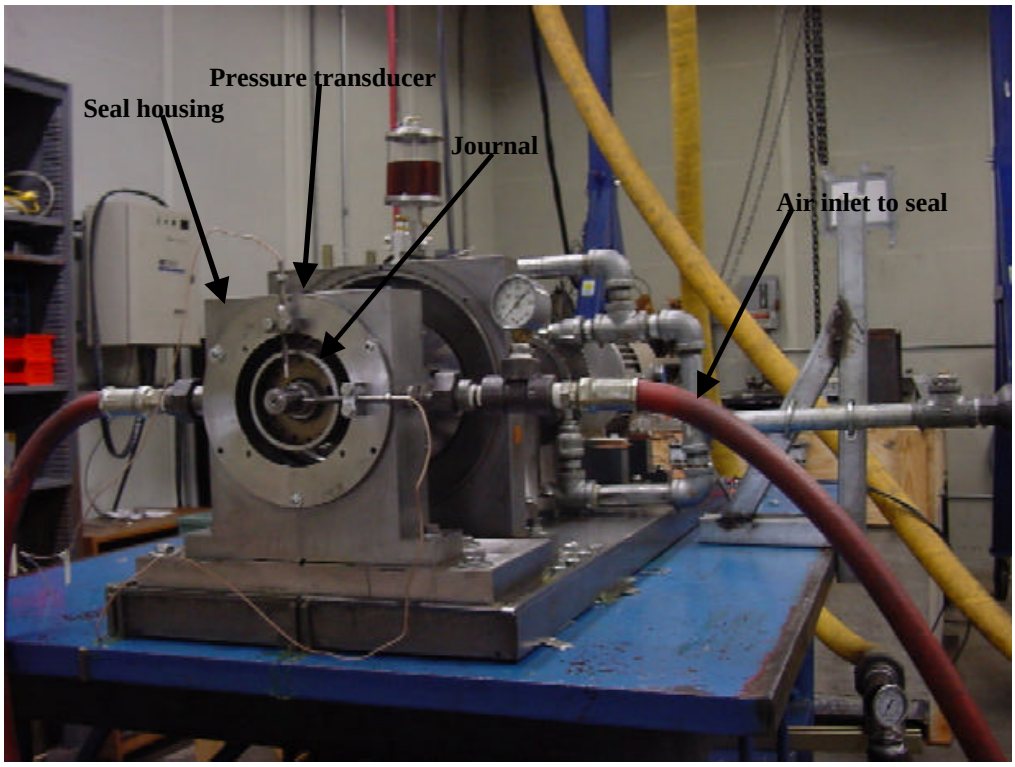

Fig. 19 End view of the PDS test rig

i. The test rig is supported by 1.5 inches (38.1 mm) thick steel plate attached to the structure using four bolts of 0.5 inches (12.7 mm) diameter.

ii. The base plate, also made of steel, 1.8 inches (45.72 mm) thick generates alignment and parallelism of the components.

iii. A Pelton wheel type turbine driven by compressor air is used as the drive for rotor shaft. Four nozzles with a 0.25 inches (6.35 mm) diameter deliver the air to the turbine.

iv. A flexible Thomas coupling is used to prevent vibration due to misalignment of shaft.

v. A self-aligning bearing supports the drive end of the rotor shaft. On the seal journal end, a self-aligning bearing mounted in a squirrel cage supports the rotor shaft. The squirrel cage decreases the radial stiffness of the system and thereby lowers the critical speed of the system.

vi. The rotor consists of a steel shaft with a steel journal (AISI 4140) at the seal end. The journal is connected to the shaft by a tapered union.

vii. The housing is made of steel and supports the seal for testing. The axial movement of the seal and the anti-rotation are taken care by the cover plates bolted on each side of the housing.

viii. Four Bently Nevada proximity probes are installed on the housing to measure relative displacements at the outboard and inboard ends.

ix. Air for tests is supplied through two ¾" hoses located in the direction horizontal to the housing.

x. The housing can be adjusted using shims to center the seal. It could also be moved horizontally or vertically to do the same. 'O' rings are used to seal the airflow through the interface between seal housing and the seal itself.

xi. A keyphasor is attached at the drive end to be used as an input to the "ADRE" data acquisition system.

TEST INSTRUMENTATION

Figure 20 shows a photograph of the instrumentation set up. The four proximity probes attached to the housing were used to determine the rotor displacement and another other probe was used as a keyphasor. An 18 volt D.C power supply is used to power all the proximity probes. The output from all the proximitors were connected to

the DAIU (Data Acquisition Input Unit) which was connected to a computer for display. Also, the signals from the outboard proximity probes were fed into an analog oscilloscope to get the real time position of the shaft centerline. The reason for this is because of the response time of the ADRE system. The real time orbit seen on the oscilloscope must always be used to check the shaft displacement. The rotor displacement as indicated by the ADRE software clearly has a time lag and this output should never be used to judge the real-time shaft position. The seal inlet pressure was measured using a Kulite [0-300 psia (20.684 bar)] strain gauge type pressure transducer. This was mounted on the housing at the central supply plenum flush with the seal insert. The transducer was placed in such a way as not to obstruct the flow in the supply plenum of the seal. Accurate positioning of the pressure transducer is an extremely important as will be evident from further discussions in Chapter VII.

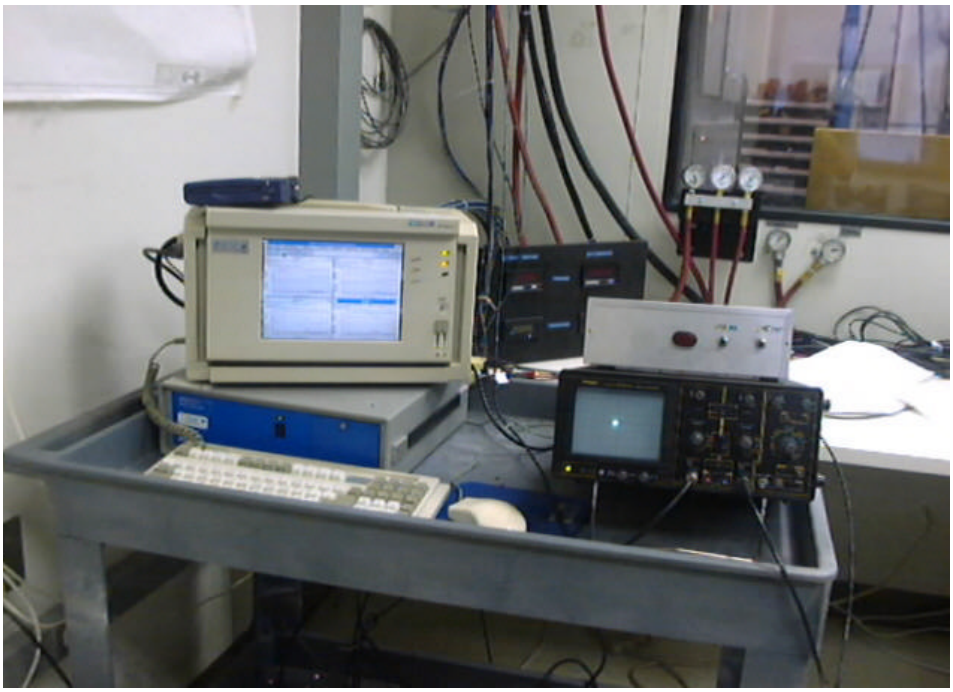

Fig. 20 Instrumentation set up for the coastdown tests

A schematic of the instrumentation set up is shown in Figure 21. “ADRE” for Windows was used to process the data and analyze the results. This software offers a variety of data to be recorded including Bode plots, shaft centerline (orbits), frequency spectra, cascade and waterfall plots. The flow rate through the seal was measured using an Omega turbine meter (FTB 938). The same power supply used for proximity probes was used to power this flowmeter. This flowmeter measured the flow rate in acfm (actual cubic feet per minute) and was connected to the 300 psig (20.684 bar) air line system.

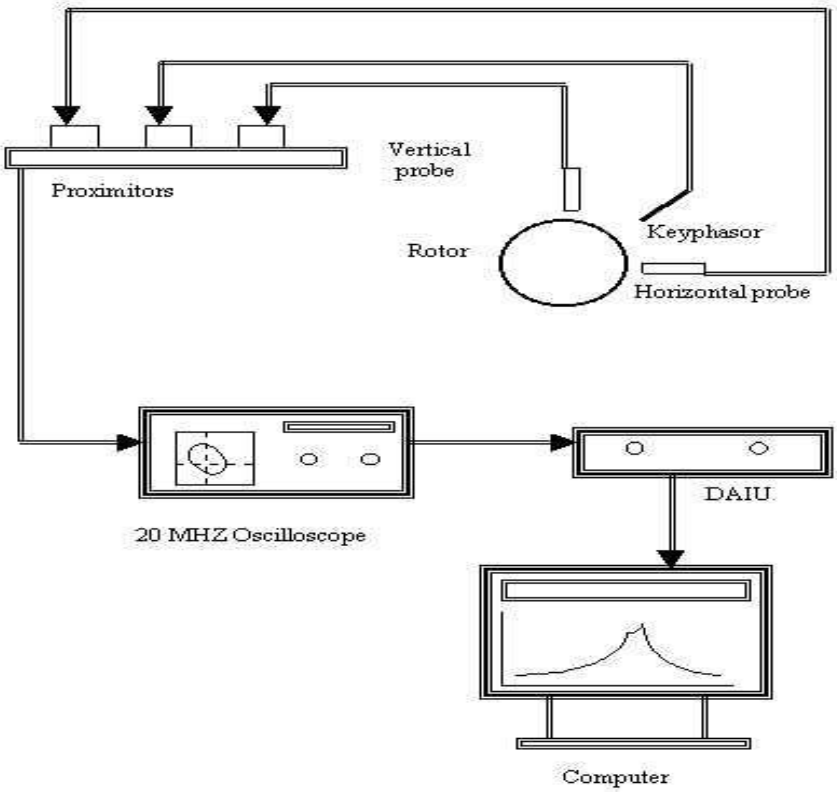

Fig. 21 Schematic of the instrumentation set up

The output (range 0-10 volts) was read from a digital multimeter. A picture of the flowmeter is shown above in Figure 22**.**

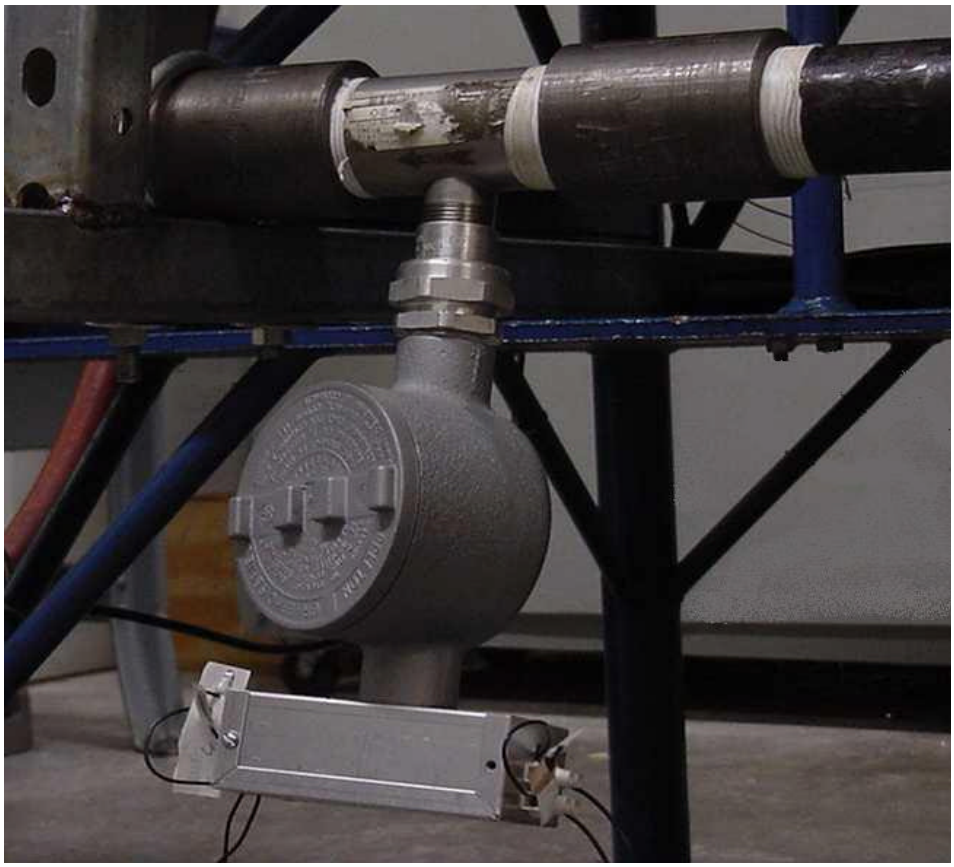

Fig. 22 Photograph of the flowmeter used for measuring leakage rates

TEST METHODOLOGY

Balancing

Keeping in mind a radial clearance of 0.004 inches (0.1016 mm) between the seal and the rotor, it was mandatory to have a vibratory amplitude of less than 0.003 inches (0.0762 mm) 0-p for the baseline testing. A single plane orbit method [15] was used to balance the rotor. The journal attached to the rotor has 16 equi-spaced 10-32 UNF tapped holes to accommodate the balance masses. Several runs were performed to

balance the rotor well enough to assure permissible synchronous response amplitudes at the critical speed. Typical baseline plots are shown in Chapter VI.

Centering the seal

The seal clearances determine how well the PDS performs. Hence it was essential that the seal have uniform clearances and be correctly centered in the housing. The seal was inserted (press fit) into the housing by gently tapping with a rubber mallet. The use of a rubber mallet ensures that the seal is not damaged and also provides a minimal force, so as to avoid any abrasion that might be caused to the seal while pushing it against the rotor. The radial clearance was measured using feeler gauges. Initially the housing bolts are kept loose. After the seal has been inserted all the way into the housing and its clearances taken care, the bolts are tightened. The clearances were once again checked using the feeler gauges to be sure that the seal was centered in both lateral and axial directions. This process sometimes took a lot of time because of the small magnitude of the clearances in this case.

Coastdown tests

The rotor was driven by the Pelton wheel turbine which was controlled by the flow of compressed air from the 125 psig (8.618 bar) pressure air line system. An inlet valve was used to vary the pressure to obtain the required running speed of the rotor. Tests were conducted by allowing the rotor to coastdown from a top speed of 10,000 rpm. This was done by gradually closing the inlet valve (for the Pelton wheel air line) after allowing the rotor to reach its peak speed. The rotor was made to pass through its first critical speed which is close to 5600 rpm (horizontal direction). At all times the real time proximity probe signals connected to the oscilloscope were monitored to estimate the vibratory amplitude. If the orbit size exceeded allowable limits then the rotor was brought to rest by cutting off the air supply. This procedure was extremely important to

avoid any contact between the rotor and the seal. The amplitude response was recorded for each run using the ADRE system. The same steps were followed for various inlet seal pressures ranging from 24.7 psia (1.703 bar) to 64.7 psia (4.46 bar) and the data was recorded.

The mass flow rate was measured from the turbine flowmeter correspondingly for each set of data. An 18 volt D.C supply was used to power the flowmeter. The output terminals of the meter were connected to a digital multimeter (DMM). The output voltage for each of the flow conditions was read out from the DMM. A calibration chart supplied by the manufacturer was used to convert the voltage into actual leakage rate in cubic feet per minute.

CHAPTER V

ROTORDYNAMIC MODEL OF THE PDS TEST RIG

A rotordynamic model of the test rig was developed by Laos [12]. The geometric plot of the model is shown in Figure 23 and the shaft material properties are listed in Table 10. Bearing files are linked at three axial locations to represent the self-aligning bearing (close to the drive end), squirrel cage and the PDS. This model has been developed by specifying the shaft dimensions and then appending the necessary element files. The characteristics of the added elements are shown in Table 11. The input files for the rotor and the bearings used in the XLTRC model are shown in Appendix A.

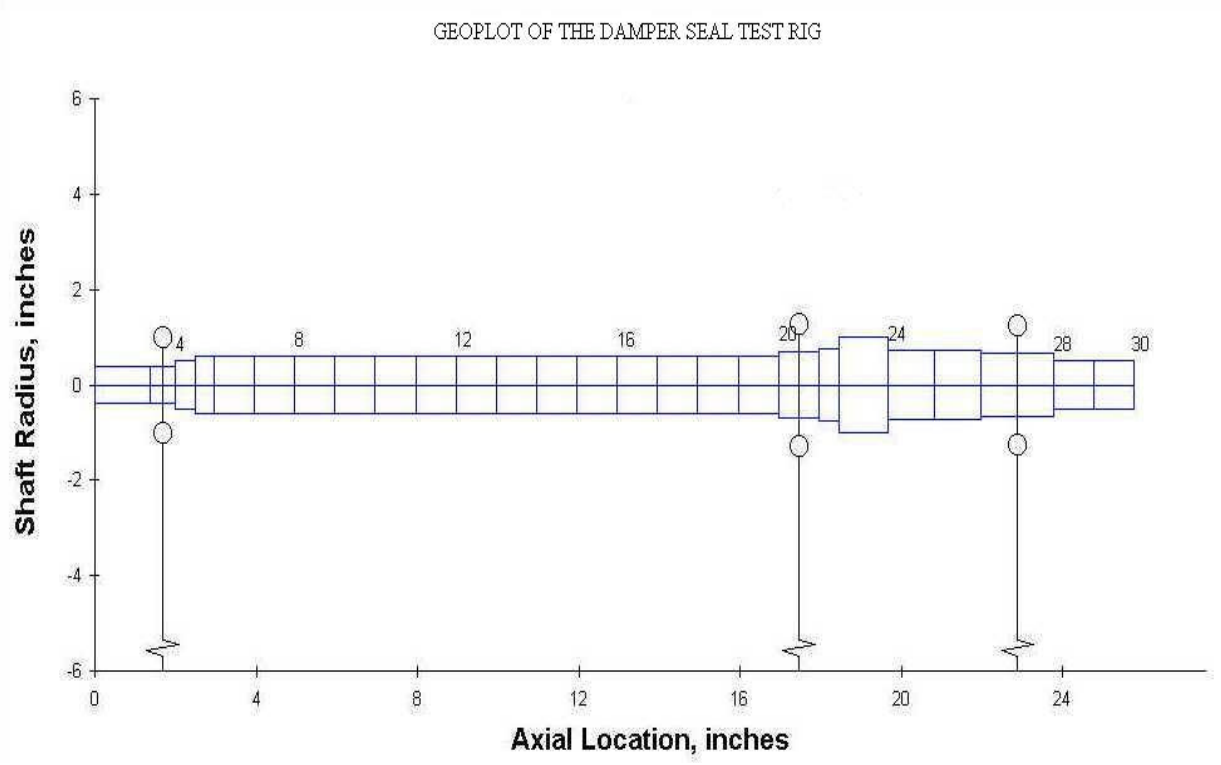

Fig. 23 Geometric plot of the rotor from XLTRC model

Table 10 Shaft material properties

Material	AISI 4140
Weight density - lb/in^3 (kg/m^3)	0.283 (7833.411)
Elastic modulus - psi (N/m^2)	$30 \cdot 10^6$ ($2.068 \cdot 10^{11}$)
Shear modulus - psi (N/m^2)	$12 \cdot 10^6$ ($8.273 \cdot 10^{10}$)

Table 11 Added mass elements

Component	Added weight lb (kg)	Added Ip lb-in^2 (kg-m^2)	Added It lb-in^2 (kg-m^2)
Self-aligning bearing	0.265 (0.120)	0.00	0.00
Squirrel cage	1.966 (0.891)	0.00	0.00
Journal	6.539 (2.966)	16.36 (0.048)	12.551 (0.037)

This model was used to simulate the imbalance response of the rotor and then to compare with the experimental Bode plots. The experimental Bode plots and the imbalance response from the XLTRC model were matched by varying the coefficients of the added elements. The baseline bearing characteristics were calculated by running the imbalance response of the model with PDS coefficients equal to zero. This denoted the system stiffness and damping without the seal. A number of iterations were performed by adjusting the squirrel cage and bearing coefficients to replicate the experimental Bode plot. Once the baseline Bode plot was matched, the direct damping and the stiffness coefficients in the PDS sheet were varied to curve fit the imbalance response at higher pressures. By fine tuning the parameters, it is possible to obtain a curve fit of the Bode plot with a very high correlation coefficient. The cross-coupled forces for the PDS have been shown to be negligible from the experiments conducted in the past. Hence they were not included in the curve fitting procedure and were always kept at zero.

CHAPTER VI

EXPERIMENTAL RESULTS AND DISCUSSION

INITIAL TESTING

Coastdown tests were conducted using the newly manufactured PDS. Before running the rotor the maximum amplitude at the critical speed was verified to be within acceptable limits [less than 0.004 inches (0.1016) 0-p]. The inherent low stiffness of the rotor affected the balancing and thus it was necessary to redo the balancing at least after a day. Typical Bode plots from ADRE after balancing the rotor are shown in Figures 24-25.

Only the horizontal probe (inboard and outboard) signals are shown here. As seen, the maximum amplitude at the critical speed is 2.85 mils (72.39 μm) and 4.61 mils (117.09 μm) p-p at the inboard and the outboard ends respectively. Considering the seal diametral clearance of 0.008 inches (0.203 mm), the rotor can safely pass through the critical speed.

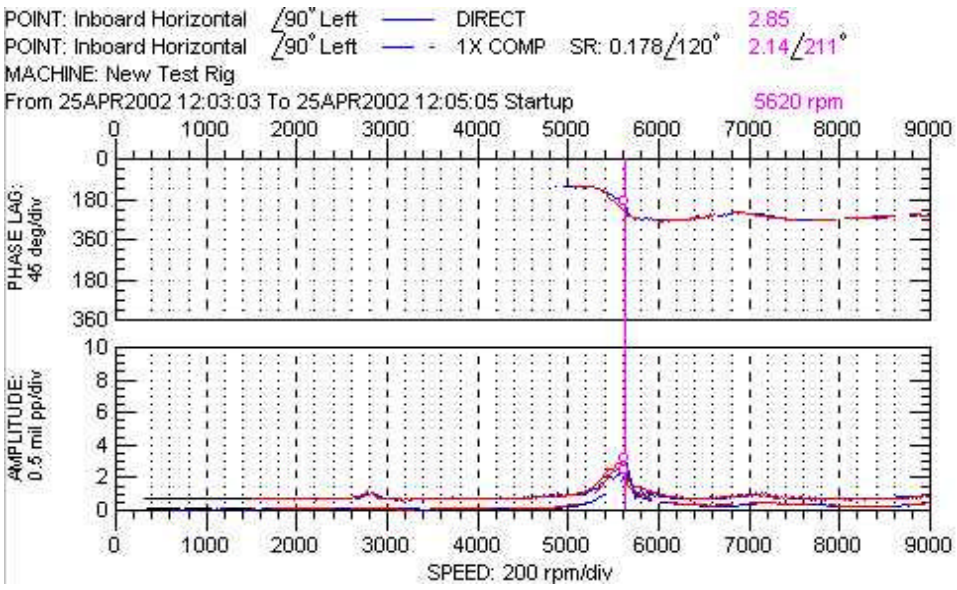

Fig. 24 Bode plots after balancing the rotor (inboard horizontal)

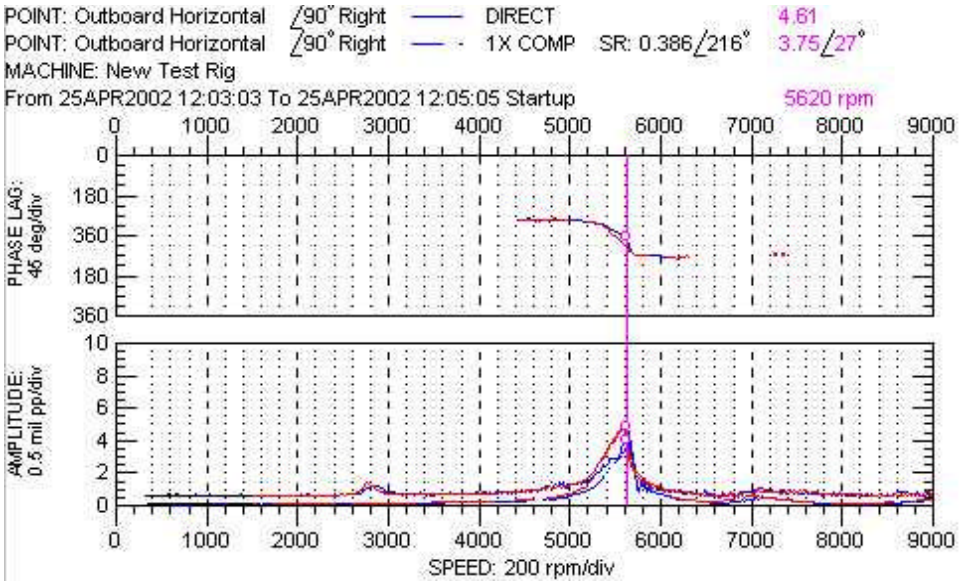

Fig. 25 Bode plots after balancing the rotor (outboard horizontal)

Effect of journal runout

Initial results from coastdown tests for various seal inlet pressures were discouraging. Contrary to the predictions, at the critical speed an increase in amplitude was observed with increase in seal inlet pressures. This is unexpected as the literature suggests that the damping tends to go up with inlet pressure. This situation is evident from the Bode plots in which the response at the critical speed of 5600 rpm seem to be increasing with inlet pressures.

Table 12 Comparison of imbalance response for the journal with runout

Imbalance response – outboard end	Baseline		37.5 psig (2.585 bar)	
	1X Amplitude p-p mils (µm)	Critical speed (rpm)	1X Amplitude p-p mils (µm)	Critical speed (rpm)
Vertical	3.58 (90.93)	5640	5.02 (127.50)	5580
Horizontal	5.22 (132.58)	5600	7.95 (201.93)	5420

The above Table 12 gives a comparison of the maximum amplitude obtained for baseline and at seal inlet pressure of 37.5 psig (2.585 bar). Figures 26-27 show the response from the horizontal and vertical probes at the outboard end. The p-p amplitude for the vertical probe for the baseline case was about 3.58 mils (90.93 μm) at a critical speed of 5640 rpm and increased to 5.02 (127.50 μm) at 5580 rpm for inlet pressure of 37.5 psig (2.585 bar). On the other hand, the horizontal probe indicated a p-p amplitude of 5.22 mils (132.58 μm) at 5420 rpm and increased to 7.95 mils (201.93 μm) at a critical of 5600 rpm at inlet pressure 37.5 psig (2.585 bar).

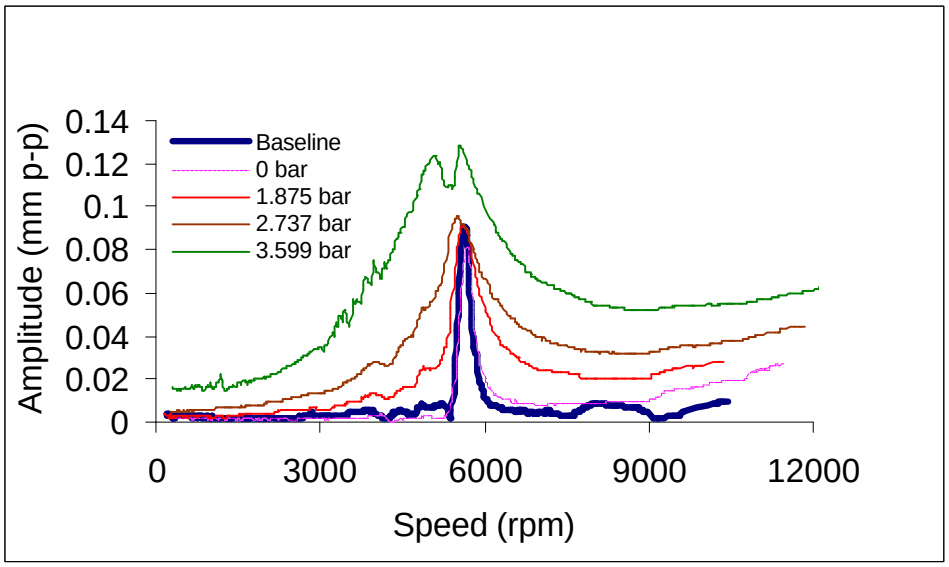

Fig. 26 Unbalance response from the outboard vertical probe, journal with runout

Investigations revealed that the journal had a runout of more than 10 mils (diametral). Analysis by Vance [16] shows that the seal journal runout can have a significant effect on synchronous vibration response, independent of the well known probe surface runout which can be subtracted from the Bode plots. The results obtained above are therefore not a true representation of the seal rotordynamic coefficients. Hence a replacement journal had to be manufactured to obtain good results. The runout on the new journal

was found to be 0.8 mils diametral, which is reasonable considering the current test conditions.

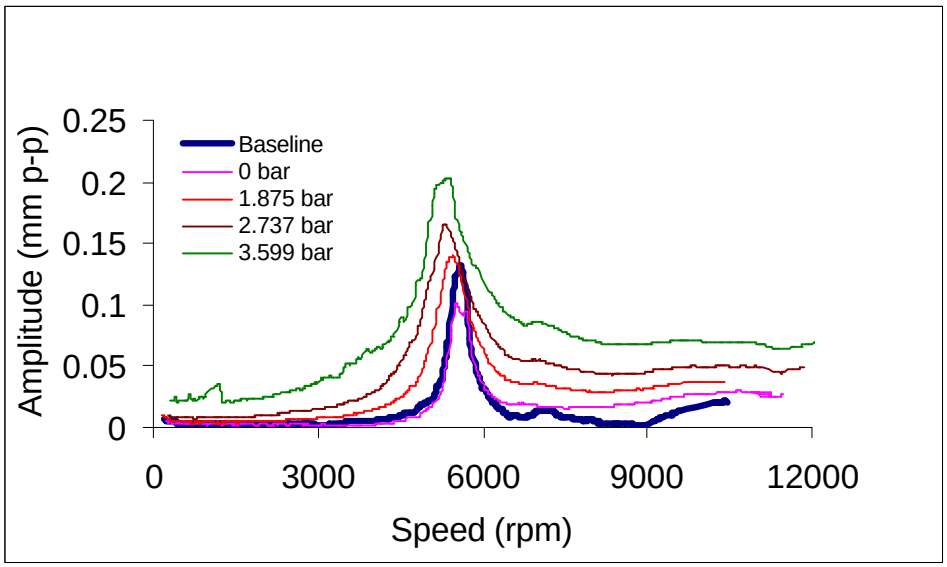

Fig. 27 Bode plot from the outboard horizontal probe, journal with runout

TEST RESULTS WITH THE NEW JOURNAL

Figures 28-39 represent the coastdown curves from the rotating tests conducted with low runout. The Bode plots are obtained through the outboard end transducers at the vertical and horizontal directions. The amplitudes shown are 1x component in the ordinates (after subtracting the runout) with running speed in the abscissa coordinates. This data was exported to Microsoft Excel to perform analysis and for conversion into easily readable forms.

It can be seen that the PDS offers good damping with increasing seal inlet pressures. The peak to peak amplitude in the vertical direction at the baseline is 2.22 mils (56.38 μm) and is subsequently reduced to less than 0.5 mils (12.7 μm) at 54.7 psia (3.771 bar). The results confirm that the PDS provide high positive damping to suppress rotor vibration. The amplitude of unbalance response (both vertical and horizontal)

decreased with increase in inlet seal pressure. It is also evident that the critical speed is reduced due to the negative stiffness of the PDS. The baseline response is also shown along with the individual plots to provide a better comparison.

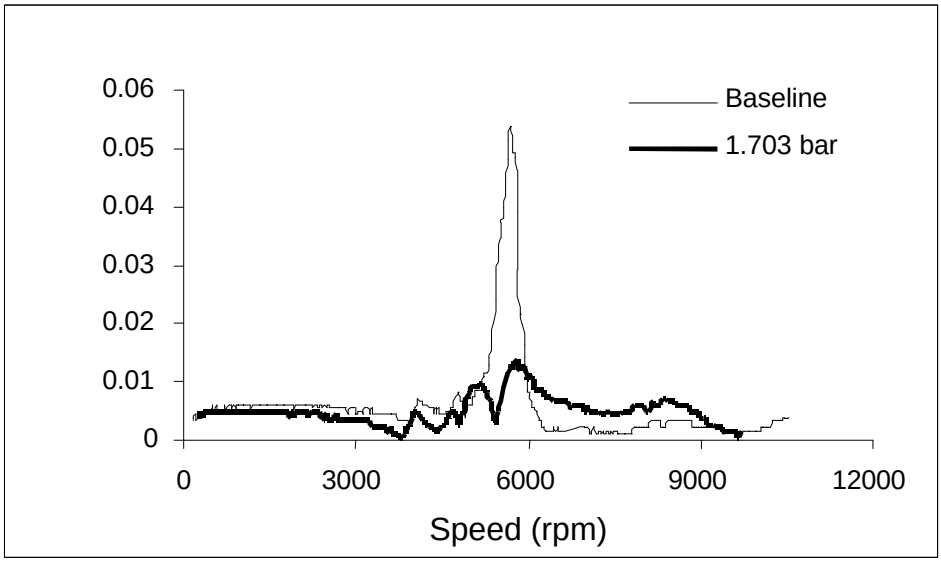

Fig. 28 Measured unbalance response in the vertical direction at the outboard end for an inlet pressure of 24.7 psia (1.703 bar)

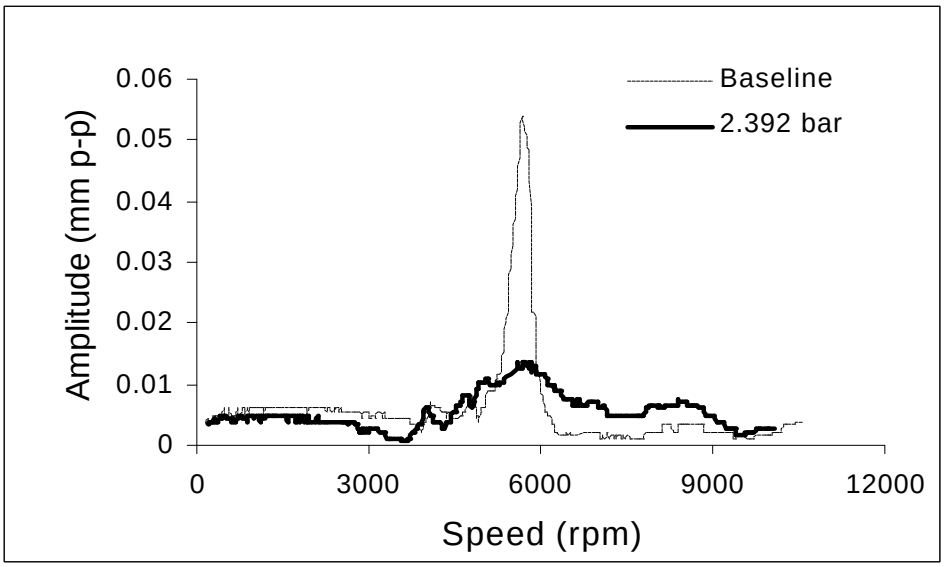

Fig. 29 Measured unbalance response in the vertical direction at the outboard end for an inlet pressure of 34.7 psia (2.392 bar)

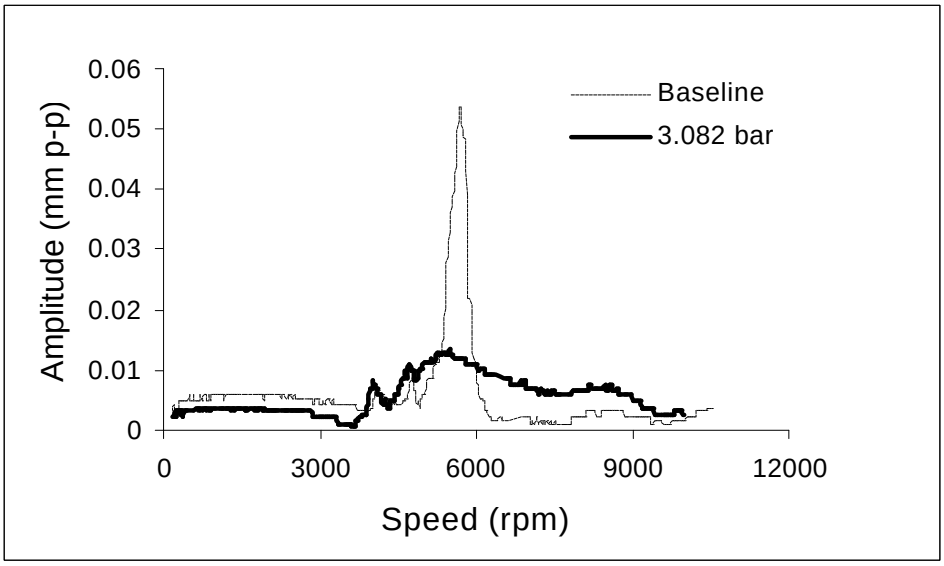

Fig. 30 Measured unbalance response in the vertical direction at the outboard end for an inlet pressure of 44.7 psia (3.082 bar)

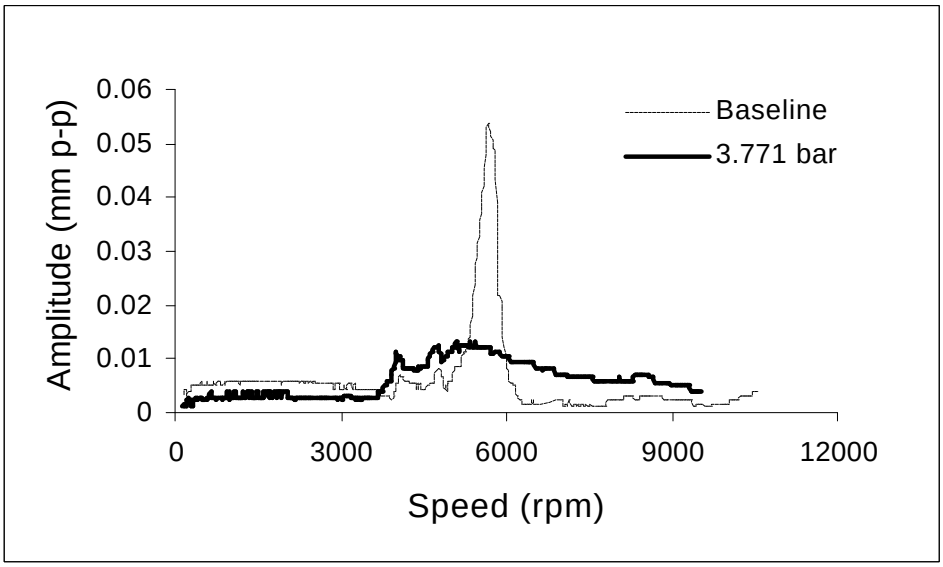

Fig. 31 Measured unbalance response in the vertical direction at the outboard end for an inlet pressure of 54.7 psia (3.771 bar)

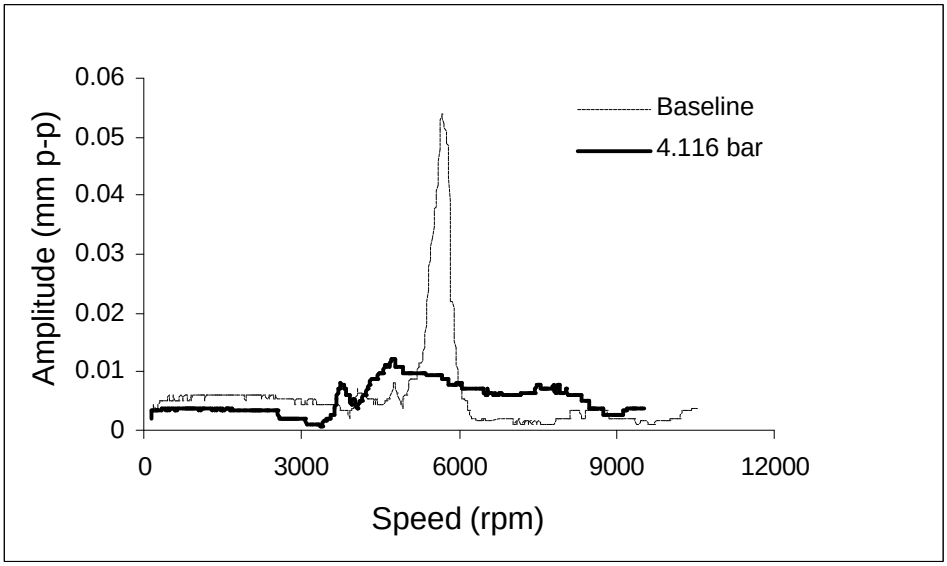

Fig. 32 Measured unbalance response in the vertical direction at the outboard end for an inlet pressure of 59.7 psia (4.116 bar)

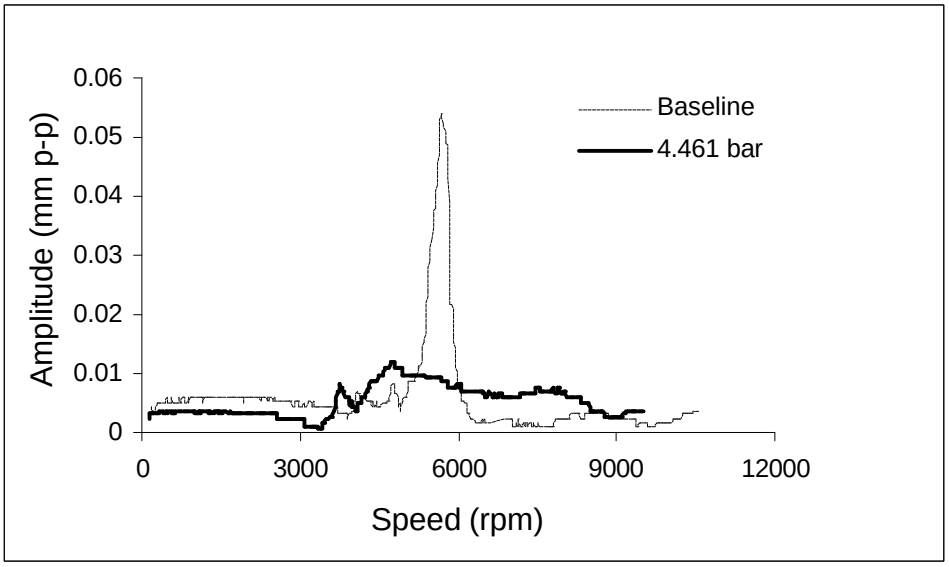

Fig. 33 Measured unbalance response in the vertical direction at the outboard end for an inlet pressure of 64.7 psia (4.461 bar)

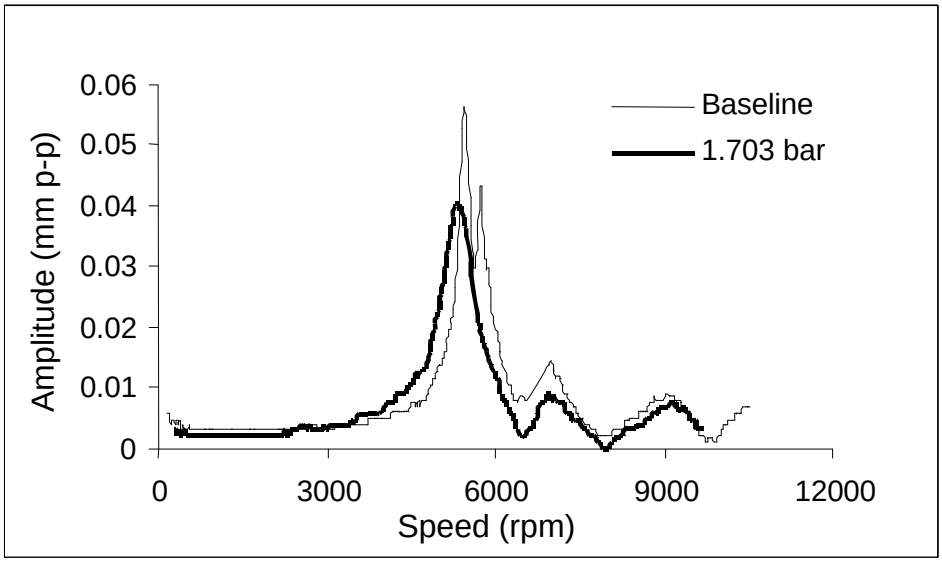

Fig. 34 Measured unbalance response in the horizontal direction at the outboard end for an inlet pressure of 24.7 psia (1.703 bar)

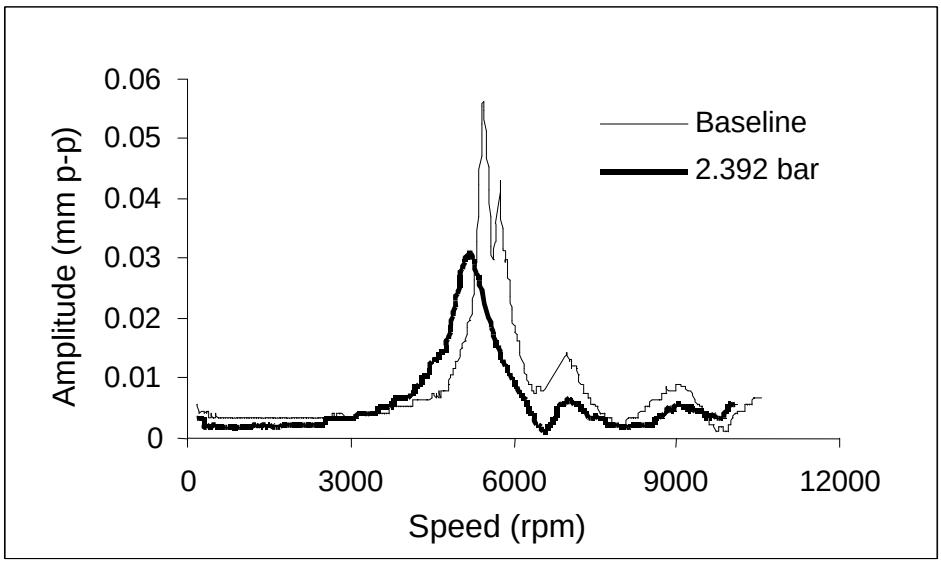

Fig. 35 Measured unbalance response in the horizontal direction at the outboard end for an inlet pressure of 34.7 psia (2.392 bar)

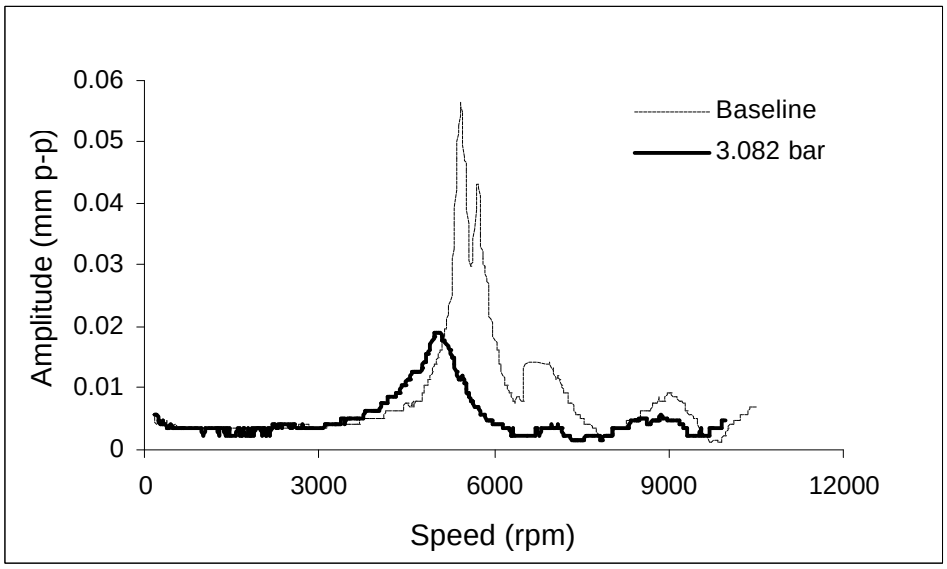

Fig. 36 Measured unbalance response in the horizontal direction at the outboard end for an inlet pressure of 44.7 psia (3.082 bar)

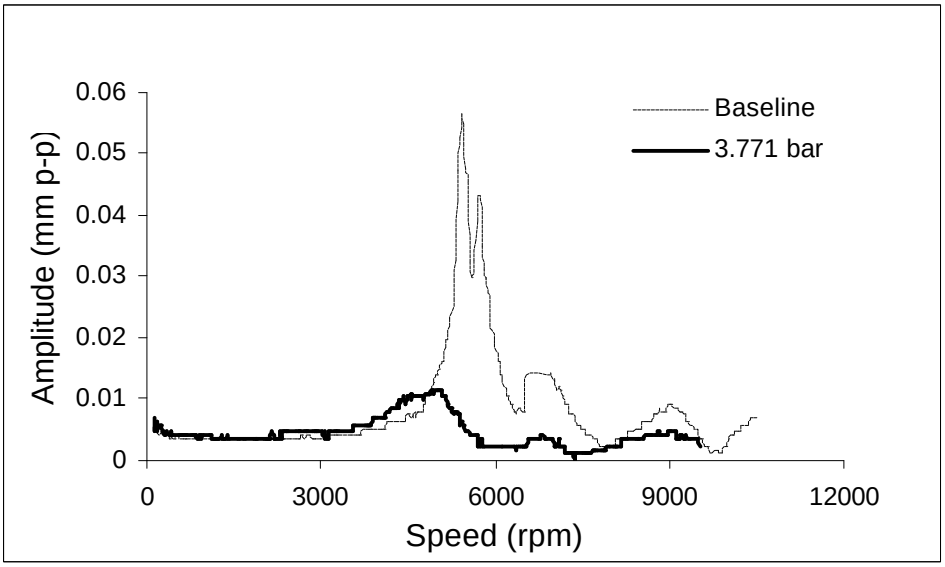

Fig. 37 Measured unbalance response in the horizontal direction at the outboard end for an inlet pressure of 54.7 psia (3.771 bar)

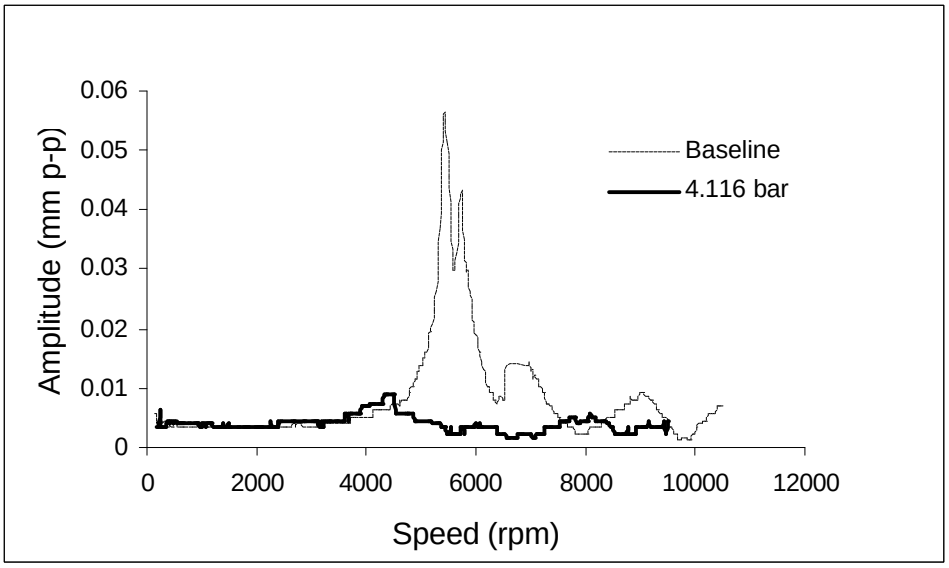

Fig. 38 Measured unbalance response in the horizontal direction at the outboard end for an inlet pressure of 59.7 psia (4.116 bar)

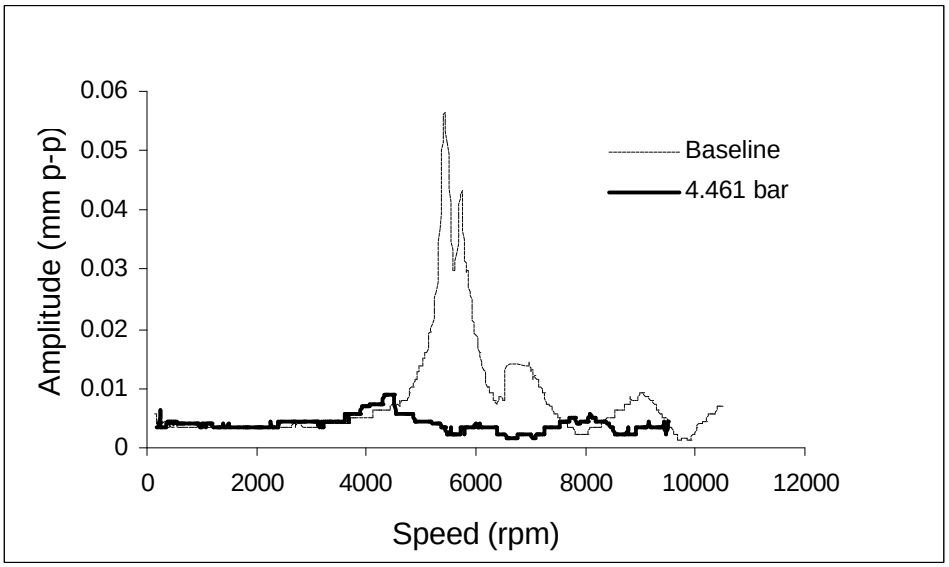

Fig. 39 Measured unbalance response in the horizontal direction at the outboard end for an inlet pressure of 64.7 psia (4.461 bar)

As seen from the above plots it is clear that the PDS is effective in suppressing synchronous response for seal inlet pressures up to 64.7 psia (4.461 bar). The baseline response in the horizontal direction was 2.22 mils (56.38 μm) p-p compared to 0.318 mils (8.07 μm) p-p at an inlet pressure of 64.7 psia (4.461 bar). Similarly the vertical response was suppressed from 2.12 mils (53.84 μm) p-p to 0.472 mils (11.98 μm) at 64.7 psia (4.461 bar). However, the PDS also produces negative stiffness. Tests could not be conducted above 64.7 psia (4.461 bar) because of the fact that the weak stiffness of the rotor caused the rotor journal to move towards the seal wall. The usual procedure in all these pressurized tests was to keep the rotor at rest and then supply air at desired pressures. As soon as the seal was pressurized to the pressure range 65 psia (4.481 bar) to 70 psia (4.4826 bar) the journal was seen to move towards the seal wall. This was confirmed in the oscilloscope where the shaft centerline was observed to move in the horizontal direction.

Further, to confirm that this movement of the seal was not because of the improper centering of the seal, numerous trials were conducted by placing the seal in

different angular positions (i.e., the seal was rotated by certain angles). In each case the rotor (at rest) started to move towards the seal at pressures around 65 psia (4.481 bar) to 70 psia (4.4826 bar), although the motion was not necessarily in the same direction. Figure 40 shows the various angular positions of the seal.

The rotor was observed to move in all the cases. The only possible cause for this effect is that the stiffness of the rotor is insufficient to overcome the negative stiffness of the seal. The stiffness of the rotor was measured and was found to be 3778 lb/in (661.603 KN/m), which is close to what the PDS produces at 64.7 psia (4.461 bar) but with a negative sign. Yet another possible cause of the behavior was explored wherein the seal was centered with the pressurized air flowing through the seal. The housing was kept loose and a rubber mallet was used to lightly tap the housing to adjust the centering of the seal. This option turned out to be extremely laborious and the flow of air through the seal made it all the more difficult to work towards centering the seal. After much struggle the seal was brought into a centered position. It can argued that the seal might not be at the geometric center of the rotor but by the judgement of clearances the seal is considered to be in the center with respect to the rotor which was deflected due to the air flow.

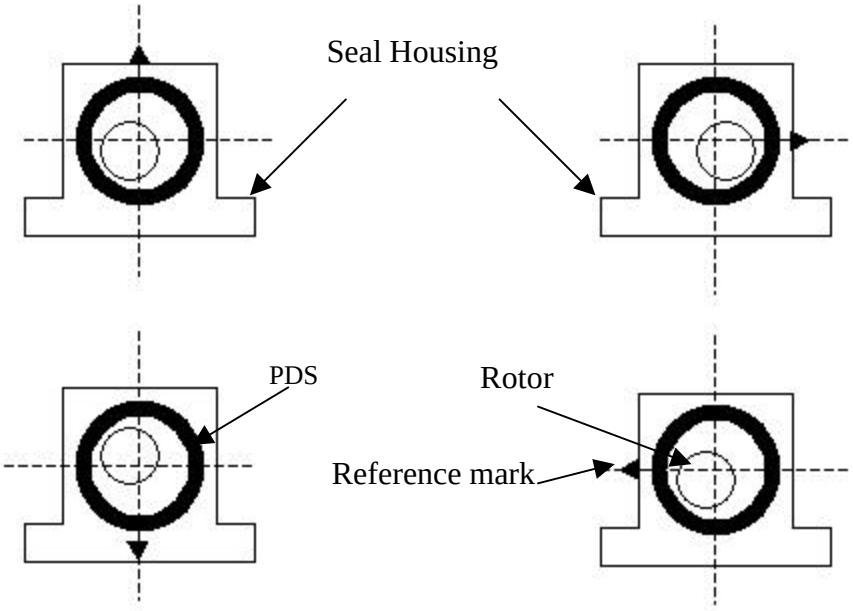

Fig. 40 Different angular positions of the PDS to check for offcentering

After carefully checking the clearances using the feeler gauges the rotor was again subjected to a coastdown test. However, during acceleration of the rotor, the oscilloscope and the ADRE plot confirmed that the response at speeds close to critical increased to values beyond limits that were considered detrimental to the seal. The rotor was thus immediately brought to rest and checked for any damage to the seal. The Bode plots for this case is shown below in Figures 41-42.

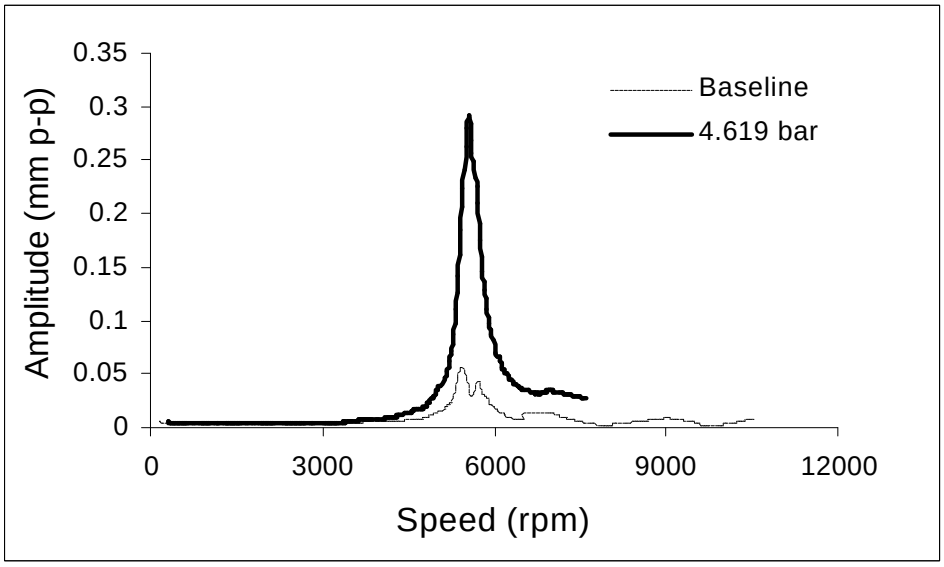

Fig. 41 Measured unbalance response in the horizontal direction at the outboard end for an inlet pressure of 67 psia (4.619 bar)

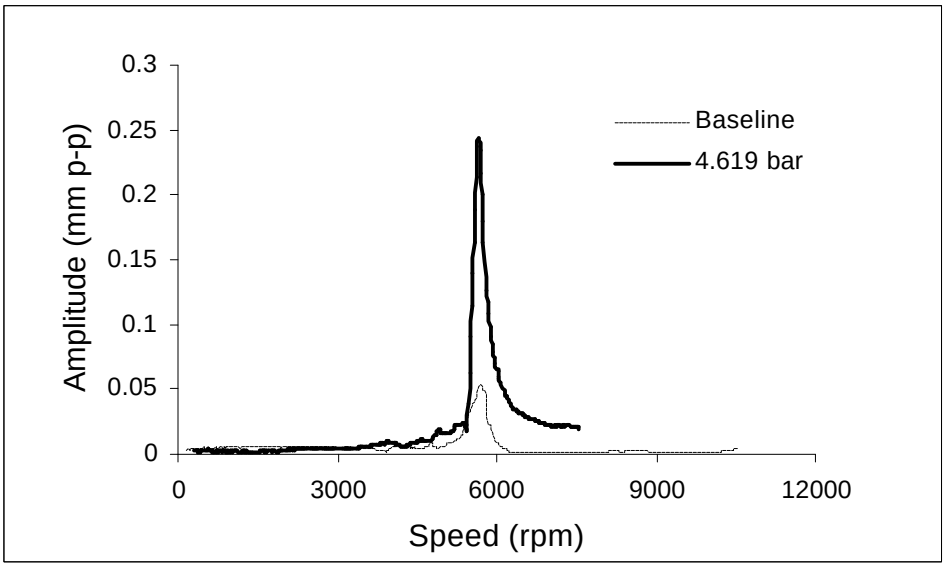

Fig. 42 Measured unbalance response in the vertical direction at the outboard end for an inlet pressure of 67 psia (4.619 bar)

Observations indicated that the rotor had rubbed with the seal. Fortunately, not much damage was done to the seal. Further inspection of the journal revealed scratches indicating contact between the PDS and the journal. Subsequent to these events, testing was restricted to inlet pressures less than 64.7 psia (4.461 bar).

EXTRACTION OF ROTORDYNAMIC COEFFICIENTS FROM EXPERIMENTAL BODE PLOTS

As explained earlier, data from the coastdown tests were analyzed using Excel™. The unbalance responses from the rotordynamic model were compared with the Bode plots obtained from the testing. The idea was to match the response of the model and the experimental plot and then obtain the coefficients (stiffness and damping) that produce the curve fit. A number of iterations were performed to obtain consistent values for the coefficients. It is possible to get more than one set of parameters which typically satisfy the experimental plots. However consistency is also checked while coming up with a set of coefficients. This approach helps to keep track of the values that are obtained and to ensure that they remain in the range in which they are expected to be.

Table 13 summarizes the direct stiffness and damping coefficients obtained from the testing. Figures 43-44 show the variation of these coefficients with inlet pressures.

Table 13 Direct damping and stiffness coefficients from coastdown tests

Seal inlet pressure		Horizontal direction			
(psia)	bar	Direct stiffness		Direct damping	
		lb/in	N/m	lb-s/in	N-s/m
24.7	1.703	-572.025	-100173	0.4125	72.237
34.7	2.392	-842.562	-147549	0.9865	172.755
44.7	3.081	-1328.64	-232671	1.364	236.863

54.7	3.771	-1512.25	-264825	2.8956	507.077
59.7	4.116	-1785.33	-312646	3.325	582.274
64.7	4.461	-1873.02	-328003	3.789	663.529
Seal inlet pressure		Vertical direction			
(psia)	bar	Direct stiffness		Direct damping	
		lb/in	N/m	lb-s/in	N-s/m
24.7	1.703	-512.356	-89723.8	0.3265	57.176
34.7	2.392	-982.289	-172018	0.8856	155.086
44.7	3.081	-1198.52	-209885	1.564	273.887
54.7	3.771	-1565.51	-274152	2.7715	485.345
59.7	4.116	-1878.95	-329042	3.365	589.278
64.7	4.461	-1956.41	-342607	3.877	678.940

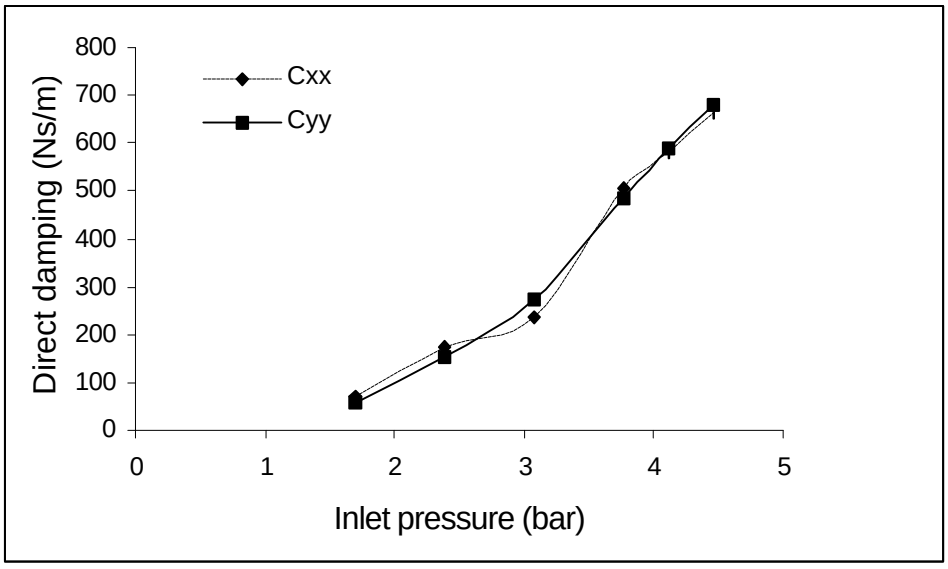

Fig. 43 Direct damping in horizontal and vertical directions from the rotating tests

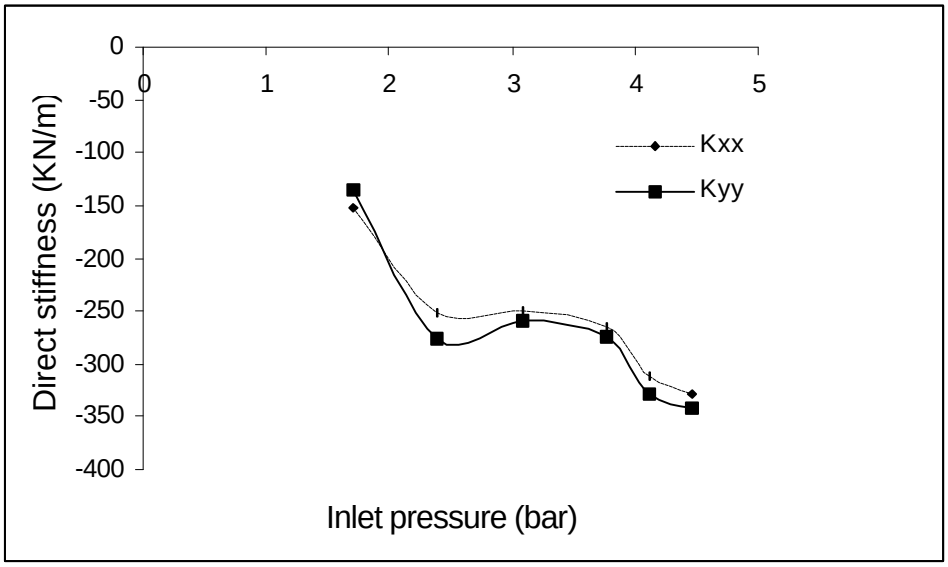

Fig. 44 Direct stiffness in horizontal and vertical directions from the rotating tests

As seen, the magnitudes of both the direct damping and stiffness coefficients increase with inlet seal pressure. The difference in the values in the horizontal and vertical directions can probably be attributed to unequal notch areas. Also, even though efforts are taken to ensure the proper centering of the seal, some offcentering is always prone to happen. Unequal clearances around the journal can cause the coefficients to be different in the orthogonal directions. This effect will be more pronounced for higher seal inlet pressures. More than one iteration was performed using the XLTRC model to come up with a consistent set of rotordynamic coefficients.

MEASUREMENTS OF MASS FLOW ACROSS THE SEAL

The leakage rate or the mass flow rate was measured using the FTB-938 turbine meter. Accuracy of the data from the flow meter was ensured by installing it in the straight portion [pipe of constant of diameter 1.5 inches (38.1 mm)] of the air line system as suggested by the manufacturer. The flow would then be laminar across the turbine meter. The output voltage for each case of inlet pressure was read out using a DMM.

This value was for two seals and later converted to actual flow in cubic feet per minute (acfm) using the calibration chart. The mass flow rates were measured with the air set at the desired pressure before conducting the coastdown test. Table 14 shows the mass flow rates obtained for the various seal inlet pressures. Figure 45 shows the mass flow rates obtained and indicates a steady rise with seal inlet pressure.

Table 14 Mass flow data from leakage tests

Seal inlet pressure psia (bar)	Mass flow	
	lb/min	kg/min
24.7 (1.703)	1.07796	0.488812
34.7 (2.392)	1.68876	0.765785
44.7 (3.081)	2.2575	1.023686
54.7 (3.771)	2.81082	1.274594
59.7 (4.116)	3.08442	1.398661
64.7 (4.461)	3.27144	1.483467

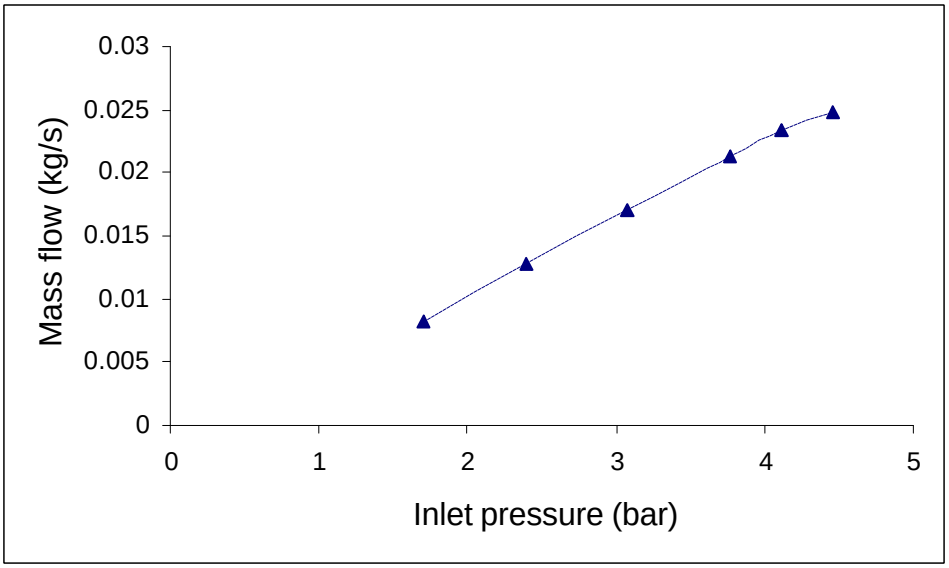

Fig. 45 Mass flow from the leakage tests

ERROR ESTIMATION IN MACHINING OF THE SEMI-CIRCULAR NOTCH

The semi-circular notch in the exit blades was machined using a three-axis machine. An end mill cutter of certain radius (depending on the seal inner diameter) was used for machining the notch. In the process of machining, the seal was fixed firmly on the machine bed and the cutting tool was moved in the radial direction by a specified amount to scrape off material from the seal surface. Figure 46 gives a snapshot of the machining process of the notch.

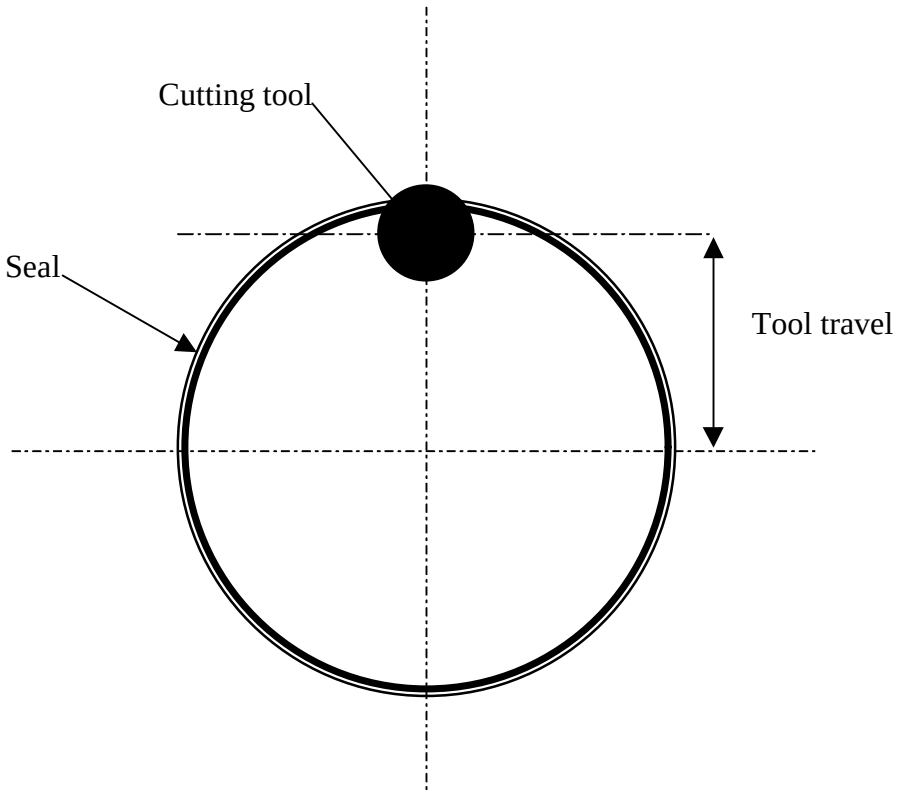

Fig. 46 Machining of the notch

The results from the running tests prompted the investigation of the notch geometry. It could be possible that the notch dimensions are erroneous and that the notch areas are not symmetrical. If this is the case then the PDS will have unequal pressure

distribution when the seal is pressurized which might cause the rotor to move towards the seal wall.

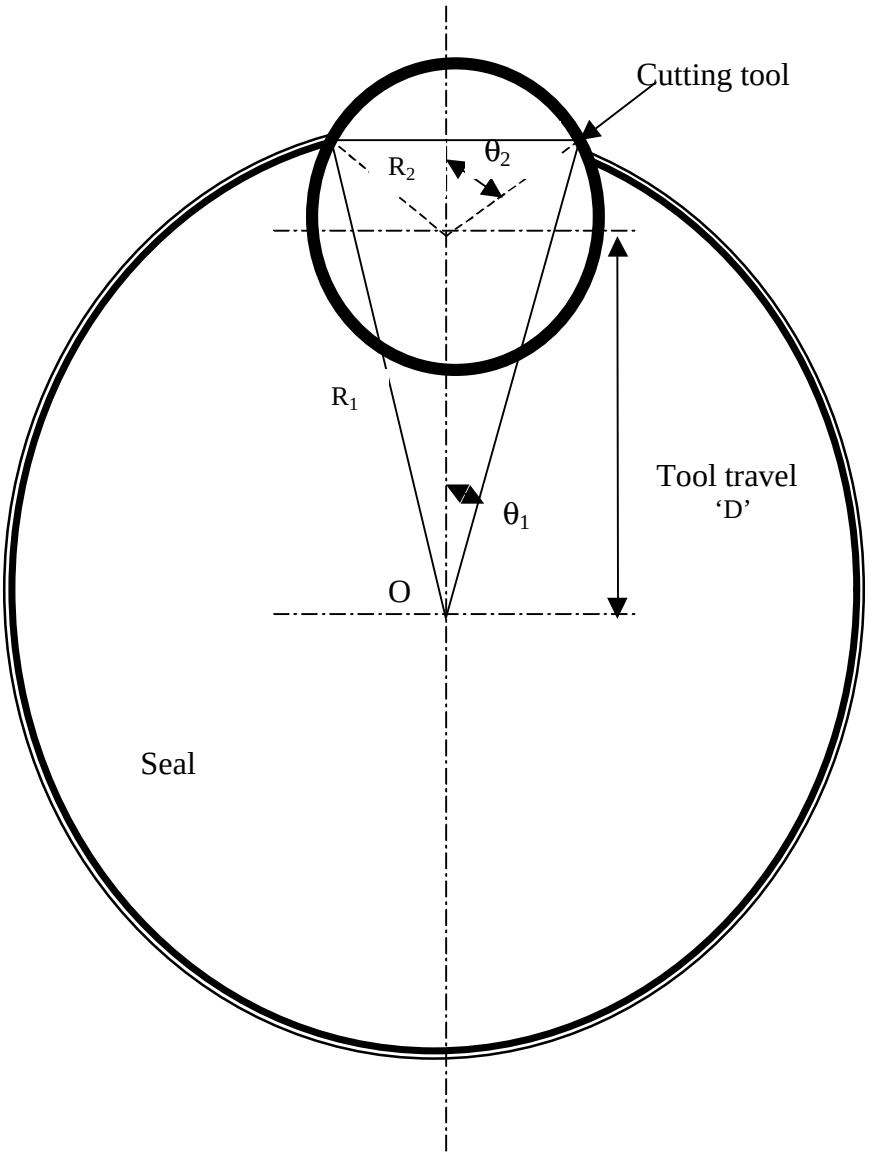

Fig. 47 Relation between tool travel and notch area

where;

R_1 Seal inner radius

R_2 Cutting tool radius

D Tool travel from the center of the seal

q_1 and q_2 are angles as shown in the figure (in degrees)

Consider Figure 47 in which the seal inner diameter and the cutting tool have been exaggerated. From simple trigonometry we have the following relation between the above parameters:

$$Notch\ \ area = \ R_2^2\, q_2 - R_1^2\, q_1 + \left(R_2\, \sin q_2\right) D \ldots\ldots\ldots\ldots\ldots\ldots\ldots\ldots\ldots\ldots\ldots\ldots(48)$$

The notch area is equal to the inlet clearance area. Using the above equation, the change in area for minute variations in the tool travel can be calculated. The radius of the cutting tool used in machining the notches on the current PDS was 0.25 inches (6.35 mm).

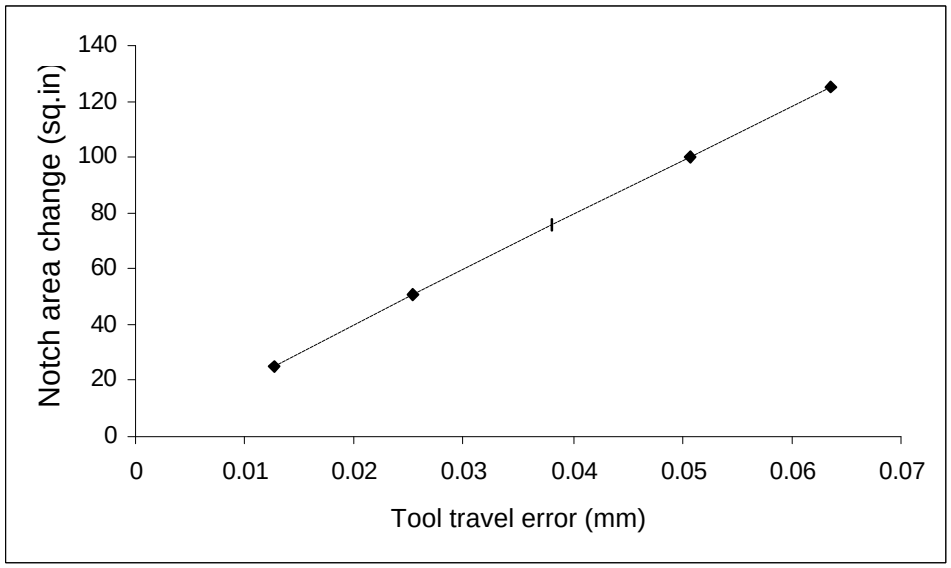

Fig. 48 Tool travel error vs change in notch area

The above Figure 48 clearly shows that even for a small error of 0.0005 inches (0.0127 mm) in the tool travel, the change in the area of the notch is enormous. In this case the area of the notch changes by approximately 25% if the tool's position is inaccurate by 0.0005 inches (0.0127 mm). This can have disastrous consequence when it comes to the proper working of the PDS. If the cutting tool's position changes by 0.001 inches (0.0254 mm) then the area of the notch becomes one and half times the required area. The area of the rectangular notch of small width used by Laos [12] is much less sensitive to the depth of cut.

CHAPTER VII

THEORY VS PREDICTIONS

COMPARISONS FOR THE FOUR BLADED PDS

Experimental results from Chapter VI will be compared with the theoretical predictions in this Chapter. The notched PDS Code 2 described in Chapter II will be used for predicting the direct stiffness and damping coefficients. Also, predictions from the other existing model (Vance – Code 1) will be compared with the test data. Both these codes use the same flow equations and methodology for obtaining the rotordynamic coefficients but the flow through the notch is considered separately in the new model. The coefficients obtained from the XLTRC model are for two seals. Hence they have to be divided by two to get the corresponding values for a single seal. Typical input sheets for Code 1 and Code 2 are shown in Figures 49 and 50 respectively.

TAMSEAL- Input and Output for One Data Point of Damping and Leakage			
Job title (in cell C2):	4" D x 1" L TAMSEAL, 40 psi		
			Input only the red font
INPUT		UNITS	DESCRIPTION
Vibe_freq	5600	cpm	VIBRATION OR WHIRL FREQUENCY (CPM)
Npair	2	none	NUMBER OF PAIRS OF LABYRINTH TEETH
Pres_hi	54.7	psia	UPSTREAM PRESSURE OF SEAL
Pres_lo	14.7	psia	DOWNSTREAM PRESSURE OF SEAL
CR_inlet	0.004	inches	INLET RADIAL CLEARANCE TO A SEAL POCKET
CR_exit	0.008	inches	EXIT RADIAL CLEARANCE TO A POCKET
Seal_lengt	1.056	inches	SEAL LENGTH (axial)
Dia_inner	4	inches	INNER DIAMETER FOR SEAL (shaft diameter)
Depth	0.40	inches	DEPTH OF SEAL POCKET
Wallthick	0.25	inches	THICKNESS OF SEPARATION WALLS
Bladethick	0.075	inches	THICKNESS OF THE LABY TEETH
PR_print	1	none	PRINTS PRESSURE RATIOS IF NOT =0
Mole_wt	29	none	29 FOR AIR, 16 FOR METHANE
Gamma	1.4	none	RATIO OF SPECIFIC HEAT, 1.4 FOR AIR, 1.3 FOR METHANE
Temprtr	80	deg F	TEMPERATURE OF GAS IN FAHRENHEIT

Fig. 49 Input sheet for Code1

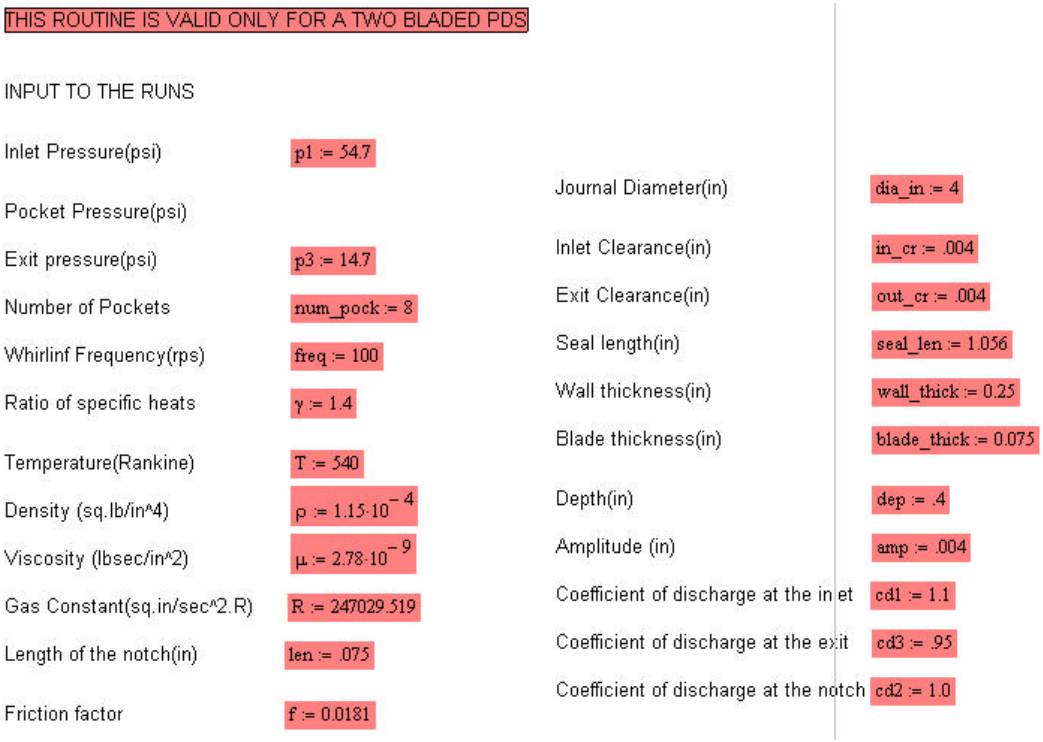

Fig. 50 Input sheet for Code2

Both the codes predict a single stiffness and damping coefficient (i.e, Kxx = Kyy and Cxx = Cyy) and do not predict any cross-coupled force coefficients. Predictions are obtained for the range of seal inlet pressures tested. The theoretical models neglect the circumferential flow in the PDS and consider the cross-coupled forces to be very minimal (Experiments by Li [9] have been conducted to justify these assumptions). Here again, the basic idea of comparing the experimental results with theoretical predictions is to support and justify the notched theoretical models.

The inlet and exit clearances are entered directly in Code 1 without giving any special emphasis on the notched portion of the exit blade. In other words, a notched PDS with a 1:2 clearance ratio (the notch is responsible for the increased clearance at the exit) is simply considered as a PDS having different blade clearances at the exit and inlet end. Recall that in a notched PDS, the blade clearances are same at the inlet and at the exit end. The provision of notches in the downstream blade of the damper cavity accounts for

the diverging clearance in the exit blades. Code 2 calculates the notch dimensions assuming an exit to inlet clearance ratio of 2:1. The PDS tested in the current research has semi-circular notches cut across the exit blades as described earlier. The actual PDS dimensions are used as inputs to the two models and the direct force coefficients are predicted for the tested inlet pressure range, from 24.7 psia (1.703 bar) to 64.7 psia (4.461 bar). In both the codes the flow condition at the last blade is checked for choking.

Figures 51-54 show the comparison curves for the inlet pressure range tested. From the damping comparison curves, it is seen that Code 1 mostly underpredicts (except at lower pressures) the damping coefficients in the horizontal direction with a deviation of 3% to 40%, depending on the inlet pressure. Code 2 also underpredicts the damping values but with a deviation range of 6% to 23%. However, the predicted damping coefficients at higher pressures agree well with the experimental values. It is seen that Code 2 gives a good prediction of the damping coefficients better than Code 1 in most cases. As the seal inlet pressure increases to about 64.7 psia (4.461 bar), both the codes tend to diverge from the experimental values. Both the codes show an increase in damping values as seal inlet pressure increases. This prediction is consistent with the experimental results which also show a trend of increasing damping coefficients with seal inlet pressures.

Experimental results and predictions both show the negative stiffness of PDS increasing in magnitude with an increase in seal inlet pressures. Codes 1 and 2 predict much higher magnitudes of stiffness coefficients than the values obtained from tests. The stiffness values of test data and predictions are in agreement at lower pressures but deviate considerably for higher pressures. The trend observed for both predictions and experimental results is the same for increase in the seal inlet pressure.

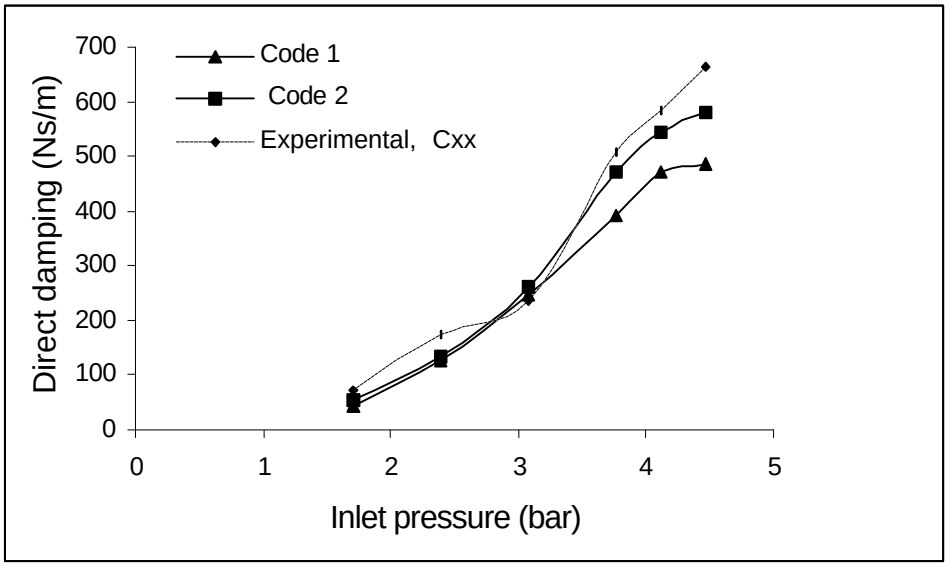

Fig. 51 Comparison of direct damping coefficients in the horizontal direction

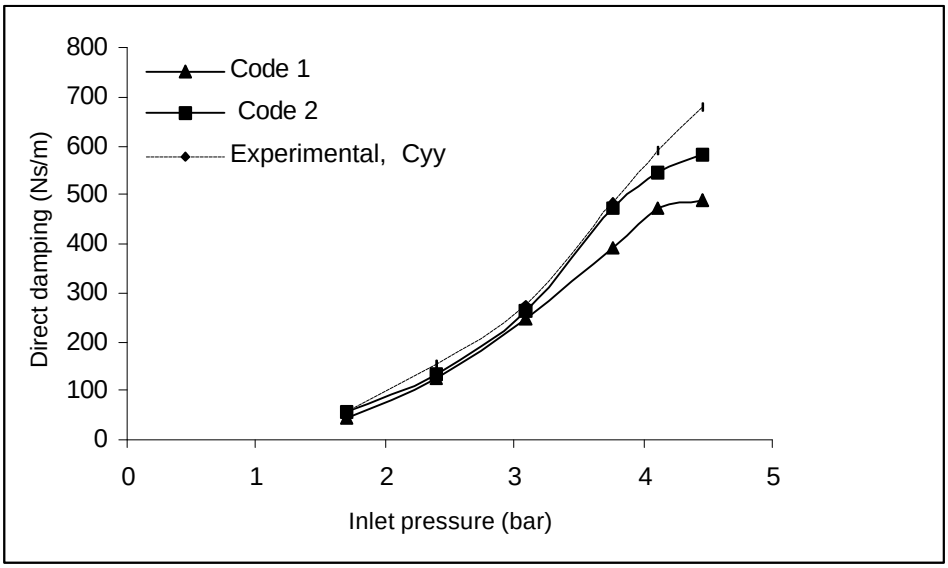

Fig. 52 Comparison of direct damping coefficients in the vertical direction

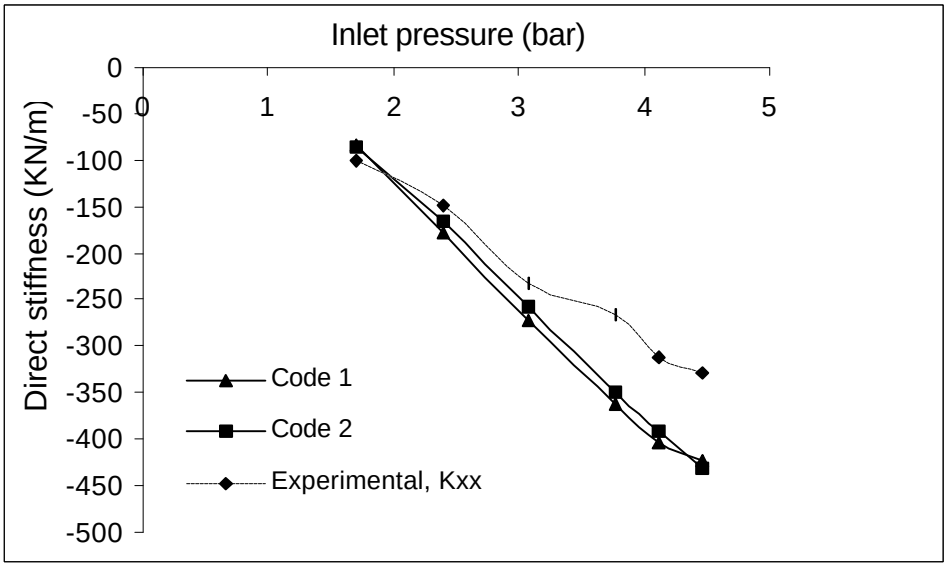

Fig. 53 Comparison of direct stiffness coefficients in the horizontal direction

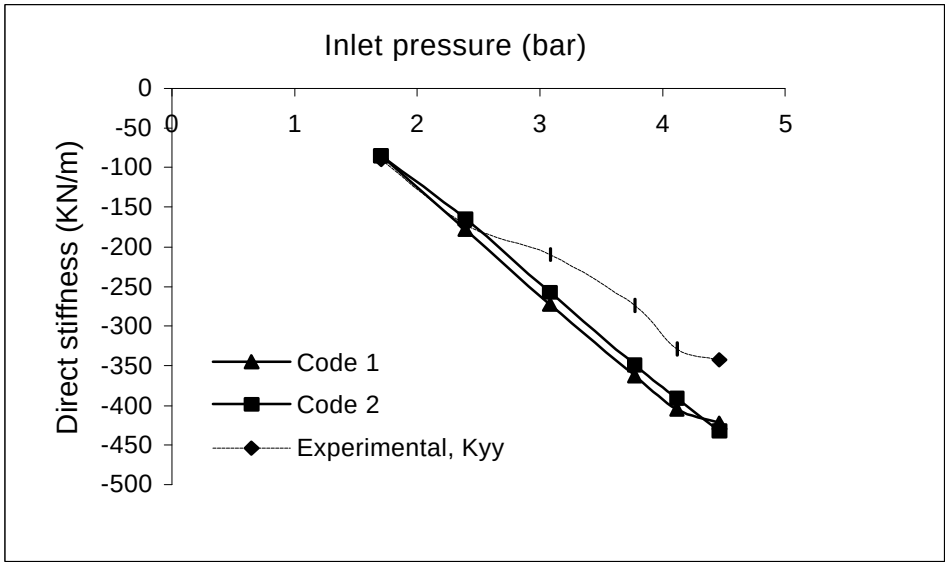

Fig. 54 Comparison of direct stiffness coefficients in the vertical direction

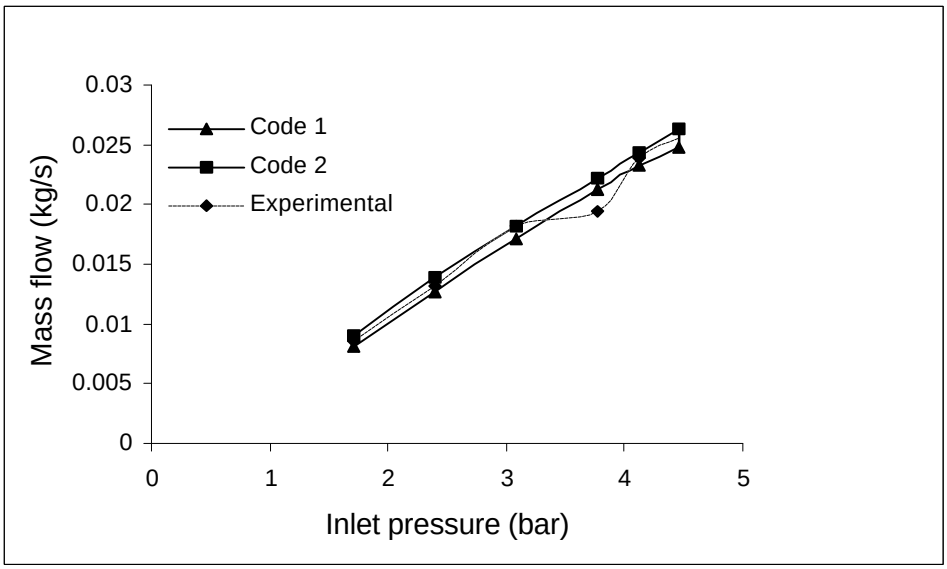

Fig. 55 Comparison of mass flow

Figure 55 compares the leakage rates obtained from the tests with those from the predictions. The predicted values are in close agreement with the measured values. Also, Code 2 predicts slightly higher pocket pressures than Code 1 because of the difference in the iterative method used.

COMPARISON OF PDS RESULTS TESTED BY LAOS

One of the most significant contributions of the various experiments conducted at the Turbomachinery Laboratory is in validation of the computer codes. The input parameters used in the models for predicting the rotordynamic coefficients have to be carefully matched to the actual conditions. The success of the theoretical predictions is measured by comparing with the experimental results. So it becomes absolutely necessary to minimize the error involved when choosing proper input parameters for the code. The following presents a plausible explanation for the discrepancies observed by Laos [12] between his theory and experiments.

Table 15 Direct damping and stiffness coefficients from testing of four bladed PDS, Laos [12]

Assumed inlet pressure psia (bar)	Direct damping in the horizontal diretcion lbs/in (Ns/m)	
	Experimental	Predicted
34.7 (2.392)	0.27 (47.2824)	1.253(219.425)
44.7 (3.082)	0.55 (96.316)	2.346 (410.831)
54.7 (3.771)	0.75 (131.34)	3.603 (631.832)
64.7 (4.461)	1.13 (197.885)	4.395 (769.652)
74.7 (5.150)	1.37 (239.914)	5.075 (888.734)
84.7 (5.834)	1.73 (302.95)	5.754(1007.64)
Assumed inlet pressure psia (bar)	Direct stiffness in the horizontal diretcion lb/in (KN/m)	
	Experimental	Predicted
34.7 (2.392)	-468 (81.956)	-1537.19 (269.192)
44.7 (3.082)	-759 (13.2916)	-2252.64 (394.482)
54.7 (3.771)	-1009 (176.696)	-2883.96 (505.039)
64.7 (4.461)	-1379 (241.490)	-3317.59 (580.976)
74.7 (5.150)	-1712 (299.805)	-3830.36 (670.772)
84.7 (5.834)	-2429 (425.366)	-4343.12 (760.567)

The above Table 15 is adapted from Laos [12]. The predicted and the experimental values for the rotordynamic coefficients are listed in the table for the four bladed eight pocket damper seal. Only values obtained in the horizontal direction are tabulated.

The following procedure was followed by Laos in predicting the direct stiffness and damping values from the code:

a) The measured pressure was assumed to be the actual inlet pressure to the seal.
b) After the seal parameters were input, the code was run to calculate the force coefficients.
c) The coefficient of discharge was then adjusted to match the predicted leakage and the measured leakage rate.
d) The direct damping and the stiffness values were then calculated.

It is seen that the predicted values are excessively high. In some cases, the percentage of error exceeds acceptable limits. This deviation is due to the following factors. First, the procedure of altering the coefficient of discharge for each run is not correct. The values of coefficients of discharge used in the runs were varied between 0.35-0.52. It is true that the flow conditions may change slightly with the rotor motion and the inlet pressure, but this fluctuation surely is much less than the variations of the coefficient of discharge. Second, a complete review also revealed that the measured pressure was different from the actual inlet pressure. This is because the inlet pressures were not measured at the inlet to the seal but instead at some point upstream of an enclosure ring with radial inlet holes. Hence the inlet pressure is actually much lesser than the measured pressure. Using the inaccurate pressures as input to the code runs introduces a considerable amount of error in predicting the damping and stiffness values. As shown earlier, the air inlet to the PDS is through the eight holes radially located in the central supply plenum. The most accurate measurement of the inlet pressure is obtained by placing the pressure transducer flush with the inside surface of the seal in the central supply plenum. As seen in Table 15, the stiffness and damping values were

consistently overpredicted by the code in Laos' work because the input pressures were measured at the wrong place.

An alternate method was developed to use the code to predict Laos' stiffness and damping coefficients in a more accurate manner. In this method, the calculated leakage was matched with the measured leakage by varying the inlet pressure. The coefficient of discharge was kept the same for all the runs. The discharge coefficients were established accurately earlier by leakage measurements. Table 16 shows the corrected values obtained by varying the inlet pressures.

Table 16 Direct damping and stiffness coefficients of PDS tested by Laos after corrections

Assumed inlet pressure psia (bar)	Corrected inlet pressure psia (bar)	Direct damping in the horizontal diretcion lbs/in (Ns/m)	
		Experimental	Predicted
34.7 (2.392)	11.95 (0.823)	0.27 (47.2824)	0.358 (62.692)
44.7 (3.082)	14.8 (1.020)	0.55 (96.316)	0.488 (85.458)
54.7 (3.771)	16.8 (1.158)	0.75 (131.34)	0.586 (102.62)
64.7 (4.461)	18.83 (1.298)	1.13 (197.885)	0.691 (121.007)
74.7 (5.150)	20.89 (1.44)	1.37 (239.914)	0.803 (140.621)
84.7 (5.834)	24.02 (1.656)	1.73 (302.95)	0.980 (171.617)
Assumed inlet pressure psia (bar)	Corrected inlet pressure psia (bar)	Direct stiffness in the horizontal diretcion lb/in (KN/m)	
		Experimental	Predicted
34.7 (2.392)	11.95 (0.823)	-468 (81.956)	-463.34 (81.140)
44.7 (3.082)	14.8 (1.020)	-759 (13.2916)	-567.041 (99.300)

54.7 (3.771)	16.8 (1.158)	-1009 (176.696)	-637.301 (111.604)
64.7 (4.461)	18.83 (1.298)	-1379 (241.490)	-706.334 (123.693)
74.7 (5.150)	20.89 (1.44)	-1712 (299.805)	-773.962 (135.536)
84.7 (5.834)	24.02 (1.656)	-2429 (425.366)	-871.994 (152.703)

As seen from the table, the predicted stiffness and damping values are more closely predicted than before. The error involved is much lesser than the previous case. The pressure drop between the position of the pressure transducer and the seal inlet is of great importance. Figures 56-57 show the variation of these coefficients with corrected seal inlet pressure.

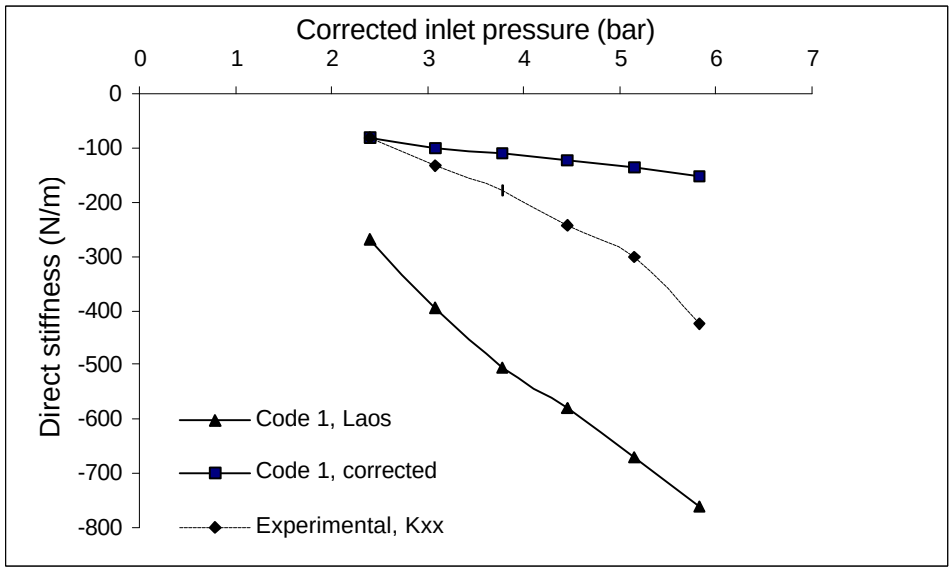

Fig. 56 Comparison of direct stiffness with corrected inlet pressure

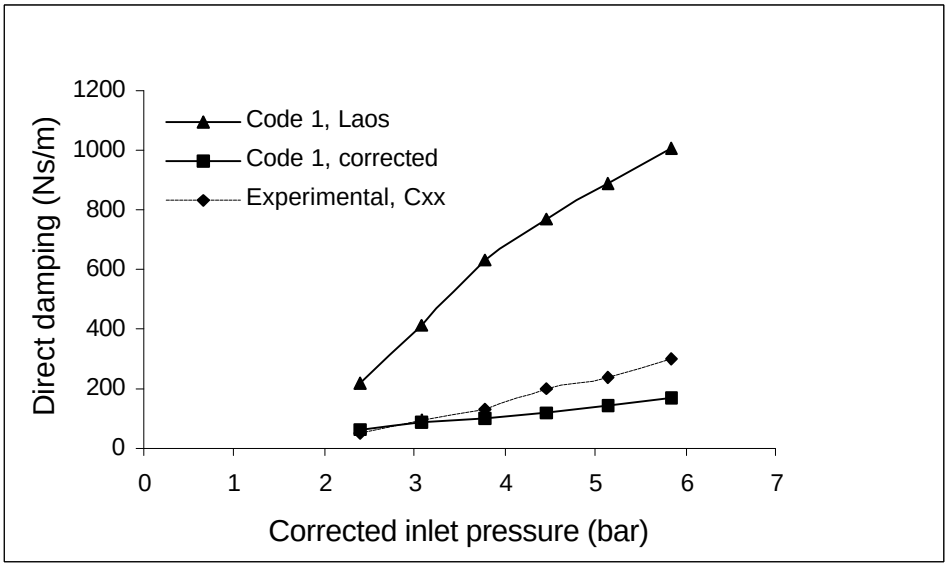

Fig. 57 Comparison of direct damping with corrected inlet pressure

The damping values are now underpredicted but the error margin has come down to a reasonable level. Conversely, the predicted stiffness values are higher in magnitude than the experimental values.

The leakage rate comparison is shown in Figure 58. As expected, the mass flow rates predicted from the code and measured by testing overlap each other. This agreement is because the leakage rates were matched to start with and then the rotordynamic coefficients are predicted from the codes. The discharge coefficients are kept the same for all the runs. The slight difference in the leakage curves is due to the tolerance used in the numerical method of the code. It is possible to exactly match the two curves by specifying a higher tolerance during the iterative process.

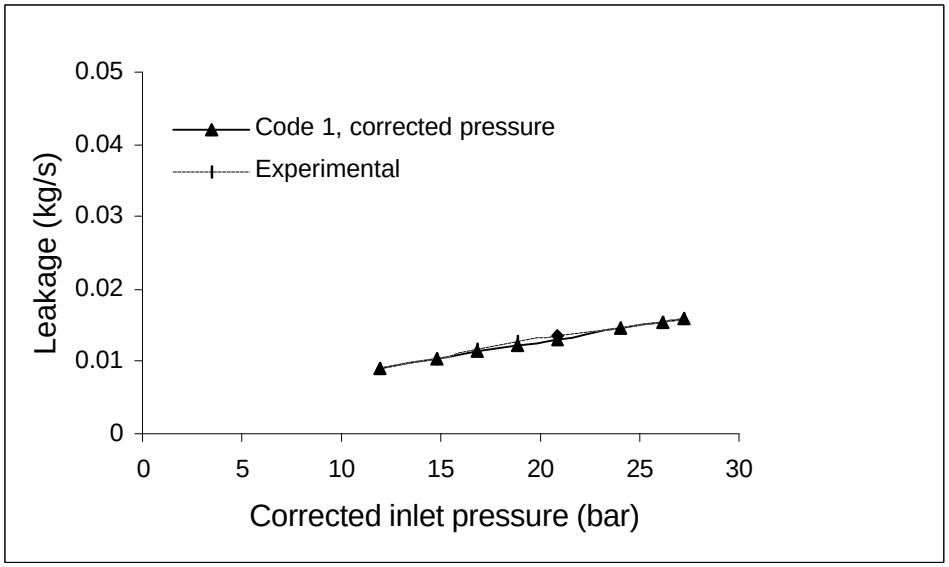

Fig. 58 Comparison of leakage rates with corrected inlet pressure

CHAPTER VIII

CONCLUSIONS

- A mathematical model for the notched PDS was completed and the theory was implemented as a computer code to predict the direct damping and stiffness coefficients.
- The notched model predicts higher direct damping coefficients in comparison to the existing model without the notch. The predictions are in agreement with the experimental results from testing of the notched PDS.
- The model predictions are in qualitative agreement with the tests conducted by Li [9] when comparisons are done for the same PDS with and without the notch. The direct damping coefficients increase when the notch is included in the analysis.
- For the case without the notch, the new theoretical model differs only slightly in predicting the direct damping coefficients from the existing model. Deviations are attributed to the difference in the algorithm used in calculating the mass flows across each blade.
- The code predictions agree reasonably with the test measurements of a notched two bladed PDS conducted by Sharma [13]. The trend predicted for both direct damping and stiffness coefficients is good. It is observed that only the direct damping coefficients are predicted well but there is considerable variation in predicting the direct stiffness of the PDS.
- The new theoretical model verifies that the mass flow across each of the PDS blades are equal once it has been calculated. This is not the case with the existing model in which the mass flows across each of the blades slightly differ and the minimum of all the values is considered for calculations in the prediction of the force coefficients.
- A new four bladed PDS with eight pockets was designed and coastdown tests and leakage tests are conducted to predict its rotordynamic coefficients.

- Initial testing with a journal with higher runout gives absurd results in which damping coefficients decrease with seal inlet pressure. These results indicate that if the runout is not within acceptable limits then it can have a detrimental effect on the damping capability of the PDS.
- Testing of the PDS with a new journal was possible only up to a seal inlet pressure of 64.7 psia (4.460 bar) because of the low stiffness of the test rotor. The low stiffness of the rotor combined with the negative stiffness produced by the PDS caused the rotor journal to move towards the seal wall when the inlet pressure is increased to the range 65 psia (4.461 bar) to 70 psia (4.4826 bar). But the results obtained below 64.7 psia (4.460 bar) are encouraging. The PDS offers positive direct damping and the damping coefficients increase with seal inlet pressures. The direct stiffness of the PDS are all negative and their magnitudes increase with seal inlet pressure.
- The results are compared with the predictions from the two available theoretical models. The experimental damping values are in close agreement with the predictions from the notched model for pressures up to 44.7 psia (3.801 bar) but the deviation is considerable for higher pressures. The deviation increases as the inlet pressure increases. Both the models predict similar direct stiffness values which is quite deviant form the measured values.
- An analysis was carried out to calculate the error involved in computing the notch area due to inaccuracies in machining the semi-circular notch and this revealed that the notch area is excessively sensitive to small errors in the cutting tool movement. Hence this method of machining the notch that was used in this study should either not be adopted or the error involved in the process should be minimized.
- An appropriate reasoning for the unusually high error between theory and experiments as detailed in [12] was provided and modifications are done to reduce the error in the comparison.

REFERENCES

1) Alford, J. S., 1965, "Protecting Turbomachinery from Self-excited Rotor Whirl," ASME J. Eng. Power, pp. 333-334 (October 1965).

2) Vance, J. M., Zierer, J. J., and Conway, E. M., 1993, "Effect of Straight Through Labyrinth Seals on Rotordynamics in Vibration of Rotating System," *Proceedings of the 14th Vibration and Noise Conference*, Albuquerque, NM, **DE-60**, pp. 159-171.

3) Benkert, H., and Wachter, J., 1980, "Flow Induced Spring Coefficients of Labyrinth Seals for Applications in Rotordynamics," *Proceedings of the 1st Workshop on Rotordynamic Instability Problems in High Performance Turbomachinery*, Texas A&M university, May 12-14, NASA CP 2133, pp.189-212.

4) Sundarajan, P., and Vance, J. M., 1995, "A Theoretical and Experimental Investigation of a Gas-Operated Bearing Damper for Turbomachinery - Part II: Experimental Results and Comparison with Theory," ASME J. Eng. Gas Turbines Power, **117**, pp. 750-756.

5) Vance, J. M., Shultz, R. R., 1993, "A New Damper Seal for Turbomachinery in Vibration of Rotating system," *Proceedings of the 14th Vibration and Noise Conference*, Albuquerque, NM, **DE-60**, ASME, pp. 139-148.

6) Shultz, R. R., 1996, "Analytical and Experimental Investigations of a Labyrinth Seal Test Rig and Damper Seals for Turbomachinery," M.S. thesis, Texas A&M University, College Station.

7) Vance, J. M., Cardon, B. P., San Andres, L. A., and Storace, A. F., 1993, "A Gas-Operated Bearing Damper for Turbomachinery," ASME J. Eng. Gas Turbines Power, **115**, pp. 383-389.

8) Li, J., 1995, "The Effect of a New Damper Seal on Rotordynamics," M.S. thesis, Texas A&M University, College Station.

9) Li, J., and Vance, J.M., 1995, “Effects of Clearance and Clearance Ratio on Two and Three Bladed TAMSEALs,” TRC-Seal-4-95, Turbomachinery Laboratory Research Progress Report, Texas A&M University, College Station.

10) Li, J., 1999, “A Bulk Flow Model of Multiple-Blade, Multiple-Pocket Gas Damper Seals,” Ph.D. dissertation, Texas A&M University, College Station.

11) Laos, H.E and Vance, J.M 1997, “Rotordynamic Effects of Pocket Damper Seals,” TRC-Seal-8-97, Turbomachinery Laboratory Research Progress Report, Texas A&M University, College Station.

12) Laos, H.E., 1999, “Rotordynamic Effects of Pocket Damper Seals,” Ph.D. dissertation, Texas A&M University, College Station.

13) Sharma, A., 2001, “High Frequency Testing of Pocket Damper Seals,” M.S. thesis, Texas A&M University, College station.

14) Saad, M.A., 1985, *Compressible Fluid Flow*, Prentice-Hall, Inc, New Jersey, pp.156-175.

15) Vance, J. M., 1998 *Rotordynamics of Turbomachinery*, John Wiley and Sons, New York, pp. 182-184, 249-260.

16) Vance, J. M., Laos, H. E., 1998, “Rotordynamic Effect of Damper Seals,” TRC-Seal-8-98, Turbomachinery Laboratory Research Progress Report, Texas A&M University, College Station.

APPENDIX A: XLTRC WORKSHEETS

In this section the various XLTRC worksheets used as part of the rotordynamic analysis are presented. The analysis is performed to match the experimental Bode plots and thereby to extract the direct damping and stiffness coefficients of the PDS.

INPUT TABLE OF BEAM AND STATION DEFINITIONS, MORE THAN ONE BEAM PER STATION IS								
Station #	Length in	OD in	ID in	Weight Density lb/in^3	Elastic Modulus psi	Shear Modulus psi	Added Weight lb	Added Ip lb-in^2
stnum	length	oda	ida	rhoa	ea	ga	awt	aip
1	1.372	0.75	0	0.283	30.0E+6	12.0E+6	0.0	0.0
2	0.314	0.7875	0	0.283	30.0E+6	12.0E+6	0.000	0.0
3	0.314	0.7875	0	0.283	30.0E+6	12.0E+6	0.265	0.0
4	0.5	1	0	0.283	30.0E+6	12.0E+6	0.0	0.0
5	0.45	1.2	0	0.283	30.0E+6	12.0E+6	0.0	0.0
6	1	1.2	0	0.283	30.0E+6	12.0E+6	0.0	0.0
7	1	1.2	0	0.283	30.0E+6	12.0E+6	0.0	0.0
8	1	1.2	0	0.283	30.0E+6	12.0E+6	0.0	0.0
9	1	1.2	0	0.283	30.0E+6	12.0E+6	0.0	0.0
10	1	1.2	0	0.283	30.0E+6	12.0E+6	0.0	0.0
11	1	1.2	0	0.283	30.0E+6	12.0E+6	0.0	0.0
12	1	1.2	0	0.283	30.0E+6	12.0E+6	0.0	0.0
13	1	1.2	0	0.283	30.0E+6	12.0E+6	0.0	0.0
14	1	1.2	0	0.283	30.0E+6	12.0E+6	0.0	0.0
15	1	1.2	0	0.283	30.0E+6	12.0E+6	0.0	0.0
16	1	1.2	0	0.283	30.0E+6	12.0E+6	0.0	0.0
17	1	1.2	0	0.283	30.0E+6	12.0E+6	0.0	0.0
18	1	1.2	0	0.283	30.0E+6	12.0E+6	0.0	0.0
19	1	1.2	0	0.283	30.0E+6	12.0E+6	0.0	0.0
20	0.5	1.378	0	0.283	30.0E+6	12.0E+6	0.000	0.0
21	0.5	1.378	0	0.283	30.0E+6	12.0E+6	1.966	0.0
22	0.5	1.5	0	0.283	30.0E+6	12.0E+6	0.0	0.0
23	1.2	2	0	0.283	30.0E+6	12.0E+6	0.0	0.0
24	1.161	1.45	0	0.283	30.0E+6	12.0E+6	0.0	0.0
25	1.17	1.45	0	0.283	30.0E+6	12.0E+6	0.0	0.0
26	0.9	1.3	0	0.283	30.0E+6	12.0E+6	0.0	0.0
27	0.9	1.3	0	0.283	30.0E+6	12.0E+6	0.000	0.000
28	1	1	0	0.283	30.0E+6	12.0E+6	0.0	0.0
29	0.969	1	0	0.283	30.0E+6	12.0E+6	0.0	0.0
30	0	1	0	0.283	30.0E+6	12.0E+6	0.0	0.0

Fig. 59 Geometry of the rotor assembly

Title:	Self_Aliagnign Ball Bearing											
Perform a Paste/Special/Link for the Title box within XLTRC to create a link to your rotor model.												
Speed	Kxx	Kxy	Kyx	Kyy	Cxx	Cxy	Cyx	Cyy	Mxx	Mxy	Myx	Myy
rpm	lb/in	lb/in	lb/in	lb/in	lb-s/in	lb-s/in	lb-s/in	lb-s/in	lb-s**2/in	lb-s**2/in	lb-s**2/in	lb-s**2/in
0	150000	0	0	150000	0	0	0	0	0	0	0	0
1000	150000	0	0	150000	0	0	0	0	0	0	0	0
2000	150000	0	0	150000	0	0	0	0	0	0	0	0
3000	150000	0	0	150000	0	0	0	0	0	0	0	0
4000	150000	0	0	150000	0	0	0	0	0	0	0	0
5000	150000	0	0	150000	0	0	0	0	0	0	0	0
6000	150000	0	0	150000	0	0	0	0	0	0	0	0
7000	150000	0	0	150000	0	0	0	0	0	0	0	0
8000	150000	0	0	150000	0	0	0	0	0	0	0	0
Insert or Delete rows to expand or contract the above table of user defined input values.												
You can use use formulas, and/or links to other spreadsheets.												

Fig. 60 Self-aligning ball bearing worksheet

Title:	BHS coefficients											
Perform a Paste/Special/Link for the Title box within XLTRC to create a link to your rotor model.												
Speed	Kxx	Kxy	Kyx	Kyy	Cxx	Cxy	Cyx	Cyy	Mxx	Mxy	Myx	Myy
rpm	lb/in	lb/in	lb/in	lb/in	lb-s/in	lb-s/in	lb-s/in	lb-s/in	lb-s**2/in	lb-s**2/in	lb-s**2/in	lb-s**2/in
0	485	0	0	490	0.2453	0	0	0.2468	0	0	0	0
1000	485	0	0	490	0.2453	0	0	0.2468	0	0	0	0
2000	485	0	0	490	0.2453	0	0	0.2468	0	0	0	0
3000	485	0	0	490	0.2453	0	0	0.2468	0	0	0	0
4000	485	0	0	490	0.2453	0	0	0.2468	0	0	0	0
5000	485	0	0	490	0.2453	0	0	0.2468	0	0	0	0
6000	485	0	0	490	0.2453	0	0	0.2468	0	0	0	0
7000	485	0	0	490	0.2453	0	0	0.2468	0	0	0	0
8000	485	0	0	490	0.2453	0	0	0.2468	0	0	0	0
Insert or Delete rows to expand or contract the above table of user defined input values.												
You can use use formulas, and/or links to other spreadsheets.												

Fig. 61 PDS worksheet

Title: Squirrel Cage Stiffness

Perform a Paste/Special/Link for the Title box within XLTRC to create a link to your rotor model.

Speed	Kxx	Kxy	Kyx	Kyy	Cxx	Cxy	Cyx	Cyy	Mxx	Mxy	Myx	Myy
rpm	lb/in	lb/in	lb/in	lb/in	lb-s/in	lb-s/in	lb-s/in	lb-s/in	lb-s**2/in	lb-s**2/in	lb-s**2/in	lb-s**2/in
0	29000	0	0	34000	0.7	0	0	3.794118	0	0	0	0
1000	29000	0	0	34000	0.7	0	0	3.794118	0	0	0	0
2000	29000	0	0	34000	0.7	0	0	3.794118	0	0	0	0
3000	29000	0	0	34000	0.7	0	0	3.794118	0	0	0	0
4000	29000	0	0	34000	0.7	0	0	3.794118	0	0	0	0
5000	29000	0	0	34000	0.7	0	0	3.794118	0	0	0	0
6000	29000	0	0	34000	0.7	0	0	3.794118	0	0	0	0
7000	29000	0	0	34000	0.7	0	0	3.794118	0	0	0	0

Insert or Delete rows to expand or contract the above table of user defined input values.
You can use use formulas, and/or links to other spreadsheets.

Fig. 62 Squirrel cage worksheet

BEARING AND SEAL DEFINITIONS

brgstn	brgtype	ucsFactor	ucsConstant		brglink
Station #	Type	UCS Factor	UCS Constant	Output Loads	Link (*Paste Special* in here)
3		1			Self_Aliagnign Ball Bearing
21		1			Squirrel Cage Stiffness
27		1			BHS coefficients

Insert or Delete rows to expand or contract the above table of bearing definitions.
You can use use formulas, and/or links to other spreadsheets.

Make the station # a reference to a cell on the 'Shaft Input' sheet if you want
the station number to automatically change when you add or delete stations from the model.

Fig. 63 Bearing and PDS definition worksheet

APPENDIX B: CALIBRATION CHARTS

A number of instruments have been used for the rotating tests conducted on the PDS. These include various proximity probes, flowmeter, etc. These have to be calibrated before using them for data acquisition. Some of the calibration charts used are shown in Figures 64-68.

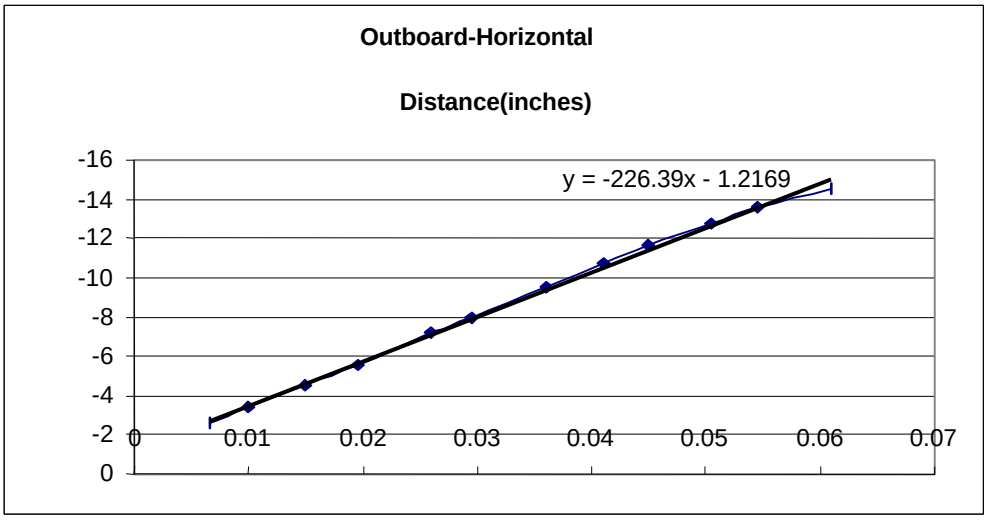

Fig. 64 Calibration chart for the outboard horizontal proximity probe

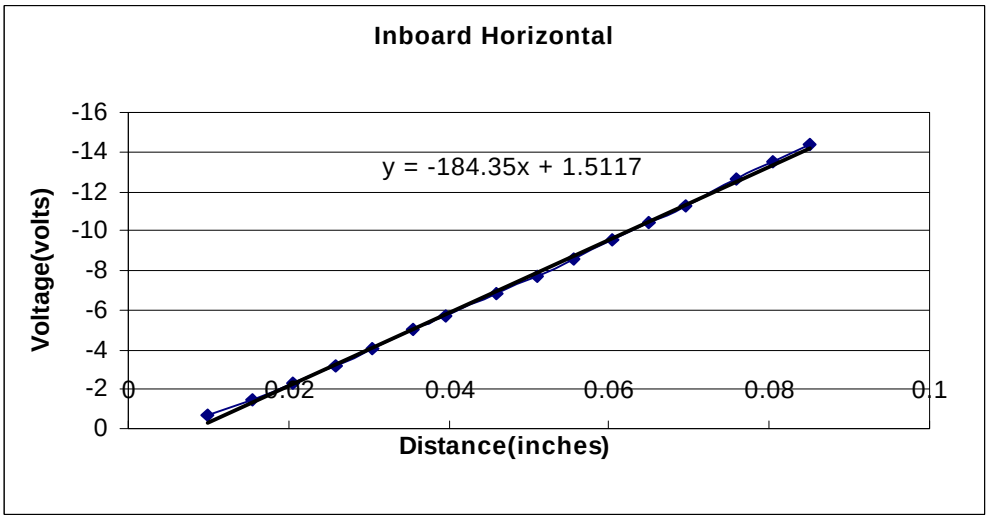

Fig. 65 Calibration chart for the inboard horizontal proximity probe

All the proximity probes are Bently Nevada probes with product number 19000-05-45-36-02.

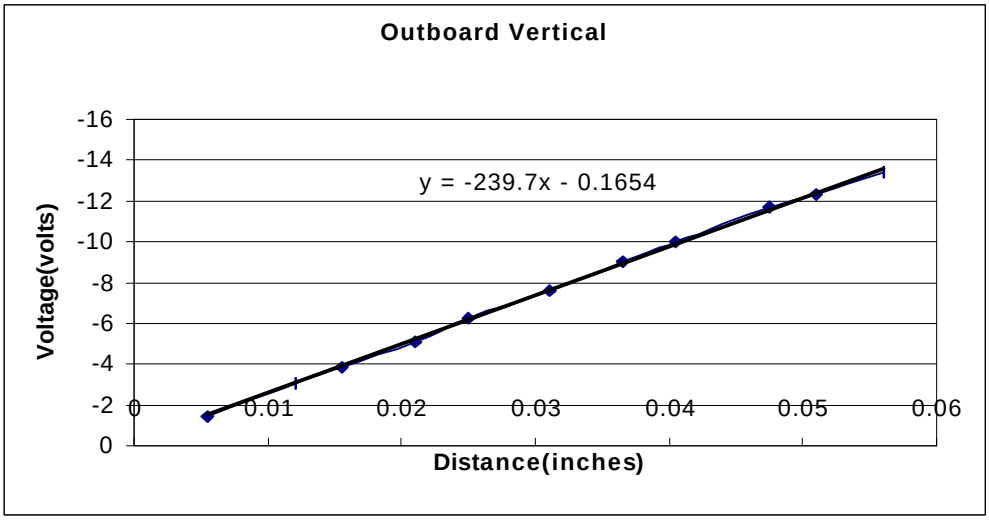

Fig. 66 Calibration chart for the outboard vertical proximity probe

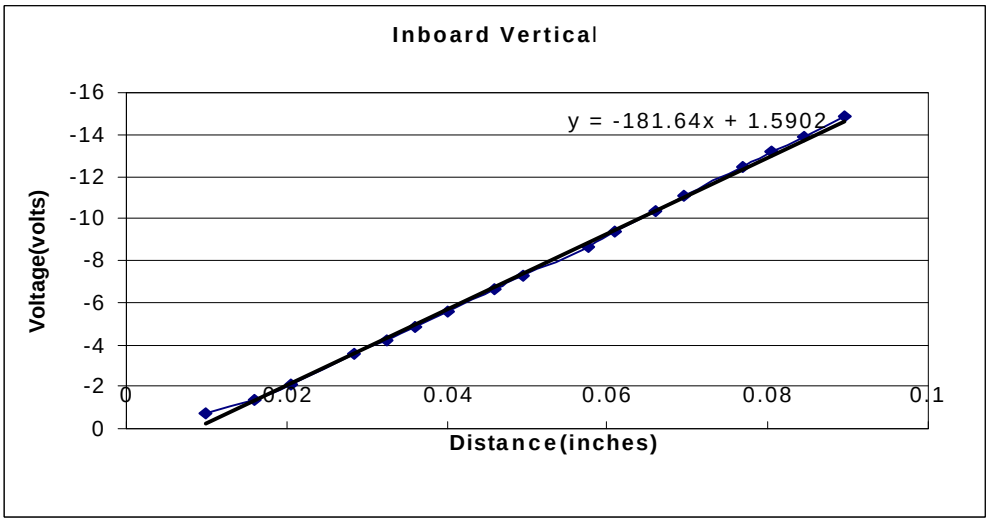

Fig. 67 Calibration chart for the inboard vertical proximity probe

Figure 68 shows the calibration chart used for converting the voltage from the flowmeter to flow rate in acfm.

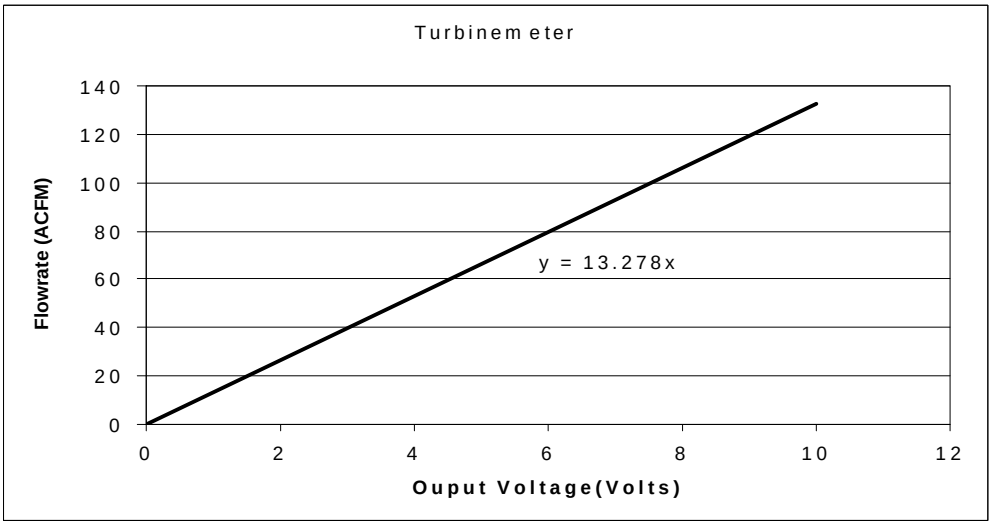

Fig. 68 Calibration chart for Omega Turbinemeter (FTB 938)

APPENDIX C: STRESS ANALYSIS ON PDS

Analysis was performed using SolidWorks™/Cosmos to check for the stresses in the PDS at high pressures during the design phase of the PDS. Figure 69 shows the mesh plot used in finding the stress distribution in the seal when a pressure of 300 psi (20.684 bar) is applied. This pressure is used in the analysis keeping in mind the maximum possible pressure difference or drop across any two blades.

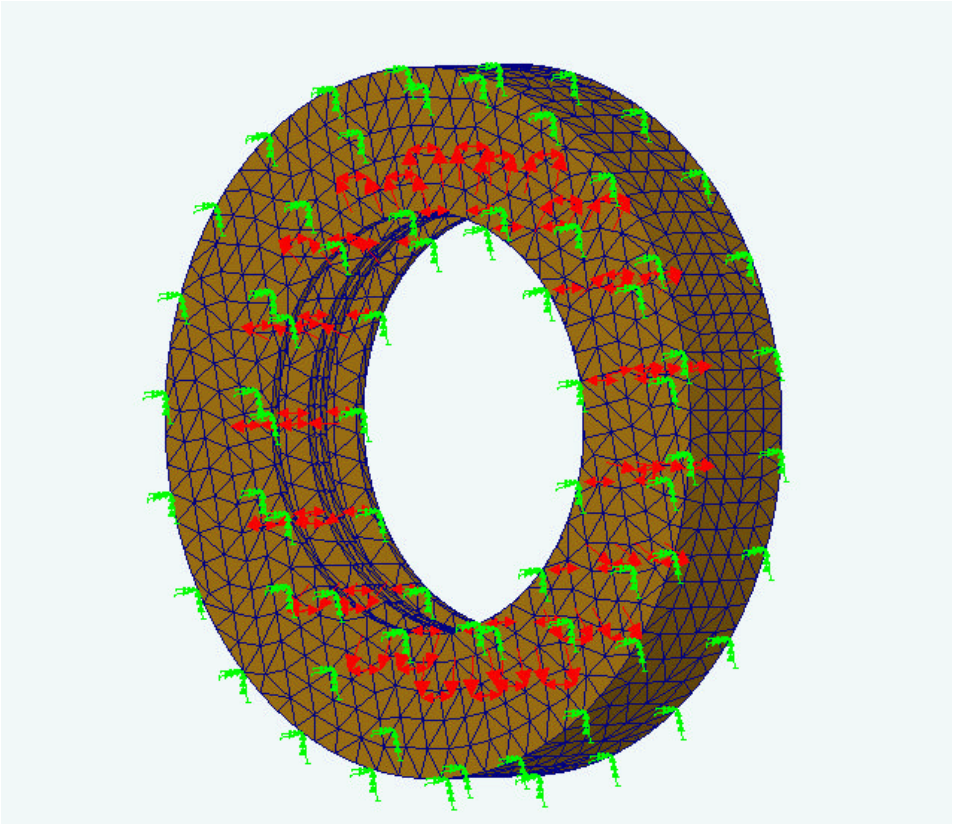

Fig. 69 Mesh plot for stress distribution in the PDS for a pressure of 300 psi (20.684 bar)

The boundary of the PDS is fixed and a uniform pressure of 300 psi (20.684 bar) is applied inside the pocket cavities. The green marks represent the constraints and the red arrows indicate the pressure applied. The least factor of safety calculated using Von

Mises stress theory turned to be 2.7. The nodal displacements are of the order 10^{-8} inches ($25.4 \cdot 10^{-7}$).

VITA

Bharathwaj Kannan Srinivas
Plt. 39, Krishnamachari Nagar, Porur,
Chennai, Tamil nadu, 600 116
India

Graduate Education
Texas A&M University
College Station, Texas
Mechanical Engineering, Master of Science
August 2000 - May 2003
Area of work: Rotordynamics and Turbomachinery

Undergraduate Education
University of Madras
Pennalur, Tamil nadu, India
Mechanical Engineering, Bachelor of Engineering
August 1996 – May 2000

Experience
Research assistant under Dr. John M. Vance.
Worked in the following projects at the Turbomachinery Laboratory:
Rotordynamic Effects of Pocket Damper Seals (August 2000 – Aug 2002).
Experimental Evaluation of Metal Mesh as a Bearing Damper Material (August 2002 - May 2003).